ABX_3 perovskite nanocrystals in porous matrices

Doctoral thesis presented by

Andrea Rubino

Supervised by

Prof. Dr. Hernán Ruy Míguez García

Dr. Mauricio Ernesto Calvo Roggiani

Inorganic Chemistry Department
Faculty of Chemistry
University of Seville

Multifunctional Optical Materials group
Institute of Materials Science of Seville
Spanish National Research Council

1 GENERAL INTRODUCTION

1.1 PEROVSKITES

The definition of perovskite embraces a class of compounds characterized by a typically pseudo-cubic crystalline habit. Generally this family of minerals, already identified in the nineteenth century,[1,2] is described by the formula ABX_3 and consists of a metal oxide organized according to a grid of cations coordinated to six oxygen atoms which leaves sufficient space for the simultaneous presence of a second cation larger than the first.[3] Since the end of the following century, however, the evidence of lead-based halogenated perovskite structures, revealing photoconduction properties, pushed the horizon of research on the valorisation of these materials forward.[4,5]

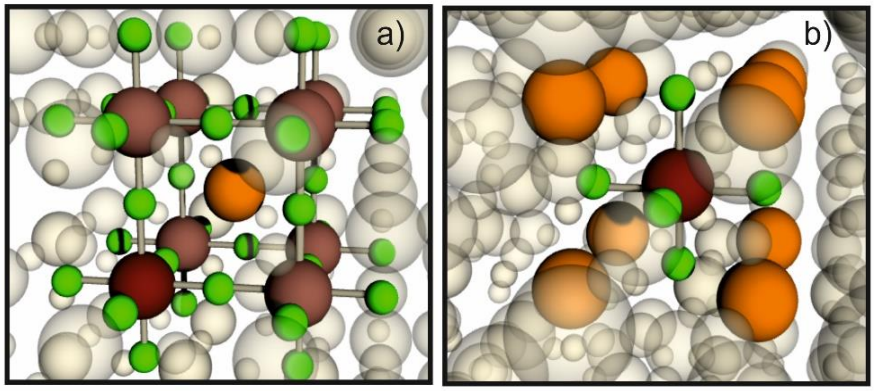

Figure 1.1 General equivalent structures of a perovskite unit cell: in a) A cation (orange element) is drawn at the centre of a cube composed by four corner-sharing BX_6 octahedrons while in b) metal cation B (red element) is represented at the centre of a cubic unit cell and coordinated to six X anions (green elements) at the centre of the cube faces with A in the corner positions.

In the case of normal three-dimensional (3D) perovskite with optoelectronic properties, the chemical composition that respects the tolerance factor, necessary to maintain the cubic structure, foresees an organic (methyl ammonium MA^+, formamidinium, FA^+) or inorganic (Cs^+) cation, A, another monoatomic cation, B, from a divalent metallic element (Pb^{2+}, Sn^{2+}, Ge^{2+}) and a halide anion, X, (Br^-, Cl^-, I^-). Metals and halides are coordinated in octahedrons that share a corner and are placed at the vertices of a cube. At the centre of the cube is located the A cation, as

illustrated in figure 1.1. A first assessment of the stability of these materials concerns the crystalline structure and for this purpose the empirical tolerance factor of Goldschimdt[6] (t) is normally taken into consideration, described as:

$$t = \frac{r_A + r_X}{\sqrt{2}\,(r_B + r_X)} \qquad (1)$$

where $r_{A,B,X}$ are the radii of the cations A and B and anion X respectively. An ideal or slightly distorted cubic conformation is maintained in a range of values of the t index between 0.71 and 1, while non-perovskite structures are formed for higher or lower values.[7] In fact molecules larger than formamidinium (ethylammonium, guanidinium, etc.) or atoms with radii smaller than cesium (e.g. rubidium or potassium) are at the limits of the tolerance factor and tend to form much less stable perovskites structures.[8,9] From the point of view of divalent metal species, lead and tin are the elements that best fit the photovoltaic requirements although, to overcome the toxicity and stability issues, variants have been studied that involve other divalent cations or mixtures of mono and trivalent metals.[10,11] The size of the perovskite crystals among the different chemical compositions, on the other hand, can vary according to the dimensions of the anion and the cation present in the lattice, affecting the perovskite crystal structure and so the bandgap (the iodide anion is larger than the bromide anion as well as formamidium is larger than methylammonium).[12,13] A derivation of 3D perovskites can result in a series of two-dimensional (2D) configurations with the formula $A_{n+1}B_nX_{3n+1}$ known as Ruddlesden-Popper (R-P) phases.[14,15] These layered perovskites are the consequence of the use of A cations consisting of large aliphatic or aromatic chains.

The interest gained around this class of semiconductors derives above all from their remarkable optical and electronic properties which are particularly appropriated in the development of the current energy context. Considering a much broader vision, the material science is constantly looking for solutions that can meet the growing demand of energy consumption and face the need to improve quality of life. In fact, in the current social context, the challenge to develop a renewable technology, of easy global access, sustainable consumption, minimal environmental impact remains open. In this regard, on both sides of the scale we find, in contrast, the production and consumption of energy. In the perspective of build up an eco-sustainable society, the paradigm would also be simple: being able to generate energy needs through clean, renewable and abundant sources and vice versa, to make careful and effective use of the "energy" available. Two of the most relevant examples in both cases, respectively, are photovoltaic technology and lighting technology (see figure 1.1c and d). The possibility of using solar radiation as a source of energy is one of the most promising alternatives to slow down or halt the exhaustion of fossil resources and eliminate, at the same time, their contaminating

effects.[16] While a significant amount of the electrical energy produced goes through public and private lighting systems, not to mention the portable technology (TV displays, computers, cell phones, etc.).[17]

In both cases, among the available tools, protagonists of this challenging research, we find semiconductor materials, already involved in many other aspects of modern technology (energy conversion, telecommunications, medicine).[18-20] The properties of these materials, in between those of an insulator and those of a conductor, have allowed an impressive technological advancement both in terms of efficiency, and energy saving together with quality and life comfort also thanks to the possibility of miniaturization (thinking of the integrated circuits).[21,22] Indeed, an interesting quality that makes these materials so attractive is their versatility. The wide range of applications derived from the use of this compounds fits perfectly with the needs of a society in which technology penetrates different aspects of life, requiring even higher levels of multi-functionality.

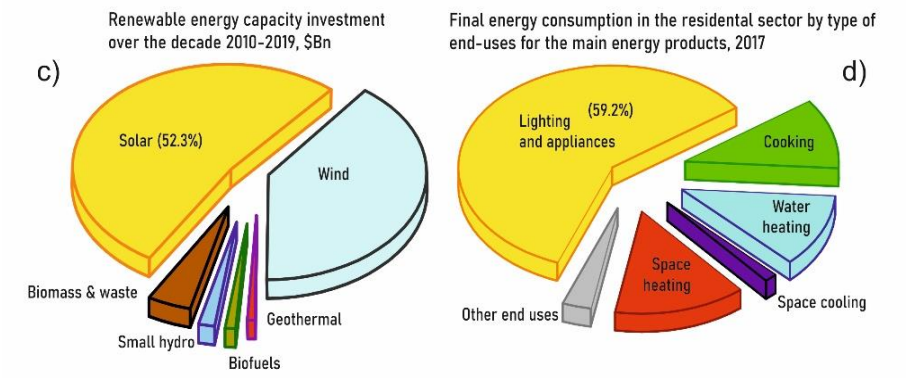

Figure 1.1 c) Percentage of investments on different alternative renewable sectors over a total investment of $2.6 trillion. Data adapted from ref.16. d) Percentage of electricity consumption in different end-use applications in households. Data adapted from ref.17.

In the wake of this pressing technological need, the discovery of the multivalent optoelectronic properties of metal-halide perovskites has been received with remarkable enthusiasm by the scientific community. The final breakthrough and the major progress date back to the last twenty years, following the introduction of perovskites in photovoltaic as an absorbent component of a dye sensitized solar cell.[23] The climb to success has been rapid and disruptive, marked by the gradual increase in efficiency of metal-halide perovskites thin film photovoltaic devices. [24,25] In the field of photovoltaics, these materials have in fact become as a potential competitor of silicon technology.

In general, however, the versatility of these semiconductor compounds also extends to many other applications. Perovskites have found use for example in light-emitting-diodes,[26,27] transistors,[28] photodetectors[29] and have been more recently considered as scintillators.[30] Another very interesting technological aspect concerns the use as an optical gain medium in distinct structural configurations (DBRs, microcavities, plasmonic structures) for the fabrication of laser devices exploiting the amplified spontaneous emission or even random lasing effects.[31] Moreover, these materials also revealed a quite strong third order nonlinear character,[32] particularly evident in 2D systems, useful for applications in communications devices. In all their applications one of the most appreciated properties of lead halide perovskites, together with low fabrication costs, is certainly the tunability of the bandgap depending on the chemical composition of the semiconductor. Specifically, the exchange of halides allows the coverage of the entire visible spectrum, from ultraviolet A (UVA) (chloride-based materials) to near infrared (iodine-based materials).[33] The advantage of this easy bandgap tuning, however, is closely linked to a contrasting phenomenon which undermines the stability of the perovskites that is the ion migration. Already known also in oxygen based perovskite compounds,[34] the migration of ionic species present in the system (A^+, B^{2+}, X^-) can be induced by various external factors, but, in any case it depends on the presence of structural defects, in particular ionic vacancies in the lattice. Among the species in movement, those with the highest probability are considered halides, whose migration is most evident in mixed perovskites, for example $MAPb(BrI)_3$, through a phase segregation effect,[35] which implicate the formations of separated domains, Br-rich and I-rich, with different electronic and optical behaviour. The ionic mobility can therefore induce a compositional change that compromises the stability of the perovskites and is in fact also associated with the main degradation factors of these materials. In particular, the presence of humidity or water and oxygen molecules and the prolonged light irradiation and heating at temperatures around 100 degrees are among the most aggressive external conditions for the survival of the perovskites as they have individually demonstrated to be able to initiate a compositional modification, but also lead directly to decomposition, reacting, for example, with organic cations to produce gaseous species and irreversibly destroy the crystalline structure.[36] Long-term stability problems are the main barriers to the marketing of perovskite-based devices. But precisely because both the argument and the materials under examination are undoubtedly complex (more degradation factors can act together and more components of a device can react distinctly), it is particularly relevant to follow the development of materials with a fundamental study of the properties and behaviour of perovskites semiconductors.

One of the most interesting developments in the investigation of these materials concerns their nanocrystals, with properties so distinctive as to generate a new field of research. As a matter of fact, since the end of the twentieth century, nanotechnology accompanied the research of applied science offering the possibility to expand the materials functionality thanks to a better control over the matter on the nanometer scale. The fabrication of low-dimensional structures has been of great help for semiconductor-based applications. Synthesis processes designed to specifically reduce the equivalent length (or size) of the three dimensions of volumetric materials (3D) have opened the field of semiconductors literally to new types of materials, such as quantum dots (0D), nanofibres (1D), nanoplatelets (2D) and a plethora of conformational variations and superstructures that can be derived from the combination of these nanomaterials.[37,38] All these new solutions have already shown enormous advantages on electronic, optical and mechanical properties and an easy integration in actual devices that have led to an amazing commercial advancement (e.g. TV displays that already use quantum dots).[39,40] Similarly, after the photovoltaic relaunch of perovskites, research naturally became interested in the development of nanocrystalline versions of these semiconductors not only from the study of their fundamental properties but also from their application in optoelectronic devices.

1.1.1 Quantum confinement effect in semiconductors

The nanoscale reduction in size of semiconducting materials is closely related to the quantum confinement (QC) phenomenon. The QC effect in semiconductors has revealed the correlation between molecules and crystals. The electronic behaviour of nanocrystals, otherwise also called quantum dots, can be seen as a compromise between the characteristics of bulk semiconductor and the discrete nature of atoms properties. In general, the properties that define a semiconductor derive in large part from the electronic configuration of the atomic elements that compose it and from the consequent overlap of orbitals that form its band structure. The direct or indirect nature of the bad gap and the energy difference between the conduction and valence bands characterize each semiconductor (and the distribution and filling of the density of states against the lattice wave vector). Starting from the very same compound, however, and reducing the volume of the crystal, until reaching dimensions comparable to the Bohr radius (typical of the bulk material), an energetic shift of the bandgap corresponding to its expansion can be observed.[41] At the nanometer scale, the number of atoms that come into play is significantly lower than the bulk, thus actually breaking the translation symmetry and preventing the Bloch condition of periodical wave functions. In these nanometer-scale materials, pseudo bands will be formed by discrete levels of electronic energy, more similar to

bonding and antibonding orbitals.[42] In this regime the optical and electronic properties become size-dependent rather than composition-dependent as in the bulk. The situation can be described from a "bottom-up" point of view considering the linear combination of atomic orbitals in molecular orbitals and then the formation of clusters up to the construction of dense bands in bulk crystals. Conversely, however, looking at this situation from a "top-down" perspective, it is possible to use the known parameters of the bulk semiconductor such as the effective mass and the dielectric constant, to predict or in a certain way describe the phenomenon of quantum confinement. From the first observations of semiconductors confined in glassy matrices[43,44] and more detailed studies on colloidal systems[45,46] various theoretical analysis have been developed on the matter. The most widely used connects the effects of quantum confinement to the particle-in-a-box problem. The term confinement, in fact, refers to the restriction or limitation of the motion of the charge carriers that can be found in a semiconductor. Concretely, photo- or thermal excitation of the semiconductor promotes electrons from the valence band to the conduction band leaving a hole in the valence band. Electrons and holes in their lowest energetic state are electrostatically bound in the so-called electron-hole pair also known as exciton. In inorganic semiconductors, the coulombic interaction between electrons and holes is generally screened by a high dielectric constant while the reduced mass of this hydrogen-like system is typically small so that the electron-hole distance exceeds the size of a unit cell of the crystal lattice. These conditions define a Wannier-type exciton, characterized by a rather low binding energy, of the order of millielectron volts (meV).[46]

When the dimensions of the semiconductor nanocrystal reach those of the exciton, the charge carriers are affected by a spatial confinement which increases their energy. Moreover, regardless of the geometric confinement, the charges in a semiconductor can also be affected by an electrical confinement when they are surrounded by a material with a different dielectric constant.[47] The effects of this type of confinement can be found in the interactions between the charge carriers. The dielectric contrast can in fact modify the surface charge at the interface between the two materials by modifying the screening that acts on the coulombic potential between the charges. This type of effect is particularly evident in the 2D systems of the R-P type perovskites in which the inorganic layers are separated with organic material with a lower dielectric constant. In this case, the dielectric confinement increases the interaction force between the charges generated in the conduction and valence bands of the lead and of the halogen in the inorganic part with a consequent increase of the exciton binding energy.[48,49]

The widest used approach for describing the bandgap shift in relation to the shrinking of a semiconductor is the one presented for the first time by Brus and

adopted both in the case of the most common inorganic semiconductors and in the case of perovskite nanocrystals.[50,51] Considering the approximation of the effective mass (parabolic energy around the minimum/maximum of the conduction/valence bands) for the kinetic energy and an approximation of the effective medium for the potential screening by the dielectric, the following expression is obtained for the correction of the bulk semiconductor bandgap, under the effect of quantum confinement:

$$E_g^{NC} \approx E_g^{bulk} + \frac{h^2}{8\mu R^2} - \frac{1.786e^2}{4\pi\varepsilon_0\varepsilon_r R} \quad (2)$$

The dependence on the radius R of the excitonic energy of the nanoparticle Eg (NC) is derived by adding two terms to the bandgap energy of the bulk, Eg (bulk). The first represents the quantization of the energy of a spherical particle-in-a-box system with infinite potential on the walls. In this term h is the Planck constant, μ is the reduced mass of the exciton and a quadratic inverse dependence on the radius can be noted. The second term takes into consideration the electrostatic interaction between charges and is characterized by an 1/R dependence. In this term, e is the charge of the electron and ε_0 and ε_r the dielectric constants of the vacuum and of the bulk semiconductor respectively. The expression was completed with the addition of a further minor correction term, given by a spatial correlation effect, but significant only for materials with low dielectric constant and in fact has not been taken into consideration in the studies carried out so far on nanocrystalline perovskites.[52] For the record, the approximations implicit in Brus formalism may not be valid in the case of so-called strong quantum confinement, that is, for extremely small crystals. In these cases, for example, the potential at the band edges loses its parabolic shape. The nanocrystals may not take on a perfectly spherical shape chosen to simplify the mathematical treatment. The potential at the limits of confinement is not exactly infinite and tunneling leaks may occur and, more generally, the nanocrystals may be affected by the external potential. Finally, assuming a static dielectric constant, that of the bulk, may not be in agreement with the change of polarization in the strong confinement. The effects of quantum confinement on the behaviour of perovskites when they are reduced to nanometer sizes underlie the substantial differences between bulk materials and nanocrystals, to the point that they can be considered as a new class of materials.

1.1.2 ABX_3 perovskite nanocrystals

One of the most interesting properties that emerged since the first synthesis of perovskite nanocrystals is the high quantum yield of their photoluminescence. They practically reached 100% in no time.[53,54] But what make these materials so relevant

for optoelectronic applications is a set of characteristics that start with the tolerance to structural defects.[55] This concept refers to the fact that defects do not interfere with the recombination or extraction processes of the charge carriers and therefore do not cause non-radiative losses. This is because, energetically, defects are distributed near the conduction and valence bands or in resonance with them (shallow traps) and not inside the bandgap (deep traps).[56,57] This particular electronic structure is attributed both to the distinctly ionic character of the bonds of the perovskites, but above all to the antibonding character of the orbitals involved in the valence band.[58] Since the conduction band is typically antibonding-like, the defects generated by the halide or non-metallic cation vacancies, they fall into the continuous of conduction or valence band. From the point of view of nanocrystals, this tolerance also facilitates their fabrication since a strict surface passivation is not necessary as in the case of inorganic core-shell semiconductors. However, to obtain control over size and shape in the nanoscale, colloidal-type preparations are used. And in this case the possible desorption of ligands in the purification phases can entail, in addition to the aggregation of the nanocrystals, an increase in surface defects (vacancies or dangling bonds), as well as favoring their reaction with external agents.[56]

An additional attractive versatility has also been demonstrated in perovskite nanocrystals thanks to the compositional tuning of the bandgap..[59,60] The use of iodine, bromine and chlorine as halide anions enables the covering of the entire visible spectrum in absorption and emission,[61,62] while the cation mainly influences the structural stability even if its exchange can play a small role on the bandgap, being able to favor some distortion of the cubic structure.[63] The ease of nanocrystals synthesis, however, makes accessible a wide range of bandgap tuning which can vary according to the shape and size when approaching the values of the exciton radius.[64] This alternative can be particularly useful in order to employ the more stable compositions. Chloride perovskites, for example, seem to be more sensitive to defects and therefore less efficient in luminescence.[65] By confining the bromide-based perovskites it is possible to obtain emission shifted in the blue using this more stable material.[66] Obviously, the precise manipulation of the bandgap, i.e. the absorption of these materials, makes the perovskite nanocrystals very interesting for the design of photovoltaic tandem systems in the production of solar energy.[67] There are already several examples of solar cells based on perovskite nanocrystals, in particular with all-inorganic perovskites for which a stable cubic phase was demonstrated, at room temperature, unlike the bulk.[68,69] Nevertheless there is still a lot of room for an optimization, in particular regarding ligands engineering (or their removal) which basically act as insulators and prevent the transport of charges.[70] Other attempts concern the use of perovskite nanowires, for example, taking advantage of the preferential charge transport along the

unconfined dimension.[71] Finally, the possibility of integrating bulk solar cells with low-dimensional materials has also given positive results. The nanocrystals at the interface between the active material and the charge transporting layers can facilitate the bands alignment and improve the carrier mobility.[72,73] Furthermore, the confined structures can offer an enhancement of conversion efficiency due to the generation of multiple excitons.[74] Another particularly interesting feature for the technological aspect is exciton binding energy. The strength of the interaction between the electron-hole pair identifies a material capable of generating free charges or stable excitons under optical or electronic stress. Consequently, we can distinguish materials that are more suitable for generating a current or generating light. Bulk perovskites are normally characterized by low binding energy values, approximately around kT.[75] But in confined structures the coulombic attraction is stronger and the binding energy increases. Consequently, the exciton does not separate in free charge carrier and the photoluminescence process becomes more effective.[76] In fact, this feature is essential in devices for lighting and lasing applications. The possibility of working with materials prepared through liquid methods also allows to improve the morphological quality, another indispensable parameter in the architecture of a device, and to facilitate the integration into more complex photonic structures for a more precise manipulation of the optical response.[77] For all this wide spectrum of applications, numerous examples already exist in the literature. Inorganic nanocrystalline perovskites have been used in LEDs, due to the greater chemical stability, and in particular 2D layered materials in which it is easy to control the confinement by adjusting the bandgap with the number of organic interlayers.[78] Always considering the application in the field of lighting, perovskites nanocrystals immediately revealed a very intense and particularly narrow photoluminescence, compared to other semiconductors, with full width at half maximum (fwhm) below 100 meV.[79] This feature is translated as an improvement in color purity for display technology. Low dimensional perovskite have found space, in fact, as materials for color conversion to obtain white light, thanks to their high color rendering index.[61,80,81]

1.2 TEMPLATED PEROVSKITE NANOCRYSTALS

Starting from the renewed interest for perovskites in photovoltaics, the attempt to apply colloidal synthesis for the fabrication of nanocrystals is relatively recent (2014/2015).[61,82] Based on the methods already widespread for the colloidal preparation of classic inorganic semiconductors such as compounds II-VI and III-V, one of the most used strategy for perovskites is the hot injection technique (HI). This approach generally consists of injecting the cationic precursor, organic or

inorganic, into a hot solution containing salts of the metal halide, together with the necessary ligands such as carboxylic acids or alkylamines dissolved in a solvent with a high boiling point.[61,83] The parameters to be kept under control in this type of system are the temperature, the precursor concentration, the ratio perovskite/ligand and the reaction time in order to control the dimensions, but also the shape of the nanocrystals. Although excellent results have already been obtained,[59] the HI technique also has some disadvantages. From a process point of view, high temperatures and specific control over the reaction conditions increase costs and limit large-scale use. As for the results, this method has been mostly used for all-inorganic perovskites, but it does not guarantee the same quality, in terms of optical properties, for organic-inorganic hybrid perovskites and more generally for more complex compositional variations.[84] The alternative commonly used, always within liquid synthetic methods, is the ligand assisted re-precipitation (LARP) technique which relies on a thermodynamic control, instead of a kinetic one. The strategy consists in fact in the "shifting" of the equilibrium state of a precursor solution in order to activate the reaction and start the crystallization. The change in the equilibrium condition can be induced by a change in temperature or by a change in concentration. The latter can occur by evaporating the solvent or by adding a solvent with different precursor ions solubility. Finally, in the presence of ligands, it is possible to have control over the precipitating crystals growth at the nanoscale. This method is certainly more versatile than HI and the milder operating conditions make it more affordable and more attractive for scale-up. However, the results are still not optimal in terms of quality and stability of the nanocrystals obtained.[84]

In addition to ligand-mediated methods, for the synthesis of perovskites in the form of nanocrystals, templated techniques have also been used in the last years. The results obtained in **this thesis** that will be described hereafter, are based on this type of perovskite nanocrystals preparation. The strategy differs from the colloidal one because of the nanometric control of the shape and size of the semiconductor crystals is made through a porous matrix where structuring agents are not needed , This alternative has proven to be quite attractive for distinct reasons. Perovskite nanocrystals grow directly within the pores of the scaffold and consequently purification processes are not necessary. Precisely for this reason, the typical self-aggregation phenomena due to detachment of ligands during the washing and deposition phases are also avoided.[56,85] The absence of organic chains around the confined perovskites improve the electrical connectivity. From the point of view of matrices, however, the advantage lies in the exploitation of the vast repertoire available by an extremely advanced research field, that of porous media. The use of porous materials, in fact, adds versatility to this synthesis method, in terms of chemical composition (organic or inorganic materials), morphology (powders or films), porosity (shape, dimensions, topology). All these features open up a new

perspective on the control and enhancement of the properties of nanocrystalline perovskites.

At the beginning of this thesis work, cases in which this synthesis strategy had been applied to the lead halide-based perovskites had not yet been reported in the literature. The research and development of an alternative to the colloidal systems, then more common, is one of the cardinal motivations of this research project, obviously together with the optimization and study, more generally, of these materials, however relatively younger in this research field, compared to the bulk counterparts on which the scientific community, in the wake of thin film technology, was more focused.

1.1.3 Porous materials

As already mentioned, the interest raised around the properties of perovskite nanocrystals is combined with the versatility of the porous materials used to guide their synthesis and manipulate their electro-optical response. Therefore, to complete the introductory context of this work, it is also necessary to shed light on the type of porous materials that can be employed and on the chemical and physical characteristics that come into play once the host-guest link has been established. Actually, the first examples of perovskites integration in porous systems can already be observed in the mesostructured solar cells in which the perovskites turned from being considered simple absorber dyes, deposited on top of a porous TiO_2 scaffold, to being the elements capable of generate and transport the charges in insulating matrices (Al_2O_3 or ZrO_2).[86,87] In these cases, however, the scaffold had a non-regular porosity and the nanocrystalline form of the perovskites was not controlled, neither analysed. Then it is starting from 2016 that a more systematic study on porous materials as templating agents emerged from the literature.[88,89] Different kinds of materials can be used for this purpose and the general encapsulation of semiconductors, like micro-particles and mesostructured films prepared with supramolecular methods, inorganic layers synthesized through electrochemical etching or simpler mesoporous systems consisting of stratifications of nanoparticles[90–95] (see figure 1.2.1 from a to f).

Among these, the former represent the most sophisticated class of compounds from a structural and functional point of view. They are obtained from the supramolecular self-assembly of surfactant or even polymeric molecules in solutions containing inorganic species (metal oxides). The intermolecular links that stabilize the structuring agents and the electrostatic interactions with the inorganic precursors lead to the formation of micellar structures that shape the surrounding inorganic phase. Once the whole matrix is condensed, the organic part can be

removed with a heat treatment leaving space for the pores of the inorganic matrix. This technique can be applied for both the fabrication of particles and films, but its potential lies in the versatility in terms of chemical composition and the spatial configuration of the porous network.[96-98]

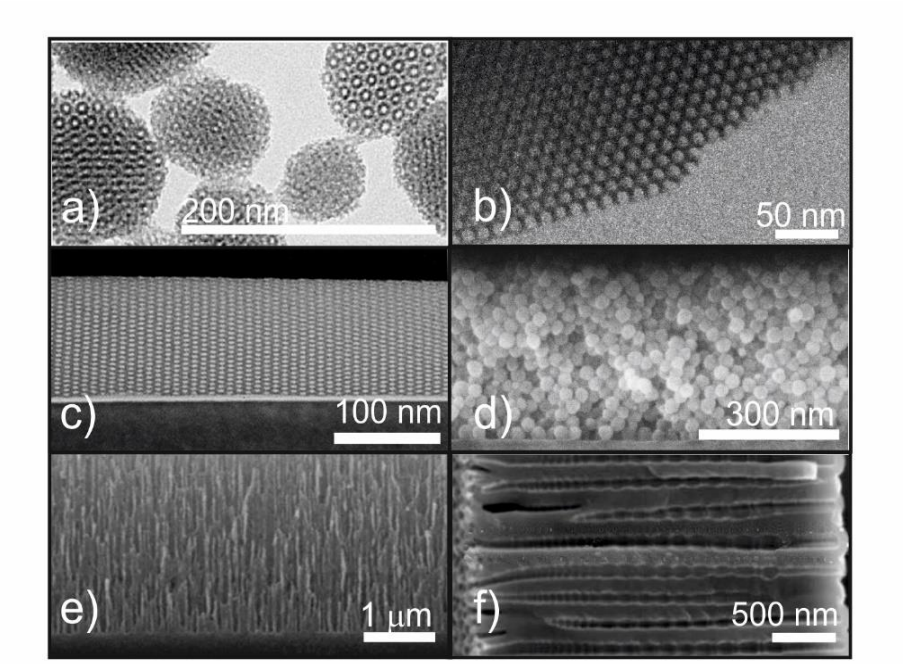

Figure 1.2.1 Examples of different porous matrices. a) HRTEM micrograph of a mesostructured silica-templated particles. b) HRTEM image of SBA-15-template particles (rods). c) HRTEM of a mesostructured film obtained from epitaxial growth of SiO2 after copolymer controlled self-assembly. d) SEM cross-section of thin film based on 30 nm size SiO2 nanoparticle dip coating. e) SEM cross-section of porous silicon prepared by electrochemical etching. f) SEM cross section of porous Al_2O_3 structured using cyclic anodization. Figures reproduced with permission from ref. 90, 91, 92, 93, 94, 95.

The use of this type of porous systems was a starting point for the development of this thesis project, as we will see later. In any case, the synthesis of semiconductors through spatial confinement within matrices of different nature is a strategy already applied to compounds of type II-VI and III-V, well before perovskites.[99-101] It is the behaviour of the latter, as already discussed, which makes this route interesting again.

1.1.4 Templated synthesis

Regarding the reaction conditions and regardless of the type of matrix that is used, two methods of synthesis are distinguished within porous structures. Figure 1.2.2a outlines the possible infiltration strategies for a porous matrix, two of which correspond to synthesis processes (route I and II). The third route shown simply indicates the possibility of encapsulating pre-formed nanocrystals ex-situ, in order to combine the properties of the semiconductor with the features and benefits of the scaffold. However, in this last case, perovskite particle size and its optical and functional properties are not related with the scaffold in which they are introduced. Route I is a two-step process. First a solution of metal halide salt (PbX) is infiltrated into the matrix which then is exposed by dipping into a solution containing the second cation (MA^+). Route II, on the other hand, consists in impregnating the matrix with a solution containing the perovskite precursors. In both cases, the contact between the precursors, inside the pores, will give rise to the nucleation of perovskites which crystallize following the evaporation of the solvent. The growth of perovskites will therefore be delimited by the size of the pores. In the development of this type of synthesis, various parameters intervene concerning the porous material on the one hand and the reaction dynamics on the other (see figure 1.2.2b and c). From the matrix point, it is necessary to take into consideration the accessible pore volume, the pore size, the tortuosity of the pore network and the functionality on the walls. The latter, in fact, will serve as anchor points where nucleation will start, but the interconnection between the pores is fundamental for the diffusion of precursors, while not only the size but also the geometry of the pores can influence those of the nanocrystals thus synthesized. The pores can be seen as nanoreactors that promote the synthesis. In general, a more easily accessible volume is obviously important for obtaining a homogeneous dispersion of the perovskite material within the matrix, especially in the case of Route III. In this regard, however, one must also be careful of the concentration of the solution to be infiltrated, containing precursors species or pre-formed crystals. Too concentrated solutions can hinder the entrance of material into the deeper pores, but on the other hand, too dilute solution would imply lack of active material inside the scaffold and therefore a weakening of the performance. But the diffusion of the species within the pore network also depends on the wettability of the matrix, or on the compatibility with the aprotic polar solvents normally used to dissolve the perovskite precursors (DMF, DMSO, GBL, etc.).

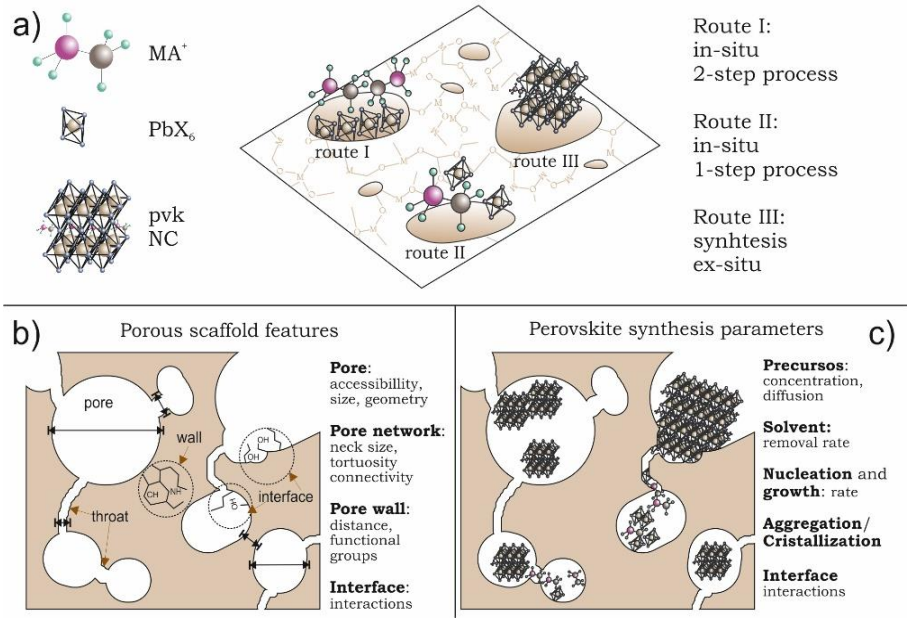

Figure 1.2.2 a) Representative illustration of different approaches for the templated synthesis ABX_3 perovskites in porous materials; Different parameters regarding porous matrices b) and synthesis dynamic c) to be considered in the templated method.

In this sense, considering the compounds most used for the preparation of porous matrices, that are SiO_2 and TiO_2, and their unwillingness to interact at the interface with the aforementioned solvents, capillary phenomena can also help impregnation. Of course, there is a limitation on the pore diameter, below which mass transport is difficult due to an increase in solvent viscosity. A solution to this type of problem can be found by using deposition techniques such as spin coating which are able to push the material thanks to the centrifugal force. Vice versa, the deposition must also be checked in order to avoid that the material comes out of the porous network and form macro-crystals at the surface or even capping layers that would otherwise have to be eliminated by adding washing cycles (that can also damage the entire process). Ultimately, temperature, an external factor, takes part in the synthesis mechanism influencing the growth dynamics, as it favors the evaporation of the solvent and therefore the perovskite crystallization.

1.3 PEROVSKITE@MATRIX COMPOSITES

In 2016, first works demonstrated the synthesis of perovskites nanocrystals confined in mesoporous SiO_2 particles with well-defined pore geometries i.e. cavities of different sizes and shape that dictate the size of the encapsulated perovskite (Figure 1.3a). In one of the reports, this method proved to be adaptable to different chemical compositions in terms of cation (MA, FA, Cs) and halide anions (Br, I) and allows authors to obtain a displacement of the photo-emission peak up to 50 nm and 100nm with respect to the bulk.[89] In another work, it has been used a similar host material, in order to obtain mixed halides perovskite nanocrystals in the range of 3.3 nm and 7.1nm (which are actually the pores sizes of the SiO_2 templates) with high control over the size and so the bandgap.[88] Some of these authors also made use a SiO_2 system (KIT-6) characterized by complex internal gyroidal geometry where it is possible to tune pore size (up to 5 nm) and the pores distance, by controlling the temperature of the hydrothermal treatment.[102]

The examples described so far, although they allow a controlled tuning of the dimensions and bandgap of perovskites and also offer an improvement in their stability, suffer from a common problem. The granular nature prevents its possible use in an actual device for which materials in laminar form with good optical quality (without light scattering effects) are required.

In this context and in parallel to these results, the effort carried out in this thesis is part of developing an alternative to colloidal synthesis, using the template technique, which was also a technologically valid solution. In particular, later we have demonstrated the usefulness of manufacturing porous matrices in the form of thin films with high optical quality so as not to alter the absorption or emission of the perovskites inside except in the extent of the quantum confinement dictated by the pore size; so much more useful as component of and optoelectronic device. This first work on ABX_3 nanocrystal synthesis in optical quality mesostructured films prepared by means of the Evaporation Induces Self Assembly process was carried out for both the case of TiO_2 and SiO_2 matrices[103] (figure 1.3b). With this technique, on varying the structuring agent it is possible to change the pore diameter, in this case from 3 to 8 nm. A strong confinement effect was attained for the case of $MAPbI_3$, with a blue shift of 0.34 eV in the photoemission. In the same period of the first silica powders based templated system previously mentioned we have optimized the parameters for the synthesis of perovskites, although the EISA technique, for the preparation of porous films, requires long matrix stabilization times and does not allow thicknesses greater than 300/400nm to be reached. Even the superposition of several layers is not easy and in any case interrupts the orderly structure of the porous skeleton.

Exploring other opportunities related to the use of scaffolds compatible with the fabrication of a device, Demchyshyn et al. proposed the synthesis of perovskites within silicon and aluminum oxide nanoporous films[104] (figure 1.3c). Both matrices, prepared by an electrochemical process, allow obtaining a film composed of aluminum oxide nanotubes of 8 nm diameter or a silicon film formed by a network of nanopores with controllable size in the range of 2 to 10 nm.

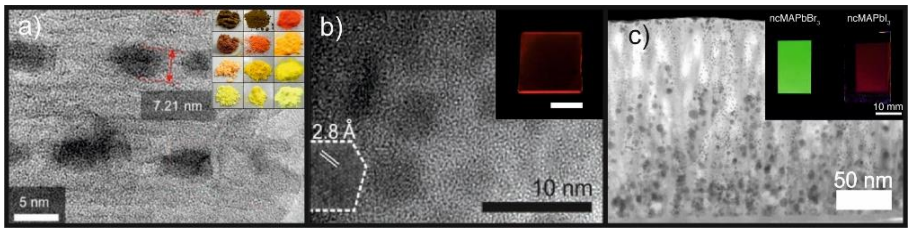

Figure 1.3 a) HRTEM image of porous SiO_2 (dark spots are $MAPbBr_3$ perovskite nanocrystals). Inset: Photographs of SiO_2@perovskite samples with different nanocrystals size and composition. b) HRTEM of TiO_2 templated mesoporous film containing $MAPbI_3$, crystallographic planes are indicated in the image. Inset: Photo of the same sample under UV-light. c) Bright Field-STEM image of nanoporous Al_2O_3 including $CsPbX_3$ nanocrystals. Inset: photographs of perovskite@AAO samples exposed to ultraviolet illumination. Reproduced with permission of ref 88, 103, 104.

Interesting also is the work on $MAPbI_3$ confinement in a mesoporous matrix consisting of a film of silicon nanotubes, reporting a blue shift up to 741 nm (from the 779 nm of the PL for the case of their perovskite bulk film reference).[105] With a one-step preparation, the solution containing the perovskite precursors infiltrates the scaffold where the nanotubes were grown through silver-assisted chemical etching. The nanocrystals are formed inside the pores along the silicon walls and it has been observed how the nanocrystals size can be controlled according to two factors: the porosity of silicon and the concentration of the precursor solution. However, the results show a fairly large dispersion in terms of nanocrystal dimensions probably also due to defects in the host mesoporous structure. Similar infiltration procedure (Route I) have been followed within thin films of F-doped TiO_2 particles with specific control over the porosity obtained through acid etching.[106]

The application of the two-step process for the synthesis in confined structures was used by Chen et al.[107] for the case of mixed-halide perovskite, $MAPbIX_2$, through a porous Metal Oxide Framework (MOF) film (HKUST-1: Copper benzene-1,3,5-tricarboxylate) first immersing the porous scaffold in a solution of PbI_2 and then dipping the MOF matrix containing PbI_2 into a solution of methylammonium halide.

Finally, much simpler porous structures consisting of a superimposition of nanoparticles with a more or less regular shape can also act as matrices in which

infiltrate perovskites precursors and synthesize nanocrystals. There are numerous deposition techniques which allow precise control over the optical quality of the nanoparticle films and their thickness.[108,109] The work of this thesis pioneer the inclusion of ABX_3 perovskite with these type of porous systems. For this reason the matrix preparation and characterization will be examined in chapter 2 of this thesis.

In general, the use of porous matrices for the synthesis of perovskite quantum dots allowed to obtain, in many cases, a considerable shift in photoluminescence towards shorter wavelengths, typical of a quantum confinement regime i.e. crystals with sizes near the exciton Bohr radius[88,89,102,103,110,111] (see figure 1.3d). So, in order to describe the quantum confinement of lead halide based perovskites nanocrystals obtained from these composite systems, most of the authors used the Brus model presented in section 1.1.1. Figure 1.3e shows data related to the size (matrix pore or nanocrystal) dependence of the energy shift (with respect to the bulk) reported in several recent publications on the case of $MAPbI_3$ and $MAPbBr_3$ perovskites, in comparison with the behavior expected by the Brus approximation.

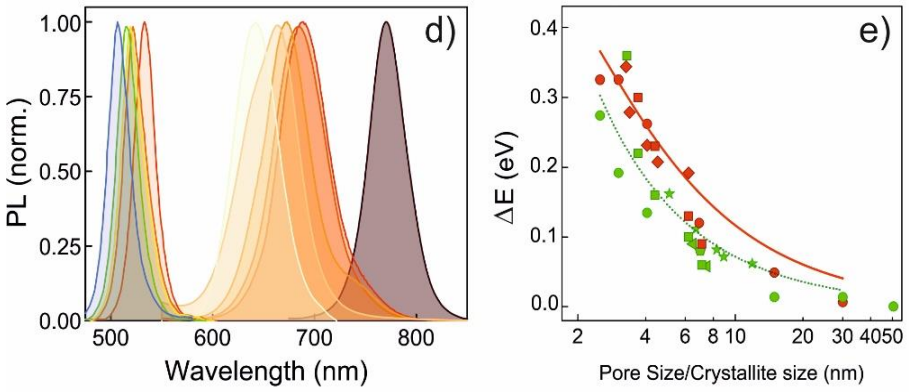

Figure 1.3 d) Emission spectra (480 nm < λ < 550 nm) of nc-$MAPbBr_3$, synthesized within a film of packed SiO_2 particles with sizes (in nm) of 11.9 (red line), 8.9 (orange line), 8.3 (yellow line), 6.7 (green line), and 5.1 (blue line); emission spectra of nc-$MAPbI_3$ (600 nm < λ < 820 nm) synthesized within mesostructured TiO_2 films with sizes of (in nm): 6.2 (dark red line), 4.5 (red line), 4.1 (dark orange line), 3.4 (orange line), and 3.3 (light grey line). Data extracted from refs. 88 and 103. The emission spectrum of a bulk film is also plotted for comparison (brown line); e) Bandgap shift, $\Delta E_g = E_{g,nc} - E_{g,bulk}$, estimated from the position of the photoemission spectra maxima, as a function of the experimentally determined crystallite size. Data adapted from ref. 89 (green and red circles), ref. 102 (green stars), ref. 88 (green and red square), ref. 103 (red diamond), ref. 110 (green pentagon) and ref. 111 (green triangles). Solid lines are the expected trends after Brus equation (2) for both $MAPbBr_3$ and $MAPbI_3$ perovskite nanocrystals (green and red lines, respectively).

1.1.5 Composites properties

The effects of the integration of perovskite nanocrystals in porous matrices are not limited to the control of the dimensions and to the tuning of the bandgap with respect to the bulk semiconductor. The matrix can also act on the optoelectronic properties of perovskites through direct interactions, as may happen at the interface between the pore walls and the nanocrystals surface, or in a more indirect way. The matrices, for example, can act as a screen or better as a filter, towards the external environment. The tortuosity of the pore network can hinder the penetration of gaseous degrading agents, especially oxygen and water vapour increasing the photo-stability of perovskites. As illustrated in the figure 1.3.1a, this beneficial effect has been demonstrated precisely in the case where a silicon-based matrix was used just to encapsulate ex-situ pre-formed $CsPbBr_3$ nanocrystals in order to increase stability and to limit their anionic segregation.[112] These composite systems have shown a better stability over temperature and illumination stress. After 96h the perovskites maintained 80% of the emission intensity, while non-encapsulated crystals lost the 60%. Likewise, integrating these systems with polymeric matrices can increase the resistance to water and oxygen, as demonstrated in some cases,[113-115] preserving the optical properties of the nanocrystals whether they are synthesized within the matrix itself or are colloidal systems subsequently encapsulated.

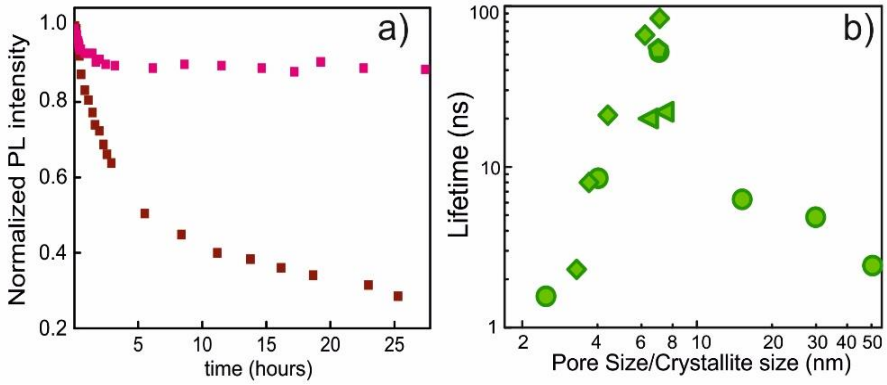

Figure 1.3.1 a) Evolution of the normalized photoluminescence during 24h of illumination of a bulk film (brown squares) and encapsulated nanocrystals (pink squares). Data adapted from ref. 104; b) Lifetime measured for different perovskite nanocrystals templated in porous systems confined perovskite as function of pore size of the host structure or the crystallite size. Data adapted from ref. 89 (green circles), ref. 88 (green diamond), ref. 110 (green pentagon), and ref. 111 (green triangles).

The porous matrix as a confined space for the synthesis of perovskites in the quantum regime can also cover other roles related to the surface chemistry of the ABX_3 nanocrystals with important consequences on their optical properties. In

colloidal ABX_3 perovskites systems, the photoluminescence quantum yield (PLQY) reaches values near 100%. However, as we mentioned before, the deposition of the colloids as thin film reduces dramatically these high PLQY values.[116] In the case of nano-templated synthesized perovskites, the reported PLQY values oscillate in a large range of values (see tables 1.3.1a and b). Interesting consequences concern also the photoemission dynamics. The reduction of the particle size implies a shortening in the lifetime of their excited states when compared with homogeneous ABX_3 bulk films, as it has been demonstrated in colloidal nanocrystalline semiconductors.[117] In general, the aforementioned behaviour was observed also in the case of templated nanocrystals.[89,103] However, it is possible that the degree of "filling" of a pore and of course the nature of the matrix may lead to the instauration of an interaction between perovskites and chemical species exposed to the pore walls. The latter, therefore, can act as a passivating agent of the traps which, as the size decreases, increases in density in the perovskite nanocrystals surface. The effect is particularly evident in cases where polymer matrices are used, in which the lifetimes are comparable to those of the bulk material.[115] In this regard, Durrant and co-workers suggested a passivation effect of functional groups present on the host walls towards surface defects in perovskite nanocrystals depending on their acidity. Particularly, aluminate groups present in mesoporous alumina will harness exposed Pb ion defects in $MAPbBr_3$ nanocrystals synthesized within the pores, while this effect may not occur when silanol groups are present.[118]

In addition, different authors have reported that nanocrystals synthesized within mesoporous matrices may present either a lower density or a better harnessing of defects.[89,110] Figure 1.3.1b contains a collection of lifetime reported for most of the systems described above versus nanocrystal size. It is interesting to observe a peak around the value of 7 nm.

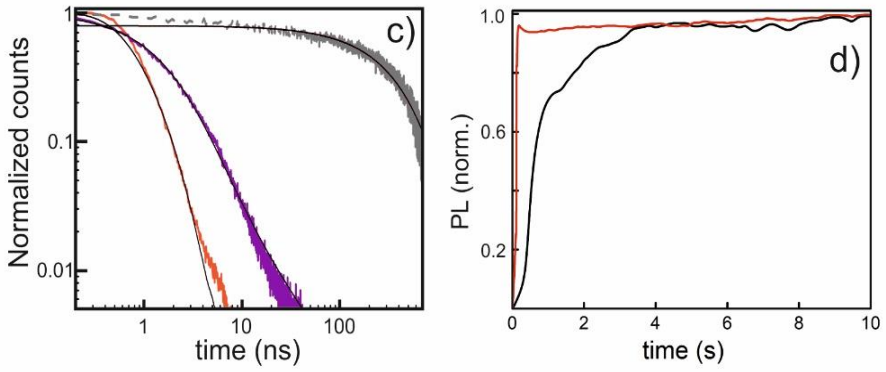

Figure 1.3.1 c) Normalized photoluminescence decay obtained from $MAPbI_3$ nanocrystals in SiO_2 (violet line) and TiO_2 (orange line) matrices. Black line represents the data obtained for a bulk film. d) Time evolution of the normalized photoluminescence (photo-activation) for nanocrystal templated system (red line) and bulk system (black line). Reproduced with permission from ref.103.

Host	Guest	pore size (nm)	λ_{max} (nm)	λ_{bulk} (nm)	QY%	ref.
MSU-H 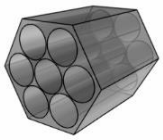	$MAPbCl_xBr_y$	7	510	/	20	89
	$FAPbCl_xBr_y$		495	/	15	
	$CsPbCl_xBr_y$		/	/	/	
	$MAPbBr_3$		540	/	22	
	$FAPbBr_3$		520	/	36	
	$CsPbBr_3$		520	/	48	
	$MAPbBr_{0.25}I_{0.75}$		660	/	2	
	$FAPbBr_{0.25}I_{0.75}$		640	/	8	
	$CsPbBr_{0.25}I_{0.75}$		630	/	15	
	$MAPbI_3$		700	/	8	
	$FAPbI_3$		705	/	15	
	$CsPbI_3$		665	/	4	
MCM-48 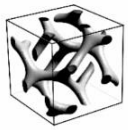	$MAPbCl_xBr_y$	3	475	/	25	
	$FAPbCl_xBr_y$		475	/	10	
	$MAPbBr_3$		470	/	8	
	$FAPbBr_3$		490	/	16	
	$MAPbBr_{0.25}I_{0.75}$		600	/	10	
	$FAPbBr_{0.25}I_{0.75}$		600	/	8	
	$MAPbI_3$		625	/	2	
	$FAPbI_3$		630	/	5	
meso-SiO_2 (MCM-41)  (SBA 15) 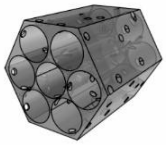	$MAPbBr_3$	7.1	525	539	2.9	88
		6.2	517		3.7	
		4.4	504		5.5	
		3.7	492		2.2	
		3.3	466		1.2	
	$MAPbBr_2I_1$	7.1	571	713	/	
		6.2	569		/	
		4.4	551		/	
		3.7	523		/	
		3.3	510		/	
	$MAPbBr_1I_2$	7.1	642	729	/	
		6.2	636		/	
		4.4	620		/	
		3.7	590		/	
		3.3	559		/	
	$MAPbI_3$	7.1	721	761	/	
		6.2	705		/	
		4.4	667		/	
		3.7	642		/	
		3.3	585		/	
KIT-6 	$MAPbBr_3$	11.9	544	559	/	102
		8.9	541		/	
		8.3	539		/	
		6.7	532		/	
		5.1	521		/	
	$MAPbI_3$	11.9	765	792	/	
		8.9	752		/	
		8.3	747		/	
		6.7	734		/	
		5.1	708		/	
SBA 15	$CsPbBr_3$	/	507	525	4.1	110

Table1.3.1a Powders: type of host (matrix) guest (ABX3 perovskite), pore size, spectral position of the maximum emission, spectral position of bulk, and photoluminescence quantum yield for powder fabrication.

Even though such a non-linear behaviour has been reported for other semiconductor, the understanding of this feature will require a deeper analysis of

the dependence of the density of deep and shallow traps since the relative energy of valence and conduction band is also changing.

Host		guest	nanocrystal size (nm)	λ_{max} (nm)	λ_{bulk} (nm)	QY%	ref.
	HKUST-1	$MAPbI_2Cl_1$	/	536	/	/	107
		$MAPbI_2Br_1$	/	655	735	/	
		$MAPbI_3$	/	715	800	/	
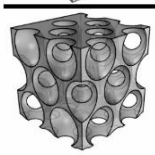	TiO_2/F127-PPG	$MAPbI_3$	6.2	692	775	1	103
	TiO_2/P123		4.52	686		1	
	TiO_2/F127		4.06	677		1	
	TiO_2/CTAB		3.4	660		1	
	TiO_2/Brij58		3.28	638		1	
	TiO_2/F127	$MAPbBr_3$	4.06	520	535	1	
	SiO_2/CTAB	$MAPbI_3$	3.4	660	775	1	
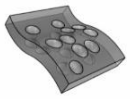	Au-PDMS (*pore size)	$MAPbCl_3$	/	424	/	/	98
		$MAPbBr_3$	9.8*	532	/	10	
			7.8*	528	/	8	
			5.6*	524	/	2	
		$MAPbI_3$	/	738	/	/	
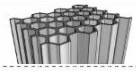	anodized Al_2O_3	$MAPbI_3$	/	729	791	25	104
		$MAPbBr_3$	/	521	535	60	
		$CsPbBr_3$	/	519	535	90	
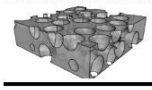	electrochemically etched Si	$MAPbI_3$	/	640	791	/	
		$MAPbBr_3$	/	485	535	/	
		$CsPbBr_3$	/	479	529	/	
		$MAPbCl_3$	/	/	/	/	
	SiO_2 nanowires	$MAPbI_3$	16	741	779	9.82	105
			5	715		/	
			/	710		/	
			/	692		/	
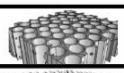	SiO_2 /P123	$CsPbBr_3$	bimodal	487-510	525	31.8	110
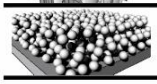	meso-ZrO_2 nanoparticles	$MAPbI_3$	/	775	>800	/	122
		$MAPbBr_3$	/	530	>550	/	
	F-doped TiO_2 nanoflowers	$MAPbI_3$	1.7	716	764	25	106
			3.3	721		13	
			5.1	737		11	
		$MAPbBr_3$	/	526	536	57	
			/	527		13	
			/	528		11	

Table1.3.1b Films: type of host (matrix) guest (ABX3 perovskite), perovskite nanocrystals size, spectral position of the maximum emission, spectral position of bulk, and photoluminescence quantum yield for thin films fabrication. The symbol * indicates pore size as no actual nanocrystal size was reported.

And for what concern the energy alignment between host and guest and the influence on decay dynamics, the porous matrices can offer a more or less favourable environment to the transfer of the charges generated by the photoexcitation. The analysis of the lifetime of the $MAPbI_3$ nanocrystals confined in two matrices based on TiO_2 and SiO_2 templated with the same pore size revealed a decay of 2 orders of magnitude faster in the titanium-based scaffold as illustrated in figure 1.3.1c. The difference is directly related to the opening of a non-radiative

deactivation channel that injects charge carriers from perovskite to the conduction band of TiO_2. This is even more evident considering the absence of steric bulky organic ligands that leads, in fact, to the possibility of charge transfer making this type of matrices more appealing for optoelectronics, although the majority of mesoporous systems in use are based on SiO_2 as we shown before. Embed nanocrystallites also demonstrated a fast photo-activation[103] (see figure 1.3.1d). A possible explanation of this effect is related to the small size of the confined perovskite crystals. So as lattice defects (surface, interstitials, vacancies) normally constitute recombination channels that quench the PL, the photo-induced ion migration that occurs in these perovskite compounds can promote the deactivation/passivation of these non-radiative paths. In consequence, this annihilation effect is much faster leading, consequently, to a quick stabilization of the PL.[119,120] It is important to mention that this proposed mechanism is different from what is postulated in colloidal perovskites where ligands act as a brake on the photo-induced ion migration.[70]

Finally, tables 1 and 2 provide a summary of the main structural features of different matrices employed to attain ABX_3 nanocrystals within their porous networks, along with the characteristic photoemission peak attained in this case.

1.1.6 Composites applications

In addition to the fundamental study, in particular on the optical response of the perovskite@matrix composite systems, some of the configurations analysed have already found a technological application. As already mentioned, the materials in the form of thin films can be more easily integrated into the multilayers architecture of a solar cell or an LED. Naturally, the insulating or conducting behaviour of the matrix and the efficiency of the charge transport between the nanocrystals and the scaffold can promote extraction or injection.[121] Titanium oxide, for example, as we have already seen, can be an excellent partner, in whose conduction band, perovskites can inject photo-generated electrons. In a work by Lee et al, (see figure 1.3.2a) in fact, the functioning of a dye sensitized solar cell based on $MAPbI_3$ nanocrystals synthesized directly in the mesoporous TiO_2 matrix is demonstrated.[122] It is interesting to note here, however, that if a high density of perovskite nanocrystals is reached through the entire porous structure so that a sufficiently tight packaging can be obtained, the percolation of the charges through the perovskites could be favoured. As regards the emission, on the other hand, $MAPbI_3$ and $CsPbBr_3$ nanocrystals synthesized in the columnar pores of an Al_2O_3 matrix have been efficiently used as active material in a light emitting diode[104] as shown in the figure 1.3.2b. The results obtained so far revealed that the use of

composite materials is promising although there is space for further improvement. In view of a possible integration in optoelectronic devices, the effort could be focused on the search for non-insulating porous materials. In fact, most of the cases concern porous silica-based structures which, thanks to the distinctive bending quality of the O-Si-O bond, allowed a preponderant advancement on the handling of these materials. From the point of view of electronic efficiency, however, the use of insulating inorganic matrices, as well as polymeric compounds, constitutes a barrier to the path of the charges. If in colloidal systems, the use of short chain ligands is one of the solutions for a better electrical connection across the nanocrystals system,[70,123] in the case of inorganic matrices a solution could be to reduce the thickness of the pore walls. In general, to improve the optoelectronic response, the research of the matrix-perovskite composite system can be made more effective by reducing the amount of inorganic material over the active semiconductor in order to decrease the electrical resistance. The risk, in this case, is that of losing the control over the perovskite confinement and consequently on the bandgap tuning.

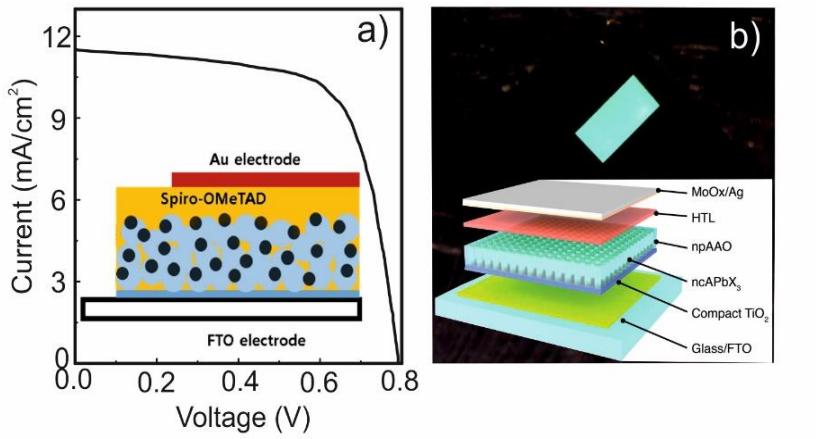

Figure 1.3.2 a) J–V curve from the DSSC based on $MAPbI_3$ nanocrystals embedded in a mesoporous TiO_2 layer (inset: architecture of the DSSC). b) Image obtained from an operating $CsPbBr_3$ LED based on nanocrystals embedded in Al_2O_3 porous system (inset: architecture of the LED). Reproduced with permission from refs 122 and 104.

In addition to the possible applications of perovskites grown in porous films, in the last chapter of this thesis, some technological solutions will be examined, both for the emission and for the absorption of light, based on perovskite nanocrystals synthesized in silicon oxide nanoparticles matrices.

1.4 MOTIVATION AND PURPOSE

What can be deduced from the current research on perovskite nanocrystals encapsulated in porous matrices might be described with the term "potential". The concept implies the existence of quality and possibilities that have not yet manifested or been realized on the basis of very promising results. The examples presented so far of how it is possible to integrate perovskites into porous materials and the effects on the properties of semiconductors, starting from the control over the dimensions to the alteration of electrical and optical properties, have also demonstrated advantages compared to other non-templated systems. Above all in view of future optoelectronic applications, improvements in stability have been observed in terms of inhibition of environmental degrading agents, emission stability and also structural stability (no self-aggregation phenomena). These systems have also added an interesting versatility and adaptability of the nanocrystalline perovskites. The results are still a proof of concept, but they certainly encourage us to continue research along this route.

The project of this thesis was born precisely in this area. With the general aim of investigating the properties offered by the confinement of perovskites in porous matrices. The results collected in this PhD thesis and the progresses around the specific field of perovskite nanocrystals templated synthesis evolved contemporary. As we seen, the state of the art reviewed in this introduction includes more recent results, but it should be considered that at the beginning of this project, in 2016, this research field was still unexplored. Thus the development of this thesis has progressed hand in hand with the discoveries of the scientific community concerning encapsulated perovskite systems, but also with respect to nanocrystals in general, characterized by a behaviour not fully explored. My work on confined perovskites began, more precisely, with the study of systems composed of mesostructured films of SiO_2 and TiO_2, already mentioned in this introduction. The pioneering result on the use of matrices in the laminar form and the singular and unpublished response of the perovskites in terms of optical properties pushed the research work carried out during the thesis.

The objective of the project was directed towards the optimization of the synthesis of organic-inorganic perovskites in matrices in the form of thin films in order to probe, also, the possible integration in devices for the absorption and / or emission of light. On the other hand, one of the most underestimated benefits, in the use of such composite systems, is the opportunity to carry out a more fundamental study on perovskites nanocrystals, otherwise much more complicated if not impossible to achieve in colloidal systems. Examples are the analysis of the growth dynamics, the study of optical constants, the analysis at low temperature and high pressure

(lattice dynamics). These insights into the behaviour of encapsulated perovskites are both part of the optimization process, but are also part of the purpose of understanding the nature of these semiconductors under the effect of confinement and the differences with bulk materials. The results obtained, concerning the chemical-physical characterization, have in fact allowed to shed light on some properties not yet observed for perovskite nanocrystals, as will be discussed later.

1.5 OVERVIEW OF THE THESIS

In the next 5 chapters the results related to the different studies that form part of the thesis entitled "ABX_3 perovskite nanocrystals in porous matrices" will be presented in the following order after this General Introduction chapter.

- The second chapter describes the synthesis method developed for the fabrication of perovskite nanocrystals in porous laminar matrices made up of silicon oxide nanoparticle layers and the structural characterization carried out on both matrices and perovskites. The analysis is enriched by a study of the growth mechanism of perovskites within the porous matrix.
- The third chapter presents the results concerning the analysis of the optical properties of Pvk-NCs@SiO_2-NPs composite materials: photoluminescence, quantum yield and lifetime. Within the emission properties, the results related to colour conversion property are also illustrated. To complete the linear optics characterization, this chapter also reports the extrapolation of the optical constants (refractive index and extinction coefficient) of the confined perovskite nanocrystals.
- In the fourth chapter we discuss the lattice dynamics influence on perovskites within the layer of silica nanoparticles. The analysis of the behaviour of these materials at low temperatures and when subjected to high pressure allows to obtain information about the influence of the crystalline network of the semiconductors on their electronic properties.
- The fifth chapter concern to the nonlinear properties of perovskite nanocrystals. The results of the third order optical response of the $FaPbBr_3$@ SiO_2 films are reported, in particular regarding the generation of third harmonics.
- In the sixth and final chapter the results related to the integration of the composite matrices in the architecture of actual devices for photovoltaics (solar cells) and lighting (LED) are presented together with the analysis of performances.

1.6 BIBLIOGRAPHY

1BHALLA, A. S.; GUO, RUYAN; ROY, RUSTUM. THE PEROVSKITE STRUCTURE—A REVIEW OF ITS ROLE IN CERAMIC SCIENCE AND TECHNOLOGY. MATERIALS RESEARCH INNOVATIONS, 2000, 4.1: 3-26.

2WELLS, HORACE LEMUEL. ÜBER DIE CÄSIUM-UND KALIUM-BLEIHALOGENIDE. ZEITSCHRIFT FÜR ANORGANISCHE CHEMIE, 1893, 3.1: 195-210.

3SCHLOM, DARRELL G., ET AL. A THIN FILM APPROACH TO ENGINEERING FUNCTIONALITY INTO OXIDES. JOURNAL OF THE AMERICAN CERAMIC SOCIETY, 2008, 91.8: 2429-2454.

4SNAITH, HENRY J. PEROVSKITES: THE EMERGENCE OF A NEW ERA FOR LOW-COST, HIGH-EFFICIENCY SOLAR CELLS. THE JOURNAL OF PHYSICAL CHEMISTRY LETTERS, 2013, 4.21: 3623-3630.

5MITZI, DAVID B. SYNTHESIS, STRUCTURE, AND PROPERTIES OF ORGANIC-INORGANIC PEROVSKITES AND RELATED MATERIALS. PROGRESS IN INORGANIC CHEMISTRY, 1999, 1-121.

6 GOLDSCHMIDT, VICTOR MORITZ. DIE GESETZE DER KRYSTALLOCHEMIE. NATURWISSENSCHAFTEN, 1926, 14.21: 477-485.

7 LI, ZHEN, ET AL. STABILIZING PEROVSKITE STRUCTURES BY TUNING TOLERANCE FACTOR: FORMATION OF FORMAMIDINIUM AND CESIUM LEAD IODIDE SOLID-STATE ALLOYS. CHEMISTRY OF MATERIALS, 2016, 28.1: 284-292.

8 SALIBA, MICHAEL, ET AL. INCORPORATION OF RUBIDIUM CATIONS INTO PEROVSKITE SOLAR CELLS IMPROVES PHOTOVOLTAIC PERFORMANCE. SCIENCE, 2016, 354.6309: 206-209.

9 ZHANG, CAI-XIN, ET AL. REVIEWING AND UNDERSTANDING THE STABILITY MECHANISM OF HALIDE PEROVSKITE SOLAR CELLS. INFOMAT.

10 KE, WEIJUN; KANATZIDIS, MERCOURI G. PROSPECTS FOR LOW-TOXICITY LEAD-FREE PEROVSKITE SOLAR CELLS. NATURE COMMUNICATIONS, 2019, 10.1: 965.

11 CHATTERJEE, SOUMYO; PAL, AMLAN J. INFLUENCE OF METAL SUBSTITUTION ON HYBRID HALIDE PEROVSKITES: TOWARDS LEAD-FREE PEROVSKITE SOLAR CELLS. JOURNAL OF MATERIALS CHEMISTRY A, 2018, 6.9: 3793-3823.

12 NOH, JUN HONG, ET AL. CHEMICAL MANAGEMENT FOR COLORFUL, EFFICIENT, AND STABLE INORGANIC–ORGANIC HYBRID NANOSTRUCTURED SOLAR CELLS. NANO LETTERS, 2013, 13.4: 1764-1769.

13 EPERON, GILES E., ET AL. FORMAMIDINIUM LEAD TRIHALIDE: A BROADLY TUNABLE PEROVSKITE FOR EFFICIENT PLANAR HETEROJUNCTION SOLAR CELLS. ENERGY & ENVIRONMENTAL SCIENCE, 2014, 7.3: 982-988.

14SHARMA, INDU BHUSHAN; SINGH, DEVINDER. SOLID STATE CHEMISTRY OF RUDDLESDEN-POPPER TYPE COMPLEX OXIDES. BULLETIN OF MATERIALS SCIENCE, 1998, 21.5: 363-374.

15 GRANCINI, GIULIA; NAZEERUDDIN, MOHAMMAD KHAJA. DIMENSIONAL TAILORING OF HYBRID PEROVSKITES FOR PHOTOVOLTAICS. NATURE REVIEWS MATERIALS, 2019, 4.1: 4-22.

16 FRANKFURT SCHOOL-UNEP CENTRE/BNEF. 2019. GLOBAL TRENDS IN RENEWABLE ENERGY INVESTMENT 2019, HTTP://WWW.FS-UNEP-CENTRE.ORG (FRANKFURT AM MAIN)

17 EUROSTAT 17-06-2019: FINAL ENERGY CONSUMPTION IN THE RESIDENTIAL SECTOR BY TYPE OF END-USES FOR THE MAIN ENERGY PRODUCTS, EU-28, 2017.

18 VINING, CRONIN B. SEMICONDUCTORS ARE COOL. NATURE, 2001, 413.6856: 577-578.

19 LEE, EL-HANG; PARK, KYOUNGWAN. POTENTIAL APPLICATIONS OF NANOSCALE SEMICONDUCTOR QUANTUM DEVICES FOR INFORMATION AND TELECOMMUNICATIONS TECHNOLOGIES. MATERIALS SCIENCE AND ENGINEERING: B, 2000, 74.1-3: 1-6.

20TOUMAZOU, CHRIS; GEORGIOU, PANTELIS. BIO-INSPIRED SEMICONDUCTORS FOR EARLY DETECTION AND THERAPY. IN: IEEE ASIAN SOLID-STATE CIRCUITS CONFERENCE 2011. IEEE, 2011. P. 129-132.

21 SINGH, R., ET AL. SEMICONDUCTOR MANUFACTURING IN THE NANOTECHNOLOGY WORLD OF THE 21ST CENTURY. IN: 2006 25TH INTERNATIONAL CONFERENCE ON MICROELECTRONICS. IEEE, 2006. P. 2-8.

22 PEERCY, PAUL S. THE DRIVE TO MINIATURIZATION. NATURE, 2000, 406.6799: 1023-1026.

23 KOJIMA, AKIHIRO, ET AL. ORGANOMETAL HALIDE PEROVSKITES AS VISIBLE-LIGHT SENSITIZERS FOR PHOTOVOLTAIC CELLS. JOURNAL OF THE AMERICAN CHEMICAL SOCIETY, 2009, 131.17: 6050-6051.

24 CORREA-BAENA, JUAN-PABLO, ET AL. THE RAPID EVOLUTION OF HIGHLY EFFICIENT PEROVSKITE SOLAR CELLS. ENERGY & ENVIRONMENTAL SCIENCE, 2017, 10.3: 710-727.

25 HTTPS://WWW.NREL.GOV/PV/INSIGHTS/ASSETS/PDFS/CELL-PV-EFF-EMERGINGPV.20200406.PDF BEST RESEARCH-CELL EFFICIENCIES, EMERGING PV, JUNE 2019.

26 QUAN, LI NA, ET AL. PEROVSKITES FOR LIGHT EMISSION. ADVANCED MATERIALS, 2018, 30.45: 1801996.

27 SUM, TZE CHIEN; RIGHETTO, MARCELLO; LIM, SWEE SIEN. QUO VADIS, PEROVSKITE EMITTERS?. THE JOURNAL OF CHEMICAL PHYSICS, 2020, 152.13: 130901.

28 SENANAYAK, SATYAPRASAD P., ET AL. UNDERSTANDING CHARGE TRANSPORT IN LEAD IODIDE PEROVSKITE THIN-FILM FIELD-EFFECT TRANSISTORS. SCIENCE ADVANCES, 2017, 3.1: E1601935.

29 RAMASAMY, PARTHIBAN, ET AL. ALL-INORGANIC CESIUM LEAD HALIDE PEROVSKITE NANOCRYSTALS FOR PHOTODETECTOR APPLICATIONS. CHEMICAL COMMUNICATIONS, 2016, 52.10: 2067-2070.

30 CHEN, QIUSHUI, ET AL. ALL-INORGANIC PEROVSKITE NANOCRYSTAL SCINTILLATORS. NATURE, 2018, 561.7721: 88-93.

31 DE GIORGI, MARIA LUISA; ANNI, MARCO. AMPLIFIED SPONTANEOUS EMISSION AND LASING IN LEAD HALIDE PEROVSKITES: STATE OF THE ART AND PERSPECTIVES. APPLIED SCIENCES, 2019, 9.21: 4591.

32 ABDELWAHAB, IBRAHIM, ET AL. HIGHLY ENHANCED THIRD-HARMONIC GENERATION IN 2D PEROVSKITES AT EXCITONIC RESONANCES. ACS NANO, 2018, 12.1: 644-650.

33 SALIBA, MICHAEL, ET AL. PEROVSKITE SOLAR CELLS: FROM THE ATOMIC LEVEL TO FILM QUALITY AND DEVICE PERFORMANCE. ANGEWANDTE CHEMIE INTERNATIONAL EDITION, 2018, 57.10: 2554-2569.

34 CHERRY, M.; ISLAM, M. SAIFUL; CATLOW, C. R. A. OXYGEN ION MIGRATION IN PEROVSKITE-TYPE OXIDES. JOURNAL OF SOLID STATE CHEMISTRY, 1995, 118.1: 125-132.

35 SLOTCAVAGE, DANIEL J.; KARUNADASA, HEMAMALA I.; MCGEHEE, MICHAEL D. LIGHT-INDUCED PHASE SEGREGATION IN HALIDE-PEROVSKITE ABSORBERS. ACS ENERGY LETTERS, 2016, 1.6: 1199-1205.

36 KUNDU, SOUMYA; KELLY, TIMOTHY L. IN SITU STUDIES OF THE DEGRADATION MECHANISMS OF PEROVSKITE SOLAR CELLS. ECOMAT.

37 ZHU, PENGCHEN; ZHU, JIA. LOW-DIMENSIONAL METAL HALIDE PEROVSKITES AND RELATED OPTOELECTRONIC APPLICATIONS. INFOMAT, 2020, 2.2: 341-378.

38 BUHRO, WILLIAM E.; COLVIN, VICKI L. SHAPE MATTERS. NATURE MATERIALS, 2003, 2.3: 138-139.

39 FANG, JINGZHI, ET AL. RECENT ADVANCES IN LOW-DIMENSIONAL SEMICONDUCTOR NANOMATERIALS AND THEIR APPLICATIONS IN HIGH-PERFORMANCE PHOTODETECTORS. INFOMAT, 2020, 2.2: 291-317.

40 STECKEL, JONATHAN S., ET AL. QUANTUM DOTS: THE ULTIMATE DOWN-CONVERSION MATERIAL FOR LCD DISPLAYS. JOURNAL OF THE SOCIETY FOR INFORMATION DISPLAY, 2015, 23.7: 294-305.

41 MALGRAS V, NATTESTAD A, KIM JH, DOU SX, YAMAUCHI Y. UNDERSTANDING CHEMICALLY PROCESSED SOLAR CELLS BASED ON QUANTUM DOTS. SCIENCE AND TECHNOLOGY OF ADVANCED MATERIALS. 2017 DEC 31;18(1):334-50.

42 BERA, Debasis, et al. Quantum dots and their multimodal applications: a review. Materials, 2010, 3.4: 2260-2345.
43 EKIMOV, Alexey I.; EFROS, Al L.; ONUSHCHENKO, Alexei A. Quantum size effect in semiconductor microcrystals. Solid State Communications, 1985, 56.11: 921-924.
44 Ekimov A. Growth and optical properties of semiconductor nanocrystals in a glass matrix. Journal of luminescence. 1996 Oct 1;70(1-6):1-20.
45 WISE, Frank W. Lead salt quantum dots: the limit of strong quantum confinement. Accounts of Chemical Research, 2000, 33.11: 773-780.
46 EFROS, Al L.; ROSEN, M. The electronic structure of semiconductor nanocrystals. Annual Review of Materials Science, 2000, 30.1: 475-521.
47 Takagahara T. Effects of dielectric confinement and electron-hole exchange interaction on excitonic states in semiconductor quantum dots. Physical Review B. 1993 Feb 15;47(8):4569.
48 Hong X, Ishihara T, Nurmikko AV. Dielectric confinement effect on excitons in PbI 4-based layered semiconductors. Physical Review B. 1992 Mar 15;45(12):6961.
49 KAWANO, Naoki; KOSHIMIZU, Masanori; ASAI, Keisuke. The Effect of Wannier and Frenkel Exciton Resonance on the Luminescence Properties of Organic–Inorganic Layered Perovskite-Type Compounds. The Journal of Physical Chemistry C, 2012, 116.43: 22992-22995.
50 Brus LE. Electron–electron and electron-hole interactions in small semiconductor crystallites: The size dependence of the lowest excited electronic state. The Journal of chemical physics. 1984 May 1;80(9):4403-9.
51 GIORGI, Giacomo; YAMASHITA, Koichi. Zero-dimensional hybrid organic–inorganic halide perovskite modeling: insights from first principles. The journal of physical chemistry letters, 2016, 7.5: 888-899.
52 CHUKWUOCHA, Ephrem O.; ONYEAJU, Michael C.; HARRY, Taylor ST. Theoretical studies on the effect of confinement on quantum dots using the brus equation. 2012.
53 Gonzalez-Carrero S, Galian RE, Pérez-Prieto J. Maximizing the emissive properties of CH3NH3PbBr3 perovskite nanoparticles. Journal of Materials Chemistry A. 2015;3(17):9187-93.
54 LIU, Feng, et al. Highly luminescent phase-stable CsPbI3 perovskite quantum dots achieving near 100% absolute photoluminescence quantum yield. ACS nano, 2017, 11.10: 10373-10383.
55 HUANG, He, et al. Lead halide perovskite nanocrystals in the research spotlight: Stability and defect tolerance. ACS energy letters, 2017, 2.9: 2071-2083.
56 TEN BRINCK, Stephanie; ZACCARIA, Francesco; INFANTE, Ivan. Defects in lead halide perovskite nanocrystals: Analogies and (many) differences with the bulk. ACS Energy Letters, 2019, 4.11: 2739-2747.
57 KANG, Jun; WANG, Lin-Wang. High defect tolerance in lead halide perovskite CsPbBr3. The journal of physical chemistry letters, 2017, 8.2: 489-493.
58 BRANDT, Riley E., et al. Identifying defect-tolerant semiconductors with high minority carrier lifetimes: Beyond hybrid lead halide perovskites. arXiv preprint arXiv:1504.02144, 2015.
59 AKKERMAN, Quinten A., et al. Tuning the optical properties of cesium lead halide perovskite nanocrystals by anion exchange reactions. Journal of the American Chemical Society, 2015, 137.32: 10276-10281.
60 DI STASIO, Francesco, et al. Near-unity photoluminescence quantum yield in CsPbBr3 nanocrystal solid-state films via postsynthesis treatment with lead bromide. Chemistry of Materials, 2017, 29.18: 7663-7667.

61 PROTESESCU, Loredana, et al. Nanocrystals of cesium lead halide perovskites (CsPbX3, X= Cl, Br, and I): novel optoelectronic materials showing bright emission with wide color gamut. Nano letters, 2015, 15.6: 3692-3696.

62 ZHANG, Feng, et al. Brightly luminescent and color-tunable colloidal CH3NH3PbX3 (X= Br, I, Cl) quantum dots: potential alternatives for display technology. ACS nano, 2015, 9.4: 4533-4542.

63 AMAT, Anna, et al. Cation-induced band-gap tuning in organohalide perovskites: interplay of spin–orbit coupling and octahedra tilting. Nano letters, 2014, 14.6: 3608-3616.

64 KOSTOPOULOU, Athanasia, et al. Perovskite nanocrystals for energy conversion and storage. Nanophotonics, 2019, 8.10: 1607-1640.

65 SETH, Sudipta, et al. Tackling the Defects, Stability, and Photoluminescence of CsPbX3 Perovskite Nanocrystals. ACS Energy Letters, 2019, 4.7: 1610-1618.

66 HUANG, He, et al. Control of emission color of high quantum yield CH3NH3PbBr3 perovskite quantum dots by precipitation temperature. Advanced science, 2015, 2.9: 1500194.

67 ANAYA, Miguel, et al. ABX3 perovskites for tandem solar cells. Joule, 2017, 1.4: 769-793.

68 SANEHIRA, Erin M., et al. Enhanced mobility CsPbI3 quantum dot arrays for record-efficiency, high-voltage photovoltaic cells. Science advances, 2017, 3.10: eaao4204.

69 LING, Xufeng, et al. 14.1% CsPbI3 perovskite quantum dot solar cells via cesium cation passivation. Advanced Energy Materials, 2019, 9.28: 1900721.

70 LIU, Yao, et al. Dependence of carrier mobility on nanocrystal size and ligand length in PbSe nanocrystal solids. Nano letters, 2010, 10.5: 1960-1969.

71 IM, Jeong-Hyeok, et al. Nanowire perovskite solar cell. Nano letters, 2015, 15.3: 2120-2126.

72 CHA, Mingyang, et al. Enhancing perovskite solar cell performance by interface engineering using CH3NH3PbBr0. 9I2. 1 quantum dots. Journal of the American Chemical Society, 2016, 138.27: 8581-8587.

73 CHO, Kyung Taek, et al. Selective growth of layered perovskites for stable and efficient photovoltaics. Energy & Environmental Science, 2018, 11.4: 952-959.

74 LI, Mingjie, et al. Low threshold and efficient multiple exciton generation in halide perovskite nanocrystals. Nature communications, 2018, 9.1: 1-7.

75 MIYATA, Atsuhiko, et al. Direct measurement of the exciton binding energy and effective masses for charge carriers in organic–inorganic tri-halide perovskites. Nature Physics, 2015, 11.7: 582-587.

76 SWARNKAR, Abhishek, et al. Colloidal CsPbBr3 perovskite nanocrystals: luminescence beyond traditional quantum dots. Angewandte Chemie, 2015, 127.51: 15644-15648.

77 ZHANG, Yupeng, et al. Photonics and optoelectronics using nano-structured hybrid perovskite media and their optical cavities. Physics Reports, 2019.

78 SOE, Chan Myae Myae, et al. Structural and thermodynamic limits of layer thickness in 2D halide perovskites. Proceedings of the National Academy of Sciences, 2019, 116.1: 58-66.

79 KIM, Young-Hoon; CHO, Himchan; LEE, Tae-Woo. Metal halide perovskite light emitters. Proceedings of the National Academy of Sciences, 2016, 113.42: 11694-11702.

80 KO, Yun-Hyuk, et al. Super Ultra-High Resolution Liquid-Crystal-Display Using Perovskite Quantum-Dot Functional Color-Filters. Scientific reports, 2018, 8.1: 1-7.

81 PARK, DA HYE, ET AL. FACILE SYNTHESIS OF THERMALLY STABLE CSPBBR3 PEROVSKITE QUANTUM DOT-INORGANIC SIO2 COMPOSITES AND THEIR APPLICATION TO WHITE LIGHT-EMITTING DIODES WITH WIDE COLOR GAMUT. DYES AND PIGMENTS, 2018, 149: 246-252.

82 SCHMIDT, LUCIANA C., ET AL. NONTEMPLATE SYNTHESIS OF CH3NH3PBBR3 PEROVSKITE NANOPARTICLES. JOURNAL OF THE AMERICAN CHEMICAL SOCIETY, 2014, 136.3: 850-853.

83 BEKENSTEIN, YEHONADAV, ET AL. HIGHLY LUMINESCENT COLLOIDAL NANOPLATES OF PEROVSKITE CESIUM LEAD HALIDE AND THEIR ORIENTED ASSEMBLIES. JOURNAL OF THE AMERICAN CHEMICAL SOCIETY, 2015, 137.51: 16008-16011.

84 SHAMSI, JAVAD, ET AL. METAL HALIDE PEROVSKITE NANOCRYSTALS: SYNTHESIS, POST-SYNTHESIS MODIFICATIONS, AND THEIR OPTICAL PROPERTIES. CHEMICAL REVIEWS, 2019, 119.5: 3296-3348.

85 SCHEIDT, REBECCA A.; ATWELL, COREY; KAMAT, PRASHANT V. TRACKING TRANSFORMATIVE TRANSITIONS: FROM CSPBBR3 NANOCRYSTALS TO BULK PEROVSKITE FILMS. ACS MATERIALS LETTERS, 2019, 1.1: 8-13.

86 LEE, MICHAEL M., ET AL. EFFICIENT HYBRID SOLAR CELLS BASED ON MESO-SUPERSTRUCTURED ORGANOMETAL HALIDE PEROVSKITES. SCIENCE, 2012, 338.6107: 643-647.

87 BI, DONGQIN, ET AL. USING A TWO-STEP DEPOSITION TECHNIQUE TO PREPARE PEROVSKITE (CH3NH3PBI3) FOR THIN FILM SOLAR CELLS BASED ON ZRO2 AND TIO2 MESOSTRUCTURES. RSC ADVANCES, 2013, 3.41: 18762-18766

88 MALGRAS, VICTOR, ET AL. OBSERVATION OF QUANTUM CONFINEMENT IN MONODISPERSE METHYLAMMONIUM LEAD HALIDE PEROVSKITE NANOCRYSTALS EMBEDDED IN MESOPOROUS SILICA. JOURNAL OF THE AMERICAN CHEMICAL SOCIETY, 2016, 138.42: 13874-13881.

89 DIRIN, DMITRY N., ET AL. HARNESSING DEFECT-TOLERANCE AT THE NANOSCALE: HIGHLY LUMINESCENT LEAD HALIDE PEROVSKITE NANOCRYSTALS IN MESOPOROUS SILICA MATRIXES. NANO LETTERS, 2016, 16.9: 5866-5874.

90 SUTEEWONG, TEERAPORN, ET AL. HIGHLY AMINATED MESOPOROUS SILICA NANOPARTICLES WITH CUBIC PORE STRUCTURE. JOURNAL OF THE AMERICAN CHEMICAL SOCIETY, 2011, 133.2: 172-175.

91 ESCUIN, PAULA CORELL, ET AL. APPLICATION OF MESOPOROUS SILICA MATERIALS FOR THE IMMOBILIZATION OF POLYPHENOL OXIDASE. FOOD CHEMISTRY, 2017, 217: 360-363.

92 MIYATA, HIROKATSU, ET AL. LATTICE MATCHING IN THE EPITAXIAL FORMATION OF MESOSTRUCTURED SILICA FILMS. LANGMUIR, 2013, 29.2: 761-765.

93 HIDALGO, NURIA, ET AL. CHARACTERIZATION OF MESOPOROUS THIN FILMS BY SPECULAR REFLECTANCE POROSIMETRY. LANGMUIR, 2012, 28.39: 13777-13782.

94 PACHOLSKI, CLAUDIA, ET AL. BIOSENSING USING POROUS SILICON DOUBLE-LAYER INTERFEROMETERS: REFLECTIVE INTERFEROMETRIC FOURIER TRANSFORM SPECTROSCOPY. JOURNAL OF THE AMERICAN CHEMICAL SOCIETY, 2005, 127.33: 11636-11645.

95 LOSIC, DUSAN; LILLO, MICKAEL; LOSIC JR, DUSAN. POROUS ALUMINA WITH SHAPED PORE GEOMETRIES AND COMPLEX PORE ARCHITECTURES FABRICATED BY CYCLIC ANODIZATION. SMALL, 2009, 5.12: 1392-1397.

96 HUO, QUISHENG, ET AL. ORGANIZATION OF ORGANIC MOLECULES WITH INORGANIC MOLECULAR SPECIES INTO NANOCOMPOSITE BIPHASE ARRAYS. CHEM. MATER, 1994, 6: 1176.

97 BUENO-ALEJO, CARLOS J.; VILLAESCUSA, LUIS A.; GARCIA-BENNETT, ALFONSO E. SUPRAMOLECULAR TRANSCRIPTION OF GUANOSINE MONOPHOSPHATE INTO MESOSTRUCTURED SILICA. ANGEWANDTE CHEMIE, 2014, 126.45: 12302-12306.

98 CHA, WONHEE, ET AL. SIZE-CONTROLLABLE AND STABLE ORGANOMETALLIC HALIDE PEROVSKITE QUANTUM DOTS/POLYMER FILMS. JOURNAL OF MATERIALS CHEMISTRY C, 2017, 5.27: 6667-6671.

99 MARTIN, CHARLES R. NANOMATERIALS: A MEMBRANE-BASED SYNTHETIC APPROACH. SCIENCE, 1994, 266.5193: 1961-1966.

100 MOLLER, KARIN; BEIN, THOMAS. INCLUSION CHEMISTRY IN PERIODIC MESOPOROUS HOSTS. CHEMISTRY OF MATERIALS, 1998, 10.10: 2950-2963.

101 HIRAI, Takayuki; OKUBO, Hironori; KOMASAWA, Isao. Size-selective incorporation of CdS nanoparticles into mesoporous silica. The Journal of Physical Chemistry B, 1999, 103.21: 4228-4230.

102 MALGRAS, Victor, et al. Hybrid methylammonium lead halide perovskite nanocrystals confined in gyroidal silica templates. Chemical Communications, 2017, 53.15: 2359-2362.

103 ANAYA, Miguel, et al. Strong quantum confinement and fast photoemission activation in CH3NH3PbI3 perovskite nanocrystals grown within periodically mesostructured films. Advanced Optical Materials, 2017, 5.8: 1601087.

104 DEMCHYSHYN, Stepan, et al. Confining metal-halide perovskites in nanoporous thin films. Science advances, 2017, 3.8: e1700738.

105 GHOSH, Joydip; GHOSH, Ramesh; GIRI, P. K. Mesoporous Si nanowire templated controlled fabrication of organometal halide perovskite nanoparticles with high photoluminescence quantum yield for light-emitting applications. ACS Applied Nano Materials, 2018, 1.4: 1551-1562.

106 PARVEEN, Sumaiya, et al. Large exciton binding energy, high photoluminescence quantum yield and improved photostability of organo-metal halide hybrid perovskite quantum dots grown on a mesoporous titanium dioxide template. Journal of colloid and interface science, 2019, 539: 619-633.

107 CHEN, Zheng, et al. A confined fabrication of perovskite quantum dots in oriented MOF thin film. ACS applied materials & interfaces, 2016, 8.42: 28737-28742.

108 CALVO, Mauricio E., et al. Control over the structural and optical features of nanoparticle-based one-dimensional photonic crystals. Langmuir, 2009, 25.4: 2443-2448.

109 OKUYA, Masayuki; NAKADE, Koji; KANEKO, Shoji. Porous TiO2 thin films synthesized by a spray pyrolysis deposition (SPD) technique and their application to dye-sensitized solar cells. Solar energy materials and solar cells, 2002, 70.4: 425-435.

110 MALGRAS, Victor, et al. Stable blue luminescent CsPbBr3 perovskite nanocrystals confined in mesoporous thin films. Angewandte Chemie, 2018, 130.29: 9019-9023.

111RUBINO, Andrea, et al. Highly Efficient and Environmentally Stable Flexible Color Converters Based on Confined CH3NH3PbBr3 Nanocrystals. ACS applied materials & interfaces, 2018, 10.44: 38334-38340.

112 WANG, Hung-Chia, et al. Mesoporous silica particles integrated with all-inorganic CsPbBr3 perovskite quantum-dot nanocomposites (MP-PQDs) with high stability and wide color gamut used for backlight display. Angewandte Chemie International Edition, 2016, 55.28: 7924-7929.

113 RAJA, Shilpa N., et al. Encapsulation of perovskite nanocrystals into macroscale polymer matrices: enhanced stability and polarization. ACS applied materials & interfaces, 2016, 8.51: 35523-35533.

114 HE, Juan, et al. In situ synthesis and macroscale alignment of CsPbBr 3 perovskite nanorods in a polymer matrix. Nanoscale, 2018, 10.33: 15436-15441.

115 WANG, Yanan, et al. Ultrastable, highly luminescent organic–inorganic perovskite–polymer composite films. Advanced Materials, 2016, 28.48: 10710-10717.

116 GONG, Xiwen, et al. Electron–phonon interaction in efficient perovskite blue emitters. Nature materials, 2018, 17.6: 550-556.

117 RAVI, Vikash Kumar, et al. Excellent green but less impressive blue luminescence from CsPbBr3 perovskite nanocubes and nanoplatelets. Nanotechnology, 2016, 27.32: 325708.

118 GODIN, ROBERT, ET AL. TUNING CHARGE CARRIER DYNAMICS AND SURFACE PASSIVATION IN ORGANOLEAD HALIDE PEROVSKITES WITH CAPPING LIGANDS AND METAL OXIDE INTERFACES. ADVANCED OPTICAL MATERIALS, 2018, 6.5: 1701203.

119 ANAYA M, GALISTEO-LÓPEZ JF, ME C, JP E. H. MÍGUEZ. ORIGIN OF LIGHT INDUCED ION MIGRATION IN ORGANIC METAL HALIDE PEROVSKITES IN THE PRESENCE OF OXYGEN. J. PHYS. CHEM. LETT. 2018;9:3891-6.

120 GERHARD M, LOUIS B, CAMACHO R, MERDASA A, LI J, KILIGARIDIS A, DOBROVOLSKY A, HOFKENS J, SCHEBLYKIN IG. MICROSCOPIC INSIGHT INTO NON-RADIATIVE DECAY IN PEROVSKITE SEMICONDUCTORS FROM TEMPERATURE-DEPENDENT LUMINESCENCE BLINKING. NATURE COMMUNICATIONS. 2019 APR 12;10(1):1-2.

121 YOO, SO-MIN, ET AL. AN EQUIVALENT CIRCUIT FOR PEROVSKITE SOLAR CELL BRIDGING SENSITIZED TO THIN FILM ARCHITECTURES. JOULE, 2019, 3.10: 2535-2549.

122 LEE, HYO JOONG, ET AL. A FACILE PREPARATIVE ROUTE OF NANOSCALE PEROVSKITES OVER MESOPOROUS METAL OXIDE FILMS AND THEIR APPLICATIONS TO PHOTOSENSITIZERS AND LIGHT EMITTERS. ADVANCED FUNCTIONAL MATERIALS, 2018, 28.39: 1803801.

123 VICKERS, EVAN T., ET AL. IMPROVING CHARGE CARRIER DELOCALIZATION IN PEROVSKITE QUANTUM DOTS BY SURFACE PASSIVATION WITH CONDUCTIVE AROMATIC LIGANDS. ACS ENERGY LETTERS, 2018, 3.12: 2931-2939.

2 PEROVSKITE NANOCRYSTALS IN MO_X NANOPARTICLE FILMS

2.1 INTRODUCTION

Lead halide perovskites have been the subject of an intense study over the past 10 years and to date these semiconductors have been investigated in different compositions, shapes and also distinct low-dimensional configurations. The research has obviously pushed towards the optimization of the materials in order to improve their optoelectronic quality and performances. Thus, for example, perovskites with mixed A^+ cations and usually a certain proportion of iodide and bromide are used for the most efficient solar cells.[1,2] Among bulk materials, in the form of polycrystalline films, the most intense investigation concern hybrid perovskites, and, in particular, $MAPbI_3$, with the ideal optical characteristics for solar cells.[3,4] As regards the emission, however, the materials currently most used are low dimensional perovskites.[5,6] As far as perovskites nanocrystals are concerned, $CsPbX_3$ are the most popular materials and the first nano-scaled ones especially because of the ease of fabrication by colloidal synthesis and the chemical stability with respect to compositions including organic cations.[7-9]

The scientific activity developed around perovskites has been impressive and evolved exponentially so far, dragging the scientific community into a sort of gold rush. In such a context, even the choice on the material to be focused on becomes complicated, considering the rapidity of a compound to turns "obsolete" and be replaced with another that exhibit better performances. Actually it is also necessary to separate, from this point of view, the study of fundamental properties from the "technological" needs of a product. Often, in fact, by directing efforts to the result, we lose sight of how it was achieved. And the case of perovskites it is not an exception in this sense.[10] The brilliant results that have been achieved derive from a rather complex set of elements or combinations of chemical-physical properties which, for example, makes rather difficult to recognize or distinguish the factors that actually lead to an improvement from those that work only in particular conditions. Therefore, within the scope of this project, that is the study of nanocrystalline perovskites in porous matrices, the work has been focused on the use of a series of relatively simple material compositions in order to cover more carefully this research area still underexplored.[11] This thesis is focused on organic-

inorganic hybrid perovskites such as methylammonium lead halides, also in order to be able to keep a direct comparison between bulk materials and nanocrystals, for the analysis of the results. As regards the porous system, the composite materials used in this thesis are mainly made up of layers of silicon dioxide nanoparticles. These are interesting systems first of all because they are low cost and easy to prepare, but at the same time they also allow an easy manipulation in order to obtain further sophistication and functionalization which can be convenient and intriguing as we will see hereinafter. Finally, the possibility to handle these matrices in the form of a thin film is a consequence of the idea of integrating these composite materials into the architecture of an actual device and from this point of view the nanoparticles stratification is again one of the best options among the porous materials due to the their optical quality.[12,13]

2.2 PREPARATION

For the preparation of perovskites in the form of nanocrystals, a one-step method was used, which consists in the infiltration of the matrix with a solution of perovskite precursors by means of spin coating (see chapter 1). The objective, in this phase, is to synthesize perovskite nanocrystals inside the pores of a porous film and to obtain a composite matrix in which the nanocrystals size distribution is uniform and the perovskite material dispersion is as homogeneous as possible throughout the pores volume available. For this reason, the ideal infiltration technique is the spin coating which allows the precursor material to be pushed more effectively into the pores.[11] Compared to the two-step method, there are some advantages instead. The second step involves the immersion into a solution containing one of the precursors, but in this way it is more difficult to avoid the deposition of materials on the surface and in this case, washing cycles would therefore be necessary. Finally, immersion in certain polar solvents could compromise the stability of the porous matrix.[14] In general, the one-step method allows a more accurate control on the synthesis conditions thanks also to the lower number of parameters that come into play. Finally, the use of a single solution containing the precursors PbX_2 and AX is the alternative that offers a more immediate comparison with the bulk. The solution that is infiltrated in order to form the nanocrystals is, in fact, the same one that if deposited on a substrate without matrix, leads to the formation of a polycrystalline film typically used in the same optoelectronic applications.[15,16]

2.2.1 MOx Nanoparticles

As previously mentioned, mainly silicon dioxide (SiO_2) nano-spheres have been used for the preparation of a porous matrix film. In particular, we use Ludox TMA (Sigma-Aldrich) which is an aqueous colloidal dispersion of 30 nm silica nanoparticles with a rather narrow size distribution.[17] The use sub-wavelength particles of regular shape and size allow us to obtain a homogeneous porous film with optical quality. This optical quality refers to minimize light scattering effects that results in a transparent film. Also, the morphology of the film is important to improve the compatibility in multilayer structures such as those of a device, for which it would be recommended to build up a stratification with smooth and planar interfaces. Finally, using monodispersed particles with regular shape allows a certain distribution in the space, that even if it's a random packing, it is possible to obtain some porosity with a narrow pore size distribution (PSD) as it is also studied in section 2.3.1 which also helps to the optical quality of the film.[18,19] To further improve this aspect, the deposition technique used for the silica nanoparticle matrix is dip coating (see figure 2.2.1). The porous matrix can be built by covering a normal glass substrate. In this thesis, microscope slides were generally used as substrates and washed with ethanol (EtOH), acetone and isopropanol (IprOH) to ensure good adhesion and homogeneous deposition of the SiO_2 particles. Then, by adjusting the concentration of the silica suspension and the withdrawal speed of the substrate immersed, it is possible to control the thickness of the matrix from a few tens of nanometres to microns. This technique also allows uniform deposition over square centimetres, while maintaining a high degree of interconnectivity of the porous skeleton (inter-particle space) and therefore a good permeability of fluids (liquids and gas) inside with a good one-dimensional order in the stratification of the different nanoparticles sheets.[20]

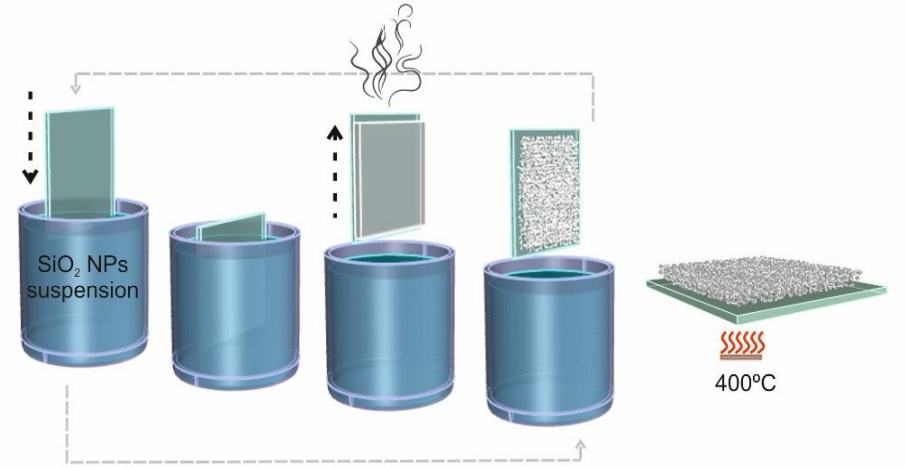

Figure 2.2.1 Graphical representation of dip-coating procedure (different cycles of dipping and drying) and final heat treatment for SiO_2 nanoparticles thin film preparation.

The process protocol developed for a SiO_2 matrix of variable thickness in the range of 30 to 2500 nm, involves a LUDOX solution diluted at 1% in methanol and a dipping process with multi depositions in rapid succession with 100 mm/min of withdrawal speed and 60 s. of waiting time between each deposition in order to evaporate the solvent. Furthermore, the dip coater (ND-R Rotary Dip Coater, Nadetech Innovations) is placed in a closed chamber to ensure control of internal humidity and therefore on evaporation. The last step of the procedure consists in a calcination heat treatment at 400 °C for one hour to definitively eliminate the solvent and all the volatile compounds, among which the stabilizers used for the LUDOX suspensions. This last step is important to guarantee mechanical stability to the porous structure, but it is also necessary to avoid an abrupt temperature change (fast ramp) and to reach a final temperature too high in order not to incur cracking phenomena[21,22] of the layer which would obviously affect the entire perovskite synthesis process. The versatility of the protocol, as well as in terms of thickness and scaling, extends to other types of matrix, such as, for example, the mesostructured systems which exploit the EISA synthesis technique (see chapter 1). In this thesis a similar dip coating process, as described above, was also applied in the preparation of porous films using particles of other metal oxides, such as TiO_2 and SnO_2. In each case, the process was adapted to the necessary stability and thickness requirements, adjusting the concentration of the colloidal suspension the withdrawal speed and the number of depositions, the drying conditions and the heat treatment. In general it is important to take into account several factors: the MO_x particles size and solubility in order to avoid particle agglomeration and subsequent scattering points in the final film; the solvent used for the colloidal suspension and the evaporation rate in order to ensure a uniform coating before the following deposition of this multistep process; the mechanical stability depending on the thickness and the heat treatment and distinctive for each MO_x suspension.

2.2.2 Perovskites

The actual synthesis of perovskites generally consists of a crystallization process by evaporation of the solvents in which the precursors were dissolved. This rapid precipitation can be modified by the addition of an "antisolvent" during the spin coating stage.[23,24] The approach between anionic and cationic species, in solution, lead to a first step of nucleation and formation of clusters and nuclei with the typical crystalline structure of the perovskites. Subsequently, the removal of the solvent implies a change in the conditions of concentration and the primary particles formed act as points of nucleation of rest of dispersed precursors. In this way its growth is promoted. As for bulk perovskites, the solution precipitates (single crystals) or can be deposited on a substrate and evaporated rapidly at 100 °C (thin

films). With the porous matrix the idea is to force the formation of perovskites inside the pores, using them as nano-reactors in which limit the space for perovskite crystals growth. For this purpose, the porous materials described above are infiltrated, at room temperature, by a solution of dimethylformamide (DMF) containing PbX_2 and MAX reagents in different molar ratios. More concretely, the solution is deposited by spin coating as shown in the figure 2.2.2. Finally the sample is heated up to 100 °C for one hour, in order to completely evaporate the solvent and favour the crystallization. The entire synthesis process of perovskites synthesis (preparation of solutions, deposition and heating) is conducted in a glovebox. The inert atmosphere is in fact essential to avoid the degradation due to oxygen and environmental humidity.[25,26]

Special consideration should be given to the deposition step in order to ensure the complete infiltration of the precursor solution into the pores of the matrix, but, at the same time, avoiding the accumulation of precursors material at the surface that can lead to the formation of bulky crystals (size larger than 50 nm) or even a capping layer.[11,27] In this sense, it is necessary to optimize the concentration of the precursor solution, the thickness of the matrix and the rotational speed of the spin coating.

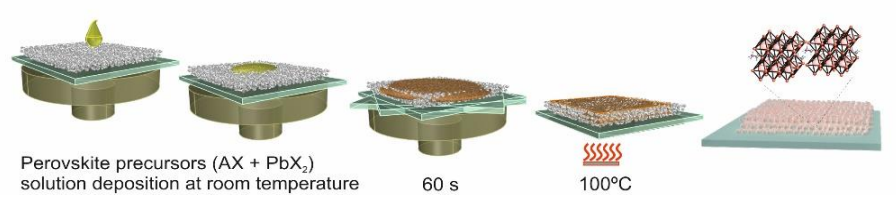

Figure 2.2.2 Graphical representation of spin-coating procedure and final heat treatment for perovskite nanocrystals one-step synthesis within the porous SiO_2 thin film.

The result can be monitored through the analysis of photoluminescence. The presence of bulk material is in fact recognizable by the spectral position of the peak corresponding to that of the polycrystalline film, while the infiltrated nanocrystals show the characteristic blue-shift with respect to the same peak. In general, we observed that a 1000 nm thick silica matrix can be infiltrated by a saturated precursors solution (solubility depends on the species involved in the different perovskite compositions) with a rotation speed of 5000 rpm for 60 s. These are the regular conditions used for the synthesis of perovskites nanocrystals during this thesis. Some changes to this procedure have been introduced during the work for specific project needs. The details will be indicated when necessary in the dedicated chapter or paragraph.

2.2.3 Size control

The synthetic system developed in this work allows to control the size of perovskite nanocrystals by varying the concentration of the precursor solution. Beyond the control of the template infiltration to prevent the formation of bulk crystals, the deposition of more diluted solutions in the same matrix leads to crystals of smaller dimensions. The result is particularly evident in the precise displacement of the photoluminescence peak which shifts to shorter wavelengths due to the increase of the bandgap. This feature is directly correlated with the reduction in the size of the nanocrystal (see chapter 1) as illustrated in figure 2.2.3 for the case of the as-prepared $MAPbBr_3$ perovskite nanocrystals when lowering the precursor solution concentration and compared to the bulk thin film. Further confirmations are appreciable in the structural analysis presented in sub-paragraph 2.3.2.

In order to understand the possibility of modify the crystals size even below the dimensions of the pores of the matrix, it is necessary to consider the kinetics of the formation steps of the perovskites inside the matrix, during the spin-coating step. In the absence of typical structuring agents of colloidal synthesis, the nucleation and growth of the crystals, within a single heterogeneous phase, will be dictated by the elimination of the solvent as already seen for the bulk. The difference in the case of the process occurring inside the matrix lies in the diffusion of the reagents and vapours, limited by the tortuosity of the porous network.

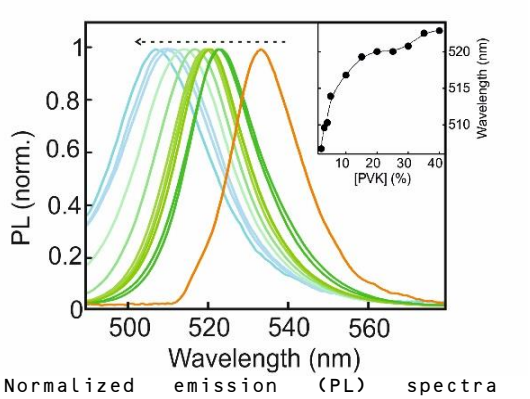

Figure 2.2.3 Normalized emission (PL) spectra of $MAPbBr_3$ nanocrystals synthesized, inside the SiO_2 scaffold, starting from solutions with different precursor concentrations (% of $MABr+PbBr_2$ in DMF). Gradual shift of the maximum of emission is registered from 523 nm, 40 wt% to 504 nm, 2 wt%. The arrow points the decrease in concentration and the spectral shift with respect to the bulk photoluminescence (orange curve with maximum emission at 533 nm). Inset: Evolution of the PL maximum with the increase of perovskite precursor concentrations.

In the initial phase of the deposition, even before the beginning of the rotation, the evaporation of the solvent is still negligible, considering the low vapour pressure of the DMF. The solution then penetrates the matrix and the precursors can be homogeneously distributed throughout the entire film. Immediately after, the spin

coating rotation, pushes the solution from the centre outwards. In this way it also favours the rapid elimination of the solvent and therefore the super-saturation of the precursors inside the pores. Considering the same volume of pores, from a more diluted solution many nuclei will be formed in the first phase, but in the second step there will be less precursor material, inside a pore, to make the crystals grow. Conversely, in the case of higher concentrations, growth will be less limited by diffusion due to the larger amount of reagent species available, therefore larger nanocrystals can be obtained. Finally, in section 2.4, a more detailed study on the growth of $MAPbBr_3$ nanocrystals within the mesoporous matrices of SiO_2 NPs is presented.

2.2.4 Versatility

To conclude the description about the preparation method developed within this thesis, it is also appropriate to present its versatility, here interpreted as the possibility to be applied with different materials. For example, the metal oxide used for the matrix can be replaced with other materials that allow the infiltration by perovskite precursors as illustrated in figures 2.2.4a and b. The same perovskite confinement ability is reproduced, for example, when using a matrix of titanium dioxide nanoparticles (12 nanometres in diameter) again in the form of a porous thin film. In this case, the change in the composition of the matrix can directly affect the behaviour of the perovskites. As previously mentioned (chapter 1), the electronic structure of TiO_2 favours the extraction of photo-generated electrons from the perovskites.

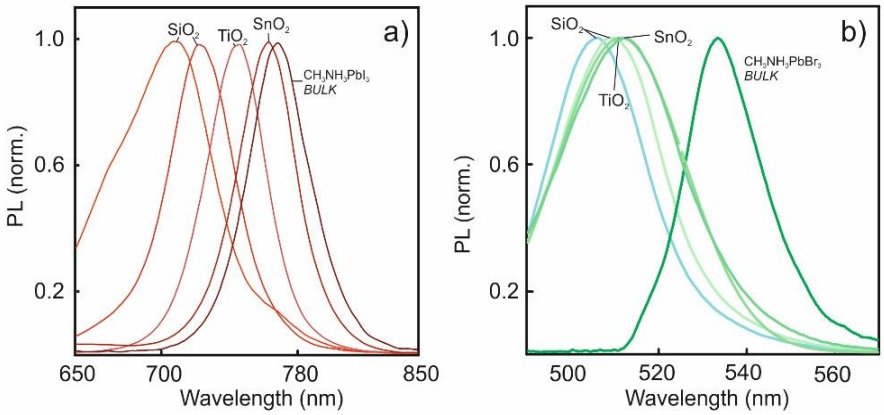

Figure 2.2.4 a) Normalized PL spectra of $MAPbI_3$ nanocrystals from a 20 wt.% concentrated solution infiltrated porous film built up with nanoparticles of TiO_2, SnO_2, SiO_2 with a diameter of 30 nm and SiO_2 with a diameter of 10 nm (the largest shift with respect to the bulk PL); b) Normalized PL spectra of MAPbBr3 nanocrystals from a 20% concentrated solution infiltrated in the same matrices as in figure 2.2.4a).

From the emission point of view, the result is a quenching of the intensity and an acceleration of the PL decay by non-radiative pathways. The template method is also effective with tin dioxide nanoparticles (8 nm) based film, but it is interesting to note the use of silicon oxide nanoparticles (Ludox CL) with smaller diameter (10 nm instead of 30 nm). As can be seen in the figure, the shift of the PL is more pronounced in the case of the smaller SiO_2 particles. In general, the diameter of the particles and their aggregation state affect the pore size of the layered film.

The versatility of the synthetic method also concerns the perovskites chemical composition. That is, the synthesis has proven to be suitable for perovskites with different halide anions and organic cations (see figure 2.2.4ab). In this thesis, $MAPbI_3$, $MAPbBr_3$ and formamidinium lead bromide ($FAPbBr_3$) have been used, each for distinct application, as will be shown in the following chapters. The difference in the preparation of these three compositions lies basically in the solution of precursors for which have typically been used the same recipes employed for the corresponding polycrystalline films. In the case of $MAPbI_3$, MAI and $PbCl_2$, (molar ratio 3 to 1) were dissolved at 40 wt% in DMF while for the case of $MAPBr_3$ and $FAPbBr_3$, MABr and FABr were dissolved with $PbBr_2$ (molar ratio 1 to 1) at 20wt%, respectively, in DMF and dimethylsulfoxide (DMSO).

2.3 STRUCTURAL CHARACTERIZATION

This paragraph will focus on the analysis of an archetypal sample (most used in this thesis), that is, $MAPbBr_3$ infiltrated in a film of SiO_2 nanoparticles of 30 nm in diameter. Some more specific characterizations will be presented in other chapters, but in this case the intention is to show the typical structure of the composite material that is obtained with the synthesis method that has been described previously. The use of solutions with distinct concentration obviously implies a different degree of filling of the pores, as well as the use of a slightly more polar and more viscous solvent than DMF, such as DMSO, or the use of smaller nanoparticles for the matrix layer. At the same time, the size of perovskite crystals depends also on the chemical composition (ions radii), as we mentioned in the introductory chapter. Apart from these variations, however, the general architecture of the composite materials prepared in this thesis can be described as follows.

2.3.1 Porosimetry

The first feature to take into consideration for the structural description of films composed of an inorganic matrix hosting perovskite nanocrystals is the porosity of

the system. For this purpose, in general, there are various analytical tools capable of studying porosimetry, that is, quantifying the characteristics of a porous material, such as the size of the pores and the total volume "occupied" by them.[28,29]

The morphological uniformity of the layer constituted by nanoparticles deposited by dip coating in a perfectly flat structure with planar interfaces (see figure 2.3.1a) together with the optical homogeneity, that means the absence of light scattering phenomena, as evidenced by the spectral behaviour in the figure 2.3.1b, allow the analysis of the total volume and size distribution of the pores, through the specular reflectance porosimetry technique.

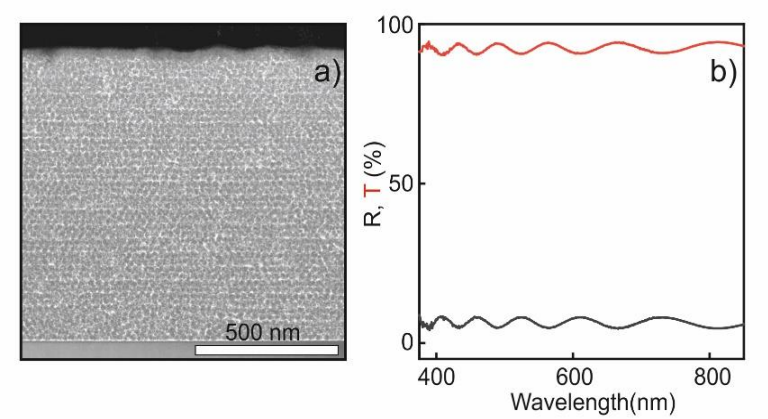

Figure 2.3.1 a) High-angle annular dark-field scanning TEM (HAADF-STEM) cross section of the SiO_2 nanoparticles stratification for the porous film; b). UV-Vis reflectance (R) and transmittance (T) of the same SiO_2 nanoparticles multilayer as in a).

This type of characterization is, in fact, based on the variation in the reflection spectrum (normal to the incident beam) produced by the increase in the effective refractive index of the porous film when a vapour condenses inside the pores. The increase in the optical thickness of the film produces a shift of the interference oscillations. For this analysis, the sample is introduced into a special chamber with a quartz window through which the incident and the reflected beam can be introduced and collected respectively. The chamber is connected through a manual valve to reservoir containing isopropanol. IprOH vapour is gradually introduced into the chamber previously evacuated up to 10^{-2} mbar. The gradual increase of isopropanol pressure (P_s) can, then, be monitored constantly and simultaneously the reflectance spectra are recorded. The figure 2.3.1c shows the evolution of the reflectance spectra of the SiO_2 NPs layer (with nanoparticles of 30 nm in diameter and a total thickness of 1000 nm), at distinct relative vapour pressures. For the optical measurement we made use of a Fourier transform Vis-NIR spectrophotometer (Bruker IFS-66) attached to a microscope with a stage to place the chamber with the sample to operate in specular reflection mode.

The measured spectra were fitted with a Matlab code based on the transfer matrix method,[30]enabling the extrapolation of the effective refractive index for the porous film on varying the isopropanol vapour pressure. By applying the Bruggeman's approximation, it is possible to separate the total pore volume V_{pore} and the volume fraction occupied by the solvent V_{ads} again as the pressure changes. In this formalism based on the effective medium theory, the system is considered as a heterogeneous medium composed of SiO_2 and IprOH for which the respective refractive indices are known. Considering the index calculated previously, it is possible to set the SiO_2 fraction for the system under vacuum, at the beginning (first reflectance measurement), without any solvent and therefore it is possible to trace the volume fraction occupied by the solvent as the pressure increases following the variation of the film index at the exact same pressures.

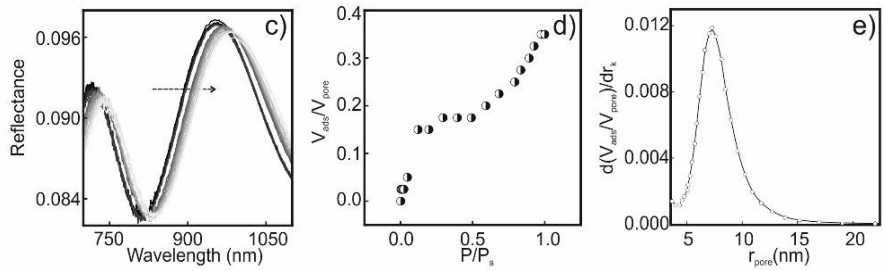

Figure 2.3.1 c) Specular reflectance spectra obtained from the SiO_2 nanoparticle film under different isopropanol vapour pressures. The arrow indicates the spectral shift as the P/P_s increases; d) Adsorption isotherm corresponding to the variation of the pores volume fraction in which the isopropanol is adsorbed; e) Pore size distributions of SiO_2 nanoparticles film extracted from the adsorption isotherm in d).

The figure 2.3.1d shows the V_{ads}/V_{pore} values as a function of the relative pressure inside the chamber. The abrupt change in the curve indicates the condensation of isopropanol within the pores. Furthermore, through the Kelvin equation[31] it is possible to establish a relationship between the condensation pressure whith it's the pore radius, $r_{pore.}$, Considering the correction parameter of Brunauer, Emmet and Teller which takes into account the initial (monolayer) absorption of the solvent on the pore walls. the pore size distribution (PSD) can be traced as shown in the figure 2.3.1 e. So, despite the irregular geometry of the porous skeleton in a SiO_2 packed particles layer, the result of this analysis indicates a distribution, albeit enlarged, but centred on a value of about 8 nm. Details on the characterization background and the PSD calculation are collected in Annex I.

2.3.2 TEM, SEM, XRD analysis

As can be seen in the figure 2.3.2a and b, the observation of the composite matrix cross-sections by scanning electron microscopy (SEM) offers a first estimate of

how the porous matrix microstructure is not affected by the infiltration of the perovskites. Furthermore, by using the backscattered electrons, it is easy to distinguish the bright regions, inside the film, where the electrons meet with the heaviest atom, that is, the lead in perovskites. The image of the entire cross section also confirms the absence of a perovskite capping layer or any macro-crystals at the surface of the silica scaffold.

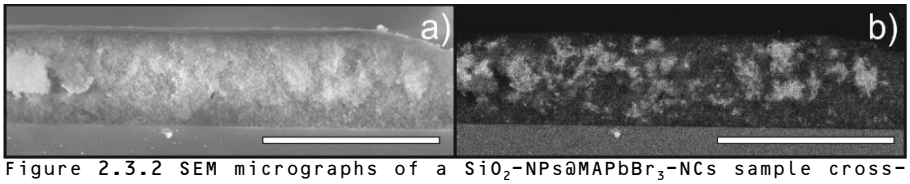

Figure 2.3.2 SEM micrographs of a SiO_2-NPs@$MAPbBr_3$-NCs sample cross-section obtained from secondary a) and backscattered b) electrons. Scale bar is 2 microns.

But it is with transmission electron microscopy (TEM) analysis that the method of confinement of perovskite nanocrystals inside the pores can be inspected closely. First of all, for this analysis a Focused Ion Beam (dual beam microscope FIB-SEM, Zeiss Auriga) was used to cut lamellae of the samples in order to obtain a much more precise and clean cross-section. The microscope used is a TEM scanning (STEM, G2F30, FEG) with a High Angle Annular Dark Field (HAADF, Wigeon) detector coupled to an EDS detector (SSD, INCA X-Max 80). The images reported in the figure 2.3.2c-j illustrate the cross section of a sample with $MAPbBr_3$ nanocrystals in the SiO_2 NPs matrix at different magnifications and from the HADDF STEM analysis to the High Resolution TEM (HRTEM). In the HADDF mode it is possible to carry out an elementary mapping of the areas selected in the zoom.

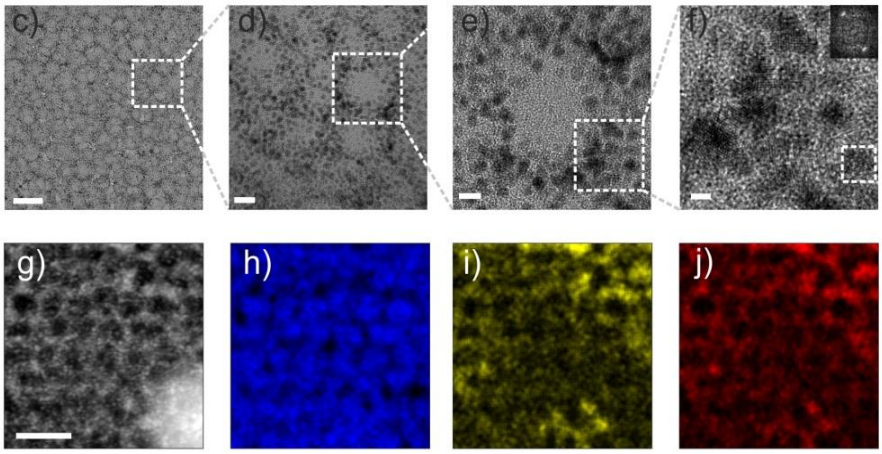

Figure 2.3.2 (c–f) HRTEM micrographs, with different magnification from figure c), of nc-$MAPbBr_3$ infiltrated in inter-particles space of the SiO_2 matrix; scale bar is 100nm in c), 10 nm in (d), 3.5 nm in (e) and 1nm in (f). The inset in (f) shows the digital diffraction pattern of area selected in the same panel; g) HAADF-STEM cross section image of the same sample as in c); scale bar is 50 nm. (h–j), EDX chemical mapping of the area selected in (g): (h) Si map; (i) Pb map; (j) Br map.

This analysis confirms the distribution of the Pb and Br elements, in the selected area, in a complementary way to the Si signal, reproducing the morphology of the SiO_2 nanoparticles infiltrated with perovskites. With the high resolution mode, on the other hand, it is possible to identify the crystalline structure of the perovskites with an interatomic distance of 0.22 nm that can be assigned to the (2,2,0) family of planes associated to the cubic phase of the $MAPbBr_3$. The HRETM images also allowed an analysis of the size distribution of the $MAPbBr_3$ nanocrystals for two distinct samples prepared from 5w% and 20% precursor solution.

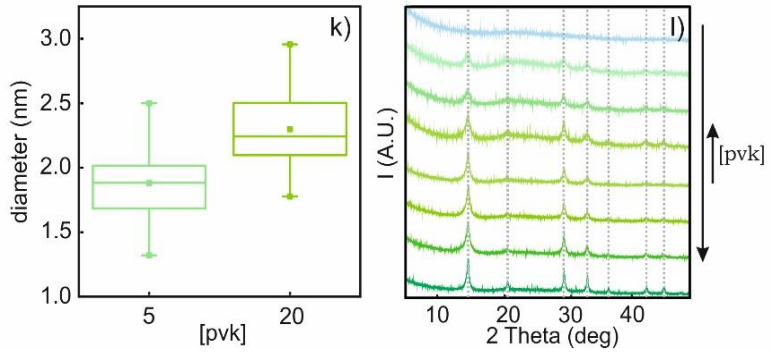

Figure 2.3.2 k) Boxplot of the size distribution of $MAPbBr_3$ nanocrystals prepared from a 5wt% and 20wt%precursor solutions infiltrated in the porous film; l) XRD diffractograms obtained from different encapsulated $MAPbBr_3$ nanocrystals prepared from precursor solution with different concentration. Grey dashed lines indicate the reference $MAPbBr_3$ bulk reference pattern.

The result shown in the figure 2.3.2k is an average diameter, respectively of 1.8 and 2.3 nm, which further confirms the control over the nanocrystals size, as the concentration of the perovskite precursor increases.

To complete the structural characterization, X-ray diffraction analysis of the SiO_2@$MAPbBr_3$ samples synthesized with different initial concentrations is shown in figure 2.3.2l In order to obtain a sufficient signal from the nanocrystals encapsulated in the matrices, the technique of grazing incidence wide-angle X-ray diffraction (GIWAX) was employed. In all cases, the diffractograms reveal the presence of $MAPbBr_3$ perovskite peaks and a gradual narrowing of the (110) peak (2θ=14.09°) as the concentration of the precursors increases. By extension, in the figure 2.3.2m-r the X-ray diffractograms of the three main perovskite compositions prepared in this work, $MAPbI_3$, $MAPbBr_3$ and $FAPbBr_3$ are presented compared with the respective crystallographic patterns[32-34] and together with each nanocrystal micrograph. In all the cases, the presence of a broad diffraction signal in the 2theta range of 15-40 due to the SiO_2 layer is also evident.

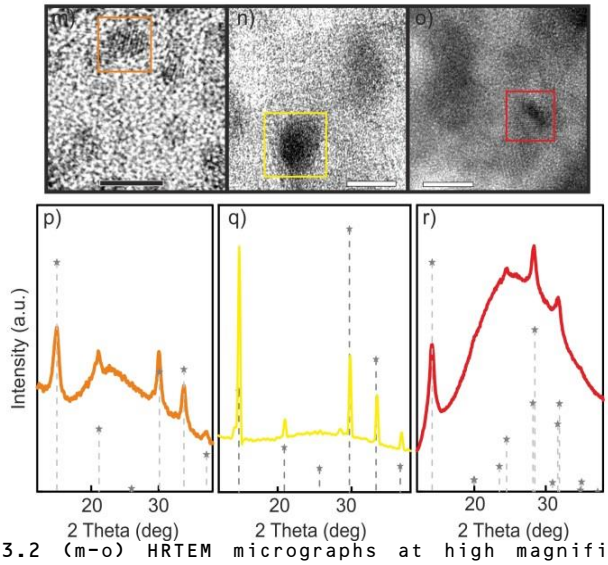

Figure 2.3.2 (m-o) HRTEM micrographs at high magnification of m) $MAPbBr_3$, n) $FaPbBr_3$, o) $MAPbI_3$ nanocrystals synthetized with templated method in the SiO_2 nanoparticles porous film; scale bar is 5 nm in m) and 10 nm in n) and o). (p-r) XRD patterns obtained from the three different perovskite compositions encapsulated in the SiO_2 nanoparticles matrix: p) $MAPbBr_3$, q) $FaPbBr_3$ and r) $MAPbI_3$ nanocrystals compared with the corresponding pattern from the literature (dashed lines).

2.4 NANOCRYSTALS GROWTH

The preparation of ABX_3 nanocrystals through the matrix assisted method have a further secondary advantage compared to colloidal systems. Taking advantage of the optical transparency of the matrix, the absence of ligands and the correlation between bandgap and size of the nanocrystals, it is possible to track the growth profile of the ABX_3 nanocrystals population inside the pores of the scaffold by monitoring the spectral change of the photoluminescence in time (see figure 2.4). This type of analysis can, in fact, contain information on the number of nanocrystals that are forming and on their quality (intensity of the PL, I_{PL}), on their diameter (spectral position of the maximum of PL, λ) and on the size distribution (amplitude of the PL, FWHM).

For a similar study, in the case of nanocrystals synthesized in solution it is necessary to extract aliquots at different reaction times or introduce microfluidic adaptations in the experimental process that can affect the measurements.[35,36] In any case it is not possible to monitor the whole process on the same population of crystals. The in situ analysis, however, also allows investigating the effect of other factors such as illumination, temperature and concentration, as will be illustrated in the following paragraphs. A clearer view of the growth process can certainly be

useful for optimizing the synthesis method, refining the theoretical models and studying and predicting the behaviour of these semiconductors in order to improve the reproducibility of the preparation.

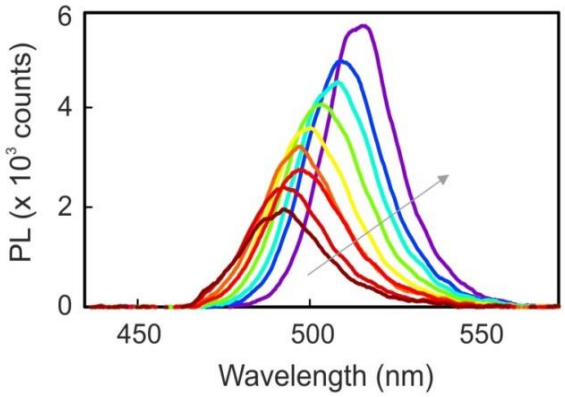

Figure 2.4 Series of photoluminescence spectra obtained from in-situ measurements at different time during the $MAPbBr_3$ nanocrystal growth inside the SiO_2 porous matrix. The arrow indicates increasing times.

2.4.1 Growth analysis

For this study, perovskite precursor solution was deposited by spin coating on top of the porous matrix at 5000 rpm, but just for 10s. The film infiltration was performed in the glovebox under inert atmosphere and then taken outside for the optical characterization without any thermal treatment. Heating accelerates the evaporation of the solvent and therefore the crystallization. Synthesis at room temperature was initially considered as a way to slow down and monitor the perovskite crystal formation process with a better accuracy. Upon depositing the precursor solution on the mesoporous matrix, nucleation takes place already during the spin-coating process. This nucleation stage is much faster than we could resolve in our experiment (5s). A change in colour, from the transparent appearance of the matrix infiltrated with the precursor solution to the greenish characteristic of the SiO_2@$MAPbBr_3$ system, is already observed in the infiltrated porous matrix when the spin coater is stopped. Following this initial stage, nanocrystals growth takes place within the pores of the matrix containing remains of the initial amount of solvent. For the emission monitoring we made use of a pulsed 405 nm laser beam (900 ps pulse duration) exciting a 100 µm spot of the sample. Then photoluminescence was collected with a fiber-coupled spectrometer (Ocean Optics USB2000). An optical set-up was built with two identical optical paths in order to measure to parts of the same sample in different conditions. The "blind" interval between the deposition stop and the first PL measurement was kept under one minute, while the PL was recorded with an integration time of 300 ms to ensure

sufficient precision but to be able to temporally separate the different phases of the growth. For those measurements demanding a reference measurement the sample was cut in two parts right after the spin coating and before taking it out of the glovebox. The figure 2.4.1abc shows the evolution of λ, I_{PL} and FWHM of the photoluminescence measurement as a function of time during the formation of $MAPbBr_3$ nanocrystals prepared from a 20 wt% precursor solution.

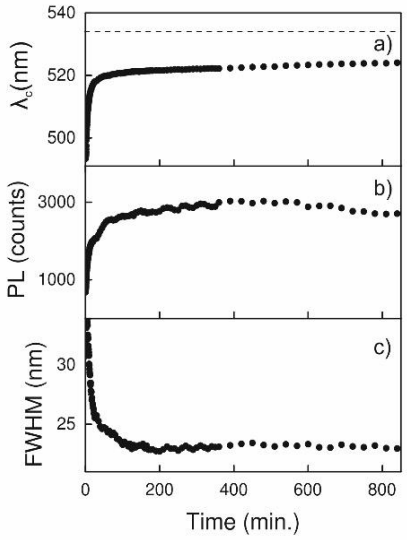

Figure 2.4.1 Time evolution of the photoluminescence peak a) spectral position, b) intensity and c) FWHM measured from a composite SiO2@ $MAPbBr_3$ sample prepared with a 20 wt% perovskite precursor solution. The horizontal dashed line in a) marks the spectral position of $MAPbBr_3$ bulk thin-film emission.

A red-shift of the peak position can be observed (from 495 nm to 525 nm) which indicates an increase in the size of the nanocrystals, without however reaching the typical position of the bulk emission thanks to the spatial confinement in the porous matrix. The monotonic increase in intensity, on the other hand, can be associated with both an increase in size and an increase in the number of emitting nanocrystals or even an improvement in quantum yield. At the same time, the FWHM undergoes a reduction from 33 nm to 23 nm normally attributed to a minimization of the nanocrystals size dispersion, or focusing,[37] which can be related to the increase in the size of the nanocrystals. The observed values of the PL FWHM are however comparable to those reported in the case of colloidal crystals and therefore indicative of a minimum dispersion of NC size.[38] As previously mentioned, the kinetics of crystallization within a porous matrix is dependent on the diffusion of the reactive species through the network of voids and also on their amount in a given volume of solvent. During the process, both solvent and precursors are subtracted because of evaporation and incorporation into nanocrystals, respectively. This is in contrast to colloidal synthesis where the solvent volume remains constant and just the precursors undergo a monotonic decrease as they are consumed through the

nanocrystals growth. At this point, to try to rationalize this process, using an analytical model, it is obviously more convenient to translate the photoluminescence spectral shift into the actual variation of nanocrystals size through the Brus equation (see equation 2 in chapter 1). For this calculation the nanocrystals size extrapolated from the TEM analysis have been used as a reference, together with the gap energy obtained from the PL, and a dielectric constant of 4.2, already reported in the literature,[39] and a reduced mass of $0.65m_0$. The latter parameter is in good agreement with the increase in binding energy reported for quantum dots[40] considering the expression

$$E_B = \varepsilon_r^2 \frac{\mu}{m_0} R_H \qquad (1)$$

valid for dimensions much lower than the Rydberg constant (R_H). The result shows an increase in the radius from 1.2 to 1.5 nm, as shown in the figure 2.4.1d(log).

To analyse this behaviour we used Lifshitz–Slyozov–Wagner (LSW) theory[41,42] through the expression:

$$R = R_0 + k(t - t_0)^{1/n} \qquad (2)$$

where R (R_0) is the radius at time t (t_0), k is a temperature-dependent reaction constant, and *n* is a parameter indicating whether the nanocrystals growth is being limited by crystallization reaction at the NC surface (n=2), diffusion of the precursors toward the NC surface (n=3) or re-dissolution of nanocrystals with a size below a given critical radius (n=4). This simplification derives from Wagner's notation

$$\tau = \frac{\nu r^2 RTkr + D}{2\sigma c_0 V_m^2 kD} \qquad (3)$$

Where ν is a stoichiometric factor, R the gas constant, T the temperature, σ the interfacial tension, c_0 the initial concentration, V_m the molar volume, k the temperature dependent reaction constant and D the diffusion coefficient. Within this model, three different limiting conditions or regimes can be distinguished: $k \cdot r \ll D$ (growth limited by phase transition reaction) in which the growth is expected to depend as a square root on time (**n=2**); $k \cdot r \gg D$ (diffusion limited) where the growth is expected to depend as a third root on time (**n=3**); and if the process is limited rather by interfacial than by volume diffusion and the dissolution of smaller particles controls the process, the growth is expected to depend as a fourth root on time (**n=4**).

Finally, we fitted the growth actually imposing that the different regimes would follow the sequence n=2-3-4, basically considering the pores volume as an environment initially rich in solvent in which the diffusion of the precursors is favoured, but that evaporation transforms into a poorly diffusive system. In the first stage it can therefore be imagined that $k \cdot r \ll D$ and the kinetics is governed by the liquid-solid phase transition reaction. Subsequently, the decrease in the diffusion coefficient turns $k \cdot r \gg D$ and so the diffusion controls the growth. In the final step, the

limiting process of crystallization becomes the re-dissolution of the smallest particles. In general, the fitting procedure was carried out using average values of k although it should vary over time and furthermore the dependence with the different powers is not applicable in the transition between two regimes. In any case, what can be extrapolated from this analysis is the evident change of limiting regimes, during the growth of the nanocrystals since the fitting to a single exponent was not applicable.

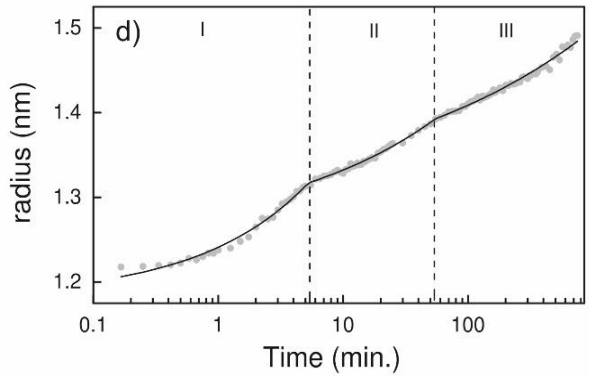

Figure 2.4.1 d) Time evolution of perovskite nanocrystals radius (estimated from Brus equation and following the PL peak position), during the growth (grey dos). Black lines correspond to the fittings with the Lifshitz– Slyozov–Wagner (LSW) model.

2.4.2 Effect of precursors concentration

We have next considered the role of precursor concentration in the growth kinetics, because, as shown previously the nanocrystals size, in the present synthesis technique, can be controlled through concentration of the spin-coated solution on the porous matrix. Figure 2.4.2ab displays results for samples grown using 20 wt%, 5 wt% and 3 wt% solutions, which leads to nanocrystals emitting in 524 nm, 516 nm, and 512 nm (λ_c) upon completion of the process. From 2.4.2a, it is evident that decreasing the concentration not only leads to a smaller nanocrystal size but also to a slower growth kinetics, as expected because of a reduced amount of precursors in the solution. Interestingly, the evolution of the size dispersion of the nanocrystals is also affected as evidenced by the results presented in figure 2.4.2b. Here, it is clear how the final FWHM increases as the precursor concentration decreases.

Further, the time evolution of the FWHM also changes with precursor concentration. This can be clearly seen in Figure 2.4.2c where FWHM, related with size dispersion, is plotted against λ_c, given by the NC size. As the concentration of precursor solution is reduced, the nanocrystal size dispersion goes from a focusing to a defocusing scenario. The above trends in the evolution of FWHM with precursor concentration

are similar to the outcome of Monte-Carlo numerical simulations employed by Talapin and co-workers to reproduce the colloidal synthesis of nanocrystals.[43]

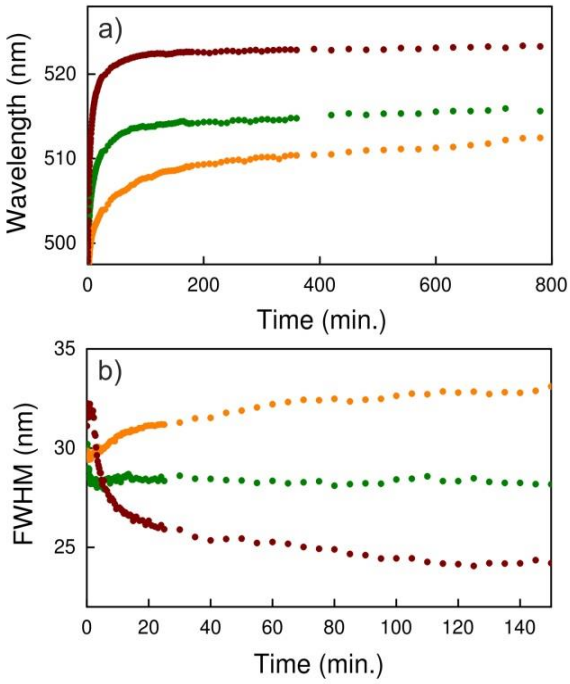

Figure 2.4.2 Time evolution of the spectral position a) and FWHM b) of the PL peak measured from composite SiO_2@$MAPbBr_3$ samples prepared with a 3% (orange dots), 5% (green dots), and 20 wt% (red dots) concentrated solutions of perovskite precursors in DMF.

There, in the presence of large amounts of precursor, a focusing of the nanocrystals size dispersion takes place in the initial stages of the process, where a population of small NCs is present, followed by a defocusing once the precursor concentration drops below a certain threshold level and Ostwald ripening dominates nanocrystal growth. In our case, when using the highest precursor concentration (20 wt%), after an initial growth in which the FWHM hardly changes, a strong focusing takes place, reducing the FWHM from 32 nm to 24 nm.

However, the precursor concentration never drops below the threshold concentration, for which NC dissolution starts and defocusing kicks in, likely because NC growth takes place together with solvent evaporation. For the intermediate case (5 wt%), precursor concentration is never large enough for the focusing process to complete and the NC growth stops in the initial stages of it. Finally, for the lowest concentration (3 wt%), the amount is initially below the threshold, leading to a defocusing, which stops once the concentration goes above the threshold level. Here, the growth process is completed when the concentration is still low and defocusing has barely started.

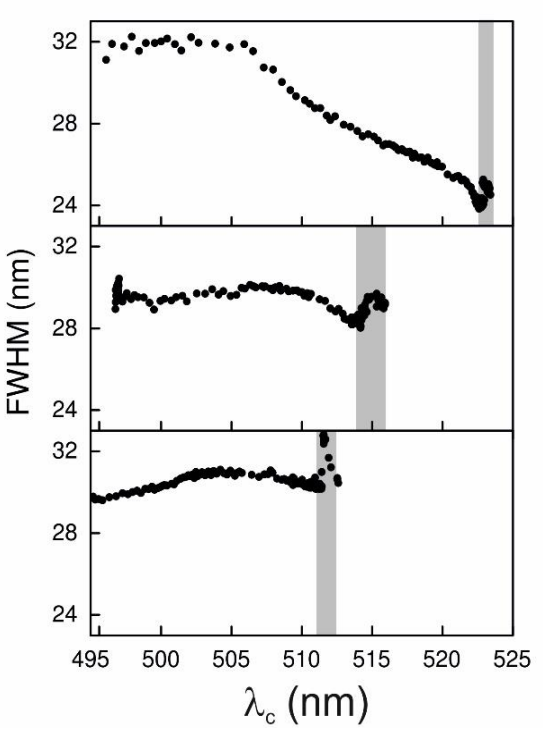

Figure 2.4.2 c) Variation of the FWHM as a function of λ_c for different precursor concentrations: 20wt% (top), 5wt% (middle) and 3wt% (bottom). Grey portions correspond to the final stages of NC growth where external illumination is reduced.

2.4.3 Effect of temperature

The role of temperature on the growth kinetics was also explored by simultaneously probing the emission from two halves of the same porous matrix infiltrated with a 20 wt% solution and placed on the two arms of the optical set-up where one of them contained a hot plate at a fixed temperature. For the case of bulk thin films, temperature has been known as a key factor during the synthesis process to induce crystallization[44]. For the case of colloidal nanocrystals, the two most widespread approaches, that is, hot injection and ligand assisted re-precipitation, take place at elevated temperatures or room temperatures, respectively (see chapter 1). Several recent works have considered the role of temperatures (RTs) on different colloidal-based synthesis of LHP NCs. It was found that, whereas increasing T leads in general to a faster growth, the final NC size can be smaller[45-47] or larger[48] than those grown at RT, depending on whether fully inorganic or hybrid organic-inorganic NCs are grown. Here, we have considered the growth for RT and 75 °C in order to evaluate the role of this parameter. Figure 2.4.3a shows the time evolution of the PL peak position and figure 2.4.3b its FWHM for the two temperatures under

consideration. Here, it is evident that increasing T lowers the growth rate and leads to a smaller final nanocrystal size, highlighted by a lower λ_c.

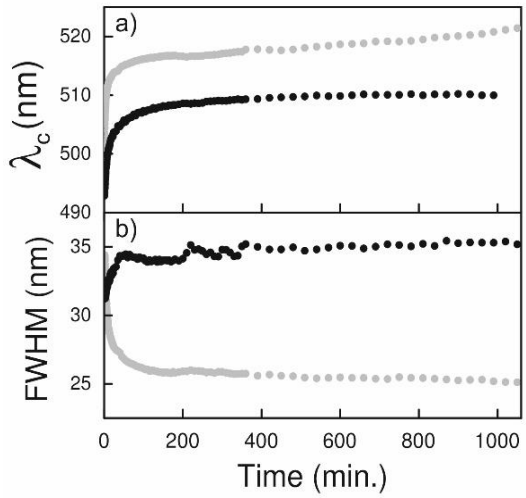

Figure 2.4.3 Time evolution of the spectral position a) and FWHM b) of the PL peak measured during the growth process at room temperature (grey dots) and 75°C (black dots) from a composite SiO_2@$MAPbBr_3$ sample prepared with a 20 wt% precursor solution.

Further, increasing T leads to a defocusing behaviour with the FWHM undergoing a rapid increase from the initial stages of monitoring. Please note that rising T gives rise to two phenomena that have opposite effects on the growth rate. On the one hand, it causes diffusion to enhance, which should imply a higher growth rate. On the other, it induces a faster solvent evaporation, which hinders growth. Our observations indicate that the latter effect prevails over the former, leading to a scenario where monomer diffusion is drastically reduced by evaporation so that growth and size focusing are quenched. Another interesting conclusion of this analysis is that limiting the synthesis volume by using nanoreactors forces crystallization even at RT, for which an incomplete reaction is known to take place for the case of their bulk counterpart.

2.4.4 Effect of illumination

In order to evaluate the role of illumination on the NC growth two samples were studied simultaneously again on the two arms of the optical set-up. One was illuminated following the pattern described in the table 2.4.4. The other was illuminated continuously for the first 360 minutes and then following the same pattern (region 7) as the reference one. Results for both samples are shown in figure 2.4.4a-c. Here it can be seen how nanocrystals growth takes place at a faster pace for the illuminated sample (see fig 2.4.4a) albeit reaching the same final nanocrystal size as evidenced by the coincidence of the spectral position of the PL

peak of both samples. This accelerated growth is accompanied by a slightly higher FWHM evidencing larger size dispersion (fig 2.4.4c).

Region	Duration	Measurement interval
1	0-1 min	5s
2	1-5 min	15s
3	5-15 min	30s
4	15-25 min	1 min
5	25-180 min	5 min
6	180-360 min	10 min
7	360-900 min	30 min

Table 2.4.4 Illumination protocol during the growth of $MAPbBr_3$ nanocrystals inside the SiO_2 porous film.

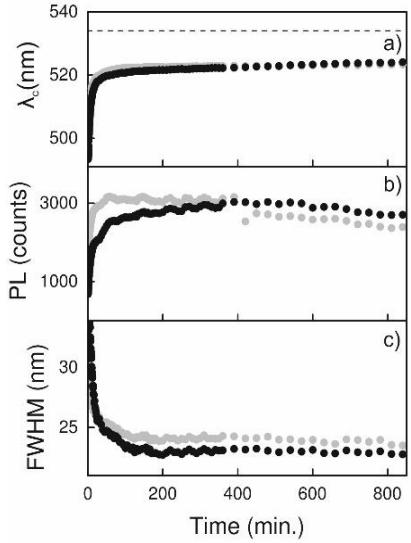

Figure 2.4.4 Time evolution of the a) spectral position, b) intensity and c) FWHM of the PL peak measured solution during the growth process under constant (grey dots) and partial illumination (black dots) from a composite $MAPbBr_3$@ SiO_2 sample prepared with a 20 wt% precursor.

While a definite explanation behind this difference in growth kinetics is not present at the time, the accelerated growth could have its origin on the formation of charged NCs upon defect-related trapping of charge carriers which can then interact with charged intermediate species.[49] Thus, for the results of figure 2.4.1, where irradiation time is 2 orders of magnitude below the constant illumination experiment, we expect a negligible effect of the probe light.

2.5 CONCLUSIONS

In this chapter a detailed overview of the method developed for the synthesis of perovskite nanocrystals has been presented. The structural characterization clearly describes the architecture of the composite materials and confirms the ability, with these systems to control the size of the nanocrystals while at the same time obtaining a homogeneous distribution in a thin film, without suffering from phenomena of self-aggregation of the particles. With these materials, as we have seen, it is possible to shed some light on the crystallization mechanism thanks to an easy *in-situ* approach. The synthesis method was adjusted in order to obtain an homogeneous distribution of perovskite nanocrystals throughout the sample but still be able to analyse the early stage of their growth. Finally, based on our observations, we proposed a growth mechanism for lead halide perovskite nanocrystals within metal-oxide mesoporous matrices where precursor concentration varies according to NC growth (deploys precursor concentration as it is incorporated into the NC surface) and solvent evaporation (increasing precursor concentration). The effect of the different parameters under consideration on the observed kinetics will depend on the way they affect these two processes. In this sense, a number of guidelines can be provided in order to optimize NC growth in this type of matrices. Regarding concentration, which has shown to be an effective way to tune the NC size, if one wants to maintain the ensemble size dispersion, a better approach can be the use of a smaller pore size in the matrix (see versatility in section 2.2.4), as changing the pore size has been shown to be an effective way to control the NC size. Further, for a given pore size, high precursor concentrations will lead to lower size dispersions although a compromise will have to be found in order not to introduce an over-layer of bulk material. As far as the reaction temperature is concerned, contrary to the bulk synthesis, RT conditions will provide the appropriate balance between growth dynamics and evaporation rate to yield high-quality larger NCs. Whereas the present study is restricted to the growth of $MAPbBr_3$ NCs, a similar mechanism is expected for other material compositions and solvents although, because of different solubility or lead-to-halide affinity, the dynamics could vary. It should be mentioned that, although out of the scope of the present work, a relevant factor to be considered in the future is the role of the surrounding atmosphere. For the case of perovskites in the shape of thin films, the role of the atmosphere during material fabrication on film morphology and optoelectronic properties has been studied over the past years.[50–52] For the case of perovskite nanocrystals growth within nano-reactors, the surrounding atmosphere will certainly play a relevant role not only in the formation of the material itself but also in the modification of the metal-oxide scaffold.

2.6 BIBLIOGRAPHY

1 REHMAN, WAQAAS, ET AL. PHOTOVOLTAIC MIXED-CATION LEAD MIXED-HALIDE PEROVSKITES: LINKS BETWEEN CRYSTALLINITY, PHOTO-STABILITY AND ELECTRONIC PROPERTIES. ENERGY & ENVIRONMENTAL SCIENCE, 2017, 10.1: 361-369.

2 SALIBA, MICHAEL, ET AL. CESIUM-CONTAINING TRIPLE CATION PEROVSKITE SOLAR CELLS: IMPROVED STABILITY, REPRODUCIBILITY AND HIGH EFFICIENCY. ENERGY & ENVIRONMENTAL SCIENCE, 2016, 9.6: 1989-1997.

3 DUAN, JIALONG, ET AL. INORGANIC PEROVSKITE SOLAR CELLS: AN EMERGING MEMBER OF THE PHOTOVOLTAIC COMMUNITY. JOURNAL OF MATERIALS CHEMISTRY A, 2019, 7.37: 21036-21068.

4 AVA, TANZILA TASNIM, ET AL. A REVIEW: THERMAL STABILITY OF METHYLAMMONIUM LEAD HALIDE BASED PEROVSKITE SOLAR CELLS. APPLIED SCIENCES, 2019, 9.1: 188.

5 YUAN, MINGJIAN, ET AL. PEROVSKITE ENERGY FUNNELS FOR EFFICIENT LIGHT-EMITTING DIODES. NATURE NANOTECHNOLOGY, 2016, 11.10: 872-877.

6 CORTECCHIA, DANIELE, ET AL. WHITE LIGHT EMISSION IN LOW-DIMENSIONAL PEROVSKITES. JOURNAL OF MATERIALS CHEMISTRY C, 2019, 7.17: 4956-4969.

7 SHAMSI, JAVAD, ET AL. METAL HALIDE PEROVSKITE NANOCRYSTALS: SYNTHESIS, POST-SYNTHESIS MODIFICATIONS, AND THEIR OPTICAL PROPERTIES. CHEMICAL REVIEWS, 2019, 119.5: 3296-3348.

8 KOVALENKO, MAKSYM V.; BODNARCHUK, MARYNA I. LEAD HALIDE PEROVSKITE NANOCRYSTALS: FROM DISCOVERY TO SELF-ASSEMBLY AND APPLICATIONS. CHIMIA INTERNATIONAL JOURNAL FOR CHEMISTRY, 2017, 71.7-8: 461-470.

9 ZHANG, QIAO; YIN, YADONG. ALL-INORGANIC METAL HALIDE PEROVSKITE NANOCRYSTALS: OPPORTUNITIES AND CHALLENGES. ACS CENTRAL SCIENCE, 2018, 4.6: 668-679.

10 EXTANCE, ANDY. THE REALITY BEHIND SOLAR POWER'S NEXT STAR MATERIAL. NATURE, 2019, 570.7762: 429.

11 RUBINO, ANDREA, ET AL. MESOPOROUS MATRICES AS HOSTS FOR METAL HALIDE PEROVSKITE NANOCRYSTALS. ADVANCED OPTICAL MATERIALS, 2020, 8.9: 1901868.

12 ZHANG, HUI; TOUDERT, JOHANN. OPTICAL MANAGEMENT FOR EFFICIENCY ENHANCEMENT IN HYBRID ORGANIC-INORGANIC LEAD HALIDE PEROVSKITE SOLAR CELLS. SCIENCE AND TECHNOLOGY OF ADVANCED MATERIALS, 2018, 19.1: 411-424.

13 WANG, DONG-LIN, ET AL. HIGHLY EFFICIENT LIGHT MANAGEMENT FOR PEROVSKITE SOLAR CELLS. SCIENTIFIC REPORTS, 2016, 6: 18922.

14 MORA, LAURA VIVAR, ET AL. IMPACT OF SILICA NANOPARTICLES ON THE MORPHOLOGY AND MECHANICAL PROPERTIES OF SOL-GEL DERIVED COATINGS. SURFACE AND COATINGS TECHNOLOGY, 2018, 342: 48-56.

15 SHI, SHAOWEI, ET AL. ADVANCEMENTS IN ALL-SOLID-STATE HYBRID SOLAR CELLS BASED ON ORGANOMETAL HALIDE PEROVSKITES. MATERIALS HORIZONS, 2015, 2.4: 378-405.

16 HOWARD, IAN A., ET AL. COATED AND PRINTED PEROVSKITES FOR PHOTOVOLTAIC APPLICATIONS. ADVANCED MATERIALS, 2019, 31.26: 1806702.

17 CALVO, MAURICIO E.; MÍGUEZ, HERNÁN. FLEXIBLE, ADHESIVE, AND BIOCOMPATIBLE BRAGG MIRRORS BASED ON POLYDIMETHYLSILOXANE INFILTRATED NANOPARTICLE MULTILAYERS. CHEMISTRY OF MATERIALS, 2010, 22.13: 3909-3915.

18 CHAIKIN, PAUL. RANDOM THOUGHTS. PHT, 2007, 60.6: 8.

19 SONG, CHAOMING; WANG, PING; MAKSE, HERNÁN A. A PHASE DIAGRAM FOR JAMMED MATTER. NATURE, 2008, 453.7195: 629-632.

20 DENKOV, N., ET AL. MECHANISM OF FORMATION OF TWO-DIMENSIONAL CRYSTALS FROM LATEX PARTICLES ON SUBSTRATES. LANGMUIR, 1992, 8.12: 3183-3190.

21 PROSSER, JACOB H., ET AL. AVOIDING CRACKS IN NANOPARTICLE FILMS. NANO LETTERS, 2012, 12.10: 5287-5291.

22 LEE, WAI PENG; ROUTH, ALEXANDER F. WHY DO DRYING FILMS CRACK?. LANGMUIR, 2004, 20.23: 9885-9888.

23 GUPTA, RAMASHANKER, ET AL. ROOM TEMPERATURE SYNTHESIS OF PEROVSKITE (MAPBI3) SINGLE CRYSTAL BY ANTISOLVENT ASSISTED INVERSE TEMPERATURE CRYSTALLIZATION METHOD. JOURNAL OF CRYSTAL GROWTH, 2020, 125598.

24 ZHANG, WEI, ET AL. ULTRASMOOTH ORGANIC–INORGANIC PEROVSKITE THIN-FILM FORMATION AND CRYSTALLIZATION FOR EFFICIENT PLANAR HETEROJUNCTION SOLAR CELLS. NATURE COMMUNICATIONS, 2015, 6.1: 1-10.

25 BRYANT, DANIEL, ET AL. LIGHT AND OXYGEN INDUCED DEGRADATION LIMITS THE OPERATIONAL STABILITY OF METHYLAMMONIUM LEAD TRIIODIDE PEROVSKITE SOLAR CELLS. ENERGY & ENVIRONMENTAL SCIENCE, 2016, 9.5: 1655-1660.

26 YUN, JAE SUNG, ET AL. HUMIDITY-INDUCED DEGRADATION VIA GRAIN BOUNDARIES OF HC (NH2) 2PBI3 PLANAR PEROVSKITE SOLAR CELLS. ADVANCED FUNCTIONAL MATERIALS, 2018, 28.11: 1705363.

27 ANAYA, MIGUEL, ET AL. STRONG QUANTUM CONFINEMENT AND FAST PHOTOEMISSION ACTIVATION IN CH3NH3PBI3 PEROVSKITE NANOCRYSTALS GROWN WITHIN PERIODICALLY MESOSTRUCTURED FILMS. ADVANCED OPTICAL MATERIALS, 2017, 5.8: 1601087.

28 VOLFKOVICH, YU M., ET AL. THE STANDARD CONTACT POROSIMETRY. COLLOIDS AND SURFACES A: PHYSICOCHEMICAL AND ENGINEERING ASPECTS, 2001, 187: 349-365.

29 BAKLANOV, M. R., ET AL. DETERMINATION OF PORE SIZE DISTRIBUTION IN THIN FILMS BY ELLIPSOMETRIC POROSIMETRY. JOURNAL OF VACUUM SCIENCE & TECHNOLOGY B: MICROELECTRONICS AND NANOMETER STRUCTURES PROCESSING, MEASUREMENT, AND PHENOMENA, 2000, 18.3: 1385-1391.

30 LOZANO, GABRIEL, ET AL. THEORETICAL ANALYSIS OF THE PERFORMANCE OF ONE-DIMENSIONAL PHOTONIC CRYSTAL-BASED DYE-SENSITIZED SOLAR CELLS. THE JOURNAL OF PHYSICAL CHEMISTRY C, 2010, 114.8: 3681-3687.

31 GREGG SJ, SING KS, SALZBERG HW. ADSORPTION SURFACE AREA AND POROSITY. JOURNAL OF THE ELECTROCHEMICAL SOCIETY. 1967 NOV 1;114(11):279C.

32 XIE, JUNJIE, ET AL. STUDY ON THE CORRELATIONS BETWEEN THE STRUCTURE AND PHOTOELECTRIC PROPERTIES OF CH3NH3PBI3 PEROVSKITE LIGHT-HARVESTING MATERIAL. JOURNAL OF POWER SOURCES, 2015, 285: 349-353.

33 JAFFE, ADAM, ET AL. HIGH-PRESSURE SINGLE-CRYSTAL STRUCTURES OF 3D LEAD-HALIDE HYBRID PEROVSKITES AND PRESSURE EFFECTS ON THEIR ELECTRONIC AND OPTICAL PROPERTIES. ACS CENTRAL SCIENCE, 2016, 2.4: 201-209.

34 PERUMAL, AJAY, ET AL. HIGH BRIGHTNESS FORMAMIDINIUM LEAD BROMIDE PEROVSKITE NANOCRYSTAL LIGHT EMITTING DEVICES. SCIENTIFIC REPORTS, 2016, 6: 36733.

35 LIGNOS, IOANNIS, ET AL. SYNTHESIS OF CESIUM LEAD HALIDE PEROVSKITE NANOCRYSTALS IN A DROPLET-BASED MICROFLUIDIC PLATFORM: FAST PARAMETRIC SPACE MAPPING. NANO LETTERS, 2016, 16.3: 1869-1877.

36 MACEICZYK, RICHARD M., ET AL. MICROFLUIDIC REACTORS PROVIDE PREPARATIVE AND MECHANISTIC INSIGHTS INTO THE SYNTHESIS OF FORMAMIDINIUM LEAD HALIDE PEROVSKITE NANOCRYSTALS. CHEMISTRY OF MATERIALS, 2017, 29.19: 8433-8439.

37 THANH, NGUYEN TK; MACLEAN, N.; MAHIDDINE, S. MECHANISMS OF NUCLEATION AND GROWTH OF NANOPARTICLES IN SOLUTION. CHEMICAL REVIEWS, 2014, 114.15: 7610-7630.

38 HUANG, HE, ET AL. GROWTH MECHANISM OF STRONGLY EMITTING CH 3 NH 3 PBBR 3 PEROVSKITE NANOCRYSTALS WITH A TUNABLE BANDGAP. NATURE COMMUNICATIONS, 2017, 8.1: 1-8.

39 SAPORI, DANIEL, ET AL. QUANTUM CONFINEMENT AND DIELECTRIC PROFILES OF COLLOIDAL NANOPLATELETS OF HALIDE INORGANIC AND HYBRID ORGANIC–INORGANIC PEROVSKITES. NANOSCALE, 2016, 8.12: 6369-6378.

40 ZHANG, FENG, ET AL. BRIGHTLY LUMINESCENT AND COLOR-TUNABLE COLLOIDAL CH3NH3PBX3 (X= BR, I, CL) QUANTUM DOTS: POTENTIAL ALTERNATIVES FOR DISPLAY TECHNOLOGY. ACS NANO, 2015, 9.4: 4533-4542.

41 LIFSHITZ, ILYA M.; SLYOZOV, VITALY V. THE KINETICS OF PRECIPITATION FROM SUPERSATURATED SOLID SOLUTIONS. JOURNAL OF PHYSICS AND CHEMISTRY OF SOLIDS, 1961, 19.1-2: 35-50.

42 WAGNER, CARL. THEORIE DER ALTERUNG VON NIEDERSCHLÄGEN DURCH UMLÖSEN (OSTWALD-REIFUNG). ZEITSCHRIFT FÜR ELEKTROCHEMIE, BERICHTE DER BUNSENGESELLSCHAFT FÜR PHYSIKALISCHE CHEMIE, 1961, 65.7-8: 581-591.

43 TALAPIN, DMITRI V., ET AL. EVOLUTION OF AN ENSEMBLE OF NANOPARTICLES IN A COLLOIDAL SOLUTION: THEORETICAL STUDY. THE JOURNAL OF PHYSICAL CHEMISTRY B, 2001, 105.49: 12278-12285.

44 DUALEH, AMALIE, ET AL. EFFECT OF ANNEALING TEMPERATURE ON FILM MORPHOLOGY OF ORGANIC–INORGANIC HYBRID PERVOSKITE SOLID-STATE SOLAR CELLS. ADVANCED FUNCTIONAL MATERIALS, 2014, 24.21: 3250-3258.

45 LIGNOS, IOANNIS, ET AL. SYNTHESIS OF CESIUM LEAD HALIDE PEROVSKITE NANOCRYSTALS IN A DROPLET-BASED MICROFLUIDIC PLATFORM: FAST PARAMETRIC SPACE MAPPING. NANO LETTERS, 2016, 16.3: 1869-1877.

46 DONG, YITONG, ET AL. PRECISE CONTROL OF QUANTUM CONFINEMENT IN CESIUM LEAD HALIDE PEROVSKITE QUANTUM DOTS VIA THERMODYNAMIC EQUILIBRIUM. NANO LETTERS, 2018, 18.6: 3716-3722.

47 ZHANG, JIBIN, ET AL. GROWTH MECHANISM OF CSPBBR 3 PEROVSKITE NANOCRYSTALS BY A CO-PRECIPITATION METHOD IN A CSTR SYSTEM. NANO RESEARCH, 2019, 12.1: 121-127.

48 MACEICZYK, RICHARD M., ET AL. MICROFLUIDIC REACTORS PROVIDE PREPARATIVE AND MECHANISTIC INSIGHTS INTO THE SYNTHESIS OF FORMAMIDINIUM LEAD HALIDE PEROVSKITE NANOCRYSTALS. CHEMISTRY OF MATERIALS, 2017, 29.19: 8433-8439.

49 HU, QIN, ET AL. IN SITU DYNAMIC OBSERVATIONS OF PEROVSKITE CRYSTALLISATION AND MICROSTRUCTURE EVOLUTION INTERMEDIATED FROM [PBI 6] 4− CAGE NANOPARTICLES. NATURE COMMUNICATIONS, 2017, 8.1: 1-9.

50 RAGA, SONIA R., ET AL. INFLUENCE OF AIR ANNEALING ON HIGH EFFICIENCY PLANAR STRUCTURE PEROVSKITE SOLAR CELLS. CHEMISTRY OF MATERIALS, 2015, 27.5: 1597-1603.

51 EPERON, GILES E., ET AL. THE IMPORTANCE OF MOISTURE IN HYBRID LEAD HALIDE PEROVSKITE THIN FILM FABRICATION. ACS NANO, 2015, 9.9: 9380-9393.

52 ZHOU, XIN, ET AL. ROLE OF MOISTURE IN THE PREPARATION OF EFFICIENT PLANAR PEROVSKITE SOLAR CELLS. ACS SUSTAINABLE CHEMISTRY & ENGINEERING, 2019, 7.21: 17691-17696.

3 PEROVSKITE NANOCRYSTALS LINEAR OPTICS

3.1 INTRODUCTION

The analysis of the optical properties of semiconductors, in general, concerns a very large set of phenomena related to the interaction between these materials and electromagnetic radiation. It is possible to divide them according to the spectral range of the light used for the investigation.[1,2] It is also possible to group them according to the type of optical response and therefore the type of information that can be obtained on the semiconductor.[3,4] As shown in the previous chapter, in the case of perovskite nanocrystals analysed in this project, the optical response can provide, for example, indications on the size and crystal growth of the nanoparticles.[5] It is also possible to distinguish the properties by considering the type of physical phenomena that may be at their origin.[6] Regarding this, most of the optical properties of semiconductors are related to the nature of their band structure, but the type of crystalline lattice may also come into play or even, especially in the case of nanocrystals, the effects of quantum confinement. Finally, looking at the question from the point of view of technological applications, it is interesting to investigate also the most macroscopic properties, such as, for example, reflection, transmission or scattering of light.[7] As regards the perovskites nanocrystals, both colloidal and templated ones, the analysis of optoelectronic properties was immediately the subject of a very intense research activity which has already brought to light interesting results such as the size-dependent shift of the absorption onset[8,9] and the tuning of the band gap over the whole visible spectrum trough halide mixing,[10] the high photoluminescence quantum yield (PLQY),[11] the defect tolerance[12] and the strength of the exciton binding energies.[13] However, a lot still remains to be explored, keeping in mind that many optical response phenomena are also intrinsically linked to the synthesis method and the type of semiconductor conformation, both in terms of structure (colloidal dispersion in solution or solid dispersion in a matrix) and composition (for example, organic ligands or inorganic matrices). After examining the morphological characteristics of composite materials consisting of hybrid metal halide perovskite nanocrystals embedded in porous SiO_2-based matrices, in this chapter we will start to investigate some of their significant linear optical properties for their use as active material in actual optoelectronic device. Some of the characterizations, as we will see later,

are made possible thanks to the laminar morphology of these composite materials and the optical quality of the matrices, already mentioned in chapter 2.

3.2 PHOTOLUMINESCENCE AND QUANTUM YIELD

It is clear that the technological field for which perovskites in the form of nanocrystals have proved to be most promising and which encourages the efforts on their study is that of lighting.[14,15] Among the most acclaimed characteristics, responsible for the excellent light emission properties of perovskite nanocrystals, we find the tolerance to defects already discussed in the introductory chapter. This electronic property has a positive effect on the ability to emit photons because the energetic position of the defects does not affect radiative recombination of the electron-hole pairs.[16] The trapping of the charge carriers by the defects implies a dispersion of the electronic energy, generally by thermal processes and therefore does not contribute to the emission of the photons. [17] The tolerance of perovskites also translates into an improvement of the energy storage performance in solar cells by reducing the recombination of the charges and facilitating, in fact, their transport to the electrodes.[18] From the photoluminescence point of view, however, a favourable ratio between radiative and non-radiative decay means a more efficient optical response to the excitation. By also implementing passivation mechanisms on the surface of the nanocrystals, the improvement in photoluminescence was clearly evident with the very high PLQY values.[19] What makes the PL of perovskite nanocrystals particularly interesting and attractive, as previously mentioned, it is also the tuning of the bandgap as a consequence of the quantum confinement effect. From the chemical composition point of view, in fact, the lead chloride based blue emitting material suffer from poorer performance because of a reduced tolerance or to better say a much deeper defects with respect to bromide and iodide based species.[20] The quantum confinement of the green emitters is therefore a valid alternative to obtain an improvement of the emissions in the shorter wavelengths range as has already been observed both with bromide-based nanoplatelets and in templated systems.[21,22] Finally, another essential parameter, especially for LED applications, is the emission spectral width (full width at half maximum, FWHM). In the case of the photoluminescence measurements from colloidal nanocrystals, at room temperature, extremely competitive FWHM values were observed with respect to the most common inorganic quantum dots.[23,24] This, however, especially concerns the suspensions in solution, while once being deposited, these colloidal systems

normally suffer from a broadening of the PL, typical of a larger polydispersity in the size of the nanocrystals, or even a red shift towards the bulk emission.[25,26]

3.2.1 Perovskite NCs emission spectral tuning

As already demonstrated in the previous chapter, the variation in concentration of the precursor solution infiltrated into the porous matrix allows us to shift on demand the bandgap of the encapsulated perovskites.

The PL of the materials in bulk form corresponds to the emission of a thin film prepared with the same solution of precursors with the highest concentration. In this case, the crystallization proceeds without spatial limitations to the crystal growth and the concentration only determines the thickness of the perovskite polycrystalline film. In consequence, the spectral position of the bulk thin films varies only slightly for very low concentrations as it can be seen in figure 3.2.1a for the case of $MAPbI_3$.

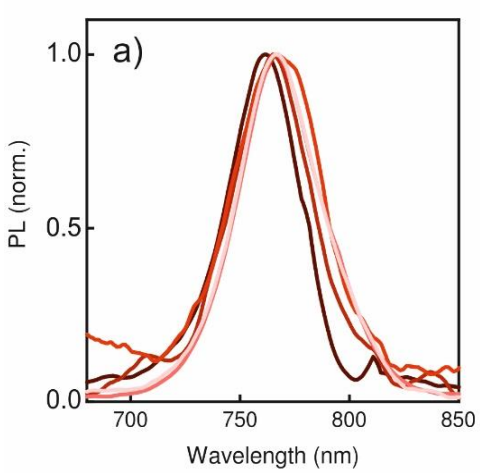

Figure 3.2.1 a) Normalized Pl emission from polycrystalline bulk films of $MAPbI_3$ prepared using perovskite precursor solution with different concentration: from 40 wt.% (light red curve) to 5 wt.% (darker red curve).

In the figure 3.2.1b it is possible to observe an example of the range of tuning possibilities in the case of $MAPbI_3$ and $MAPbBr_3$ infiltrated in the matrix described in chapter 2, concretely covering the blue-green and red regions of the visible spectrum.

Regarding the nanocrystals the linewidth of the emission is comparable, in both cases (green and red), with the results obtained for colloidal systems that is around 30 nm in the green region and around 50 nm in the red region, in both cases in the order of 90 meV. To observe the blue shift in more detail, the figures 3.2.1c and d

collect the spectral values of the maximum of the emission peak as a function of each concentration, in the case $MAPbI_3$ and $MAPbBr_3$ NCs, respectively.
Accordingly, a similar displacement of the photo-excitation edge can be seen in figure 3.2.1e. The sharp edge near the photoexcitation threshold confirms the narrow nanocrystal size distribution achieved in each infiltrated SiO_2 nanoparticle scaffold, also corroborated by the displacement of the absorption edge (see section 3.5.1).

.

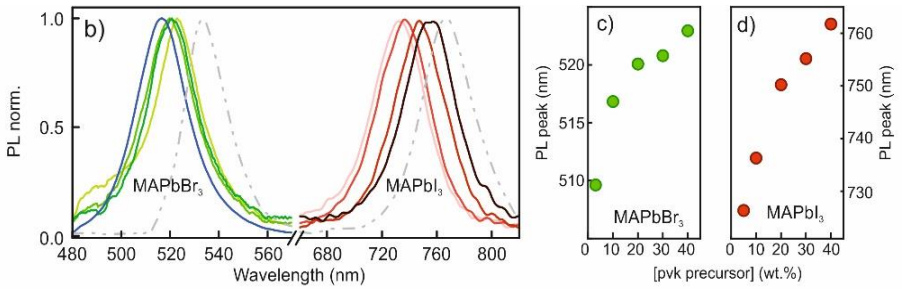

Figure 3.2.1 b) Normalized PL spectra of $MAPbBr_3$ (left greenish-blur curves) and $MAPbI_3$ (right reddish-brown curves) nanocrystals synthesized inside SiO_2 nanoparticles porous film. In both case the emission shifts towards shorter wavelengths with respect to the bulk PL spectral position (grey dashed lines) as the precursor solution concentration decrease. With this size control over perovskite nanocrystals it is possible to cover almost 160 meV in the green-blue and in the red part of the visible frequencies; PL maximum recorded for confined $MAPbBr_3$ NCs (c) and $MAPbI_3$ NCs (d) prepared using the same precursor solution as in b).

In this first part concerning the properties related to the photoluminescence of perovskite nanocrystals synthesized in porous matrices, the characterization was centred on bromine-based perovskites ($MAPbBr_3$) as the best emitters. In addition to a more intense PL, the study is also linked to the problem, already mentioned in the introduction, of the emission in the blue range and to the search for a solution through the quantum confinement of the green emitters.
The photoemission measurements were conducted using a fiber coupled spectrophotometer in which a continuous wave pump laser beam was focused with an achromatic lens producing a spot size of 250 μm^2. The excitation wavelength was selected at 450 nm for bromine-based compounds and 530 nm for iodine-based perovskites. Photo-excitation spectra were collected using a fluorometer (Fluorolog-3 from Horiba) with a double monochromator and a spot of 1×1 cm, in a front-face configuration. Finally, in figure 3.2.1f we show how it looks a series of porous SiO_2 films of identical thickness infiltrated with different concentrations of $MAPbBr_3$ precursors under ultraviolet irradiation. Images show a gradual change in the emitted colour, perceivable by the naked eye, from the neatly green emission of the larger nanocrystals to the bluish of the smallest ones. The uniformity of the

bright emission observed throughout the film surface also confirms the homogeneous infiltration over large areas.

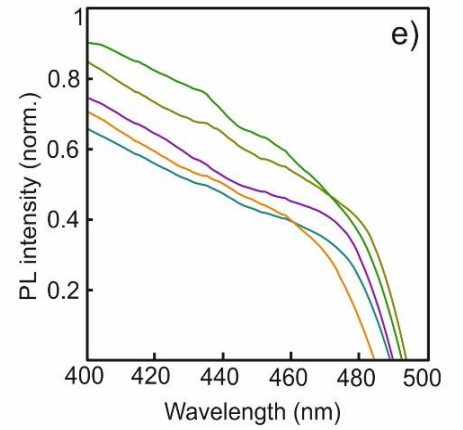

Figure 3.2.1 e) Normalized photoexcitation spectra from $MAPbBr_3@SiO_2$ samples obtained using 40 wt.% (green line), 30 wt.% (dark green line), 20 wt.% (purple line), 10 wt.% (blue line) and 5 wt.% (orange line) concentrated perovskite precursor solutions.

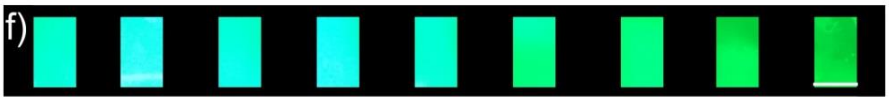

Figure 3.2.1 f) Camera photos of $MAPbBr_3@SiO_2$ samples exposed to UV light (312nm). The concentration of precursor solution employed for perovskite synthesis inside the porous matrix decreases from right (larger nanocrystals) to left (smaller nanocrystals). Scale bar is 1 cm. The images were collected using a digital camera photograph.

3.2.2 PLQY of perovskite NCs

As a more quantitative determination of the efficiency of the photoluminescence obtained from $MAPbBr_3$-based composite materials, we analysed the PL quantum yield, understood as the ratio between photons emitted and absorbed. PLQY measurements were carried out using the Hamamatsu C9920-02 absolute PLQY system that presents a xenon lamp, a monochromator, and an integrating sphere. The excitation wavelength was set to 450 nm. As can be seen from figure 3.2.2, the analysis of PLQY as a function of the concentration of the precursors reveals a strong dependence with respect to the nanocrystals size, presenting a maximum corresponding to the 1.8 nm NCs of $MAPbBr_3$ prepared at 5w% (see chapter 2), with a 35% of QY.

Even if it can be counterintuitive, considering the increase in surface to volume ratio and therefore defects density, in nanocrystals, the occurrence of a bright point as a function of particle size has also been observed in nanocrystalline colloidal semiconductors[27] as well as, in particular, in Cs-based perovskites.[28] As we know, the increase in the exciton binding energy of the nanocrystals promotes radiative

recombination and therefore improves the efficiency of the radiative emission with respect to the polycrystalline bulk material, but the increase in the surface area of the nanocrystals implies a larger number of trap states.[29] Therefore the observed trend of the QY results from the balance of different opposing phenomena.

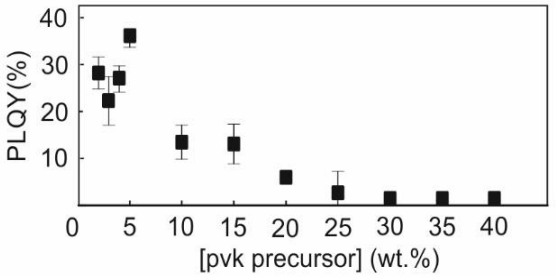

Figure 3.2.2 Photoluminescence Quantum Yield (PLQY) measured for $MAPbBr_3@SiO_2$ composite systems prepared with different initial precursor concentration (wt%).

3.2.3 Modification of the optical environment

From the point of view of the fundamental study and the characterization of the composite systems presented here, films with a more accessible porosity and the absence of ligands around the nanocrystals offer the possibility of exploring the effects of the photonic environment on perovskite nanocrystals. More concretely, for the materials of this work, we tested the effects of a polymer infiltration, also attractive for an ulterior motive illustrated in the next section. For the moment it is interesting to note that the excess of empty volume left after the infiltration of the perovskites allowed the permeation and the expansion of a polymer, poly(dimethylsiloxane) (PDMS). The results of materials composed of $MAPbBr_3$, SiO_2 and PDMS revealed an increase in PLQY with respect to the materials without PDMS (see figure 3.2.3a). In order to analyse how the emission of nc-$MAPbBr_3$ is affected once the pores are filled with PDMS, we measured the PL decay dynamics of both nc-$MAPbBr_3@SiO_2$ and PDMS@nc-$MAPbBr_3@SiO_2$ films. PL decays were measured in the same optical setup used for static PL, using a pulsed light source (Fianium SC400) in concert with a time-correlated single photon counting module (FluoroHub) and deconvoluted by means of the same measuring device. Decay curves were fitted making use of a continuous distribution in the form of a lognormal

$$\rho(\Gamma) = \frac{1}{\sigma\Gamma\sqrt{2\pi}} e^{-\frac{(ln\Gamma*\mu)^2}{2\sigma^2}} \qquad (1)$$

This distribution of the decay rates ($\rho(\Gamma)$ is centered in a most frequent value, Γ, (mode) equal to

$$\Gamma = e^{(\mu-\sigma^2)} \qquad (2)$$

A selection of the decay curves attained is displayed in a log-log plot in figure 3.2.3d. It can be readily seen that the PL of nanocrystals decays faster as a result of

the presence of PDMS in the pores. This effect is discussed next on the basis of the expected changes in the local optical environment of the emitters. Using the expression that relates QY with the decay rates $QY = \Gamma_R / (\Gamma_R + \Gamma_{NR})$ (being Γ_R and Γ_{NR} the radiative and non-radiative components of the total, measured, decay rate Γ, respectively), we can estimate Γ_R and Γ_{NR} for each composite film. The results are shown in figure 3.2.3b and c respectively.

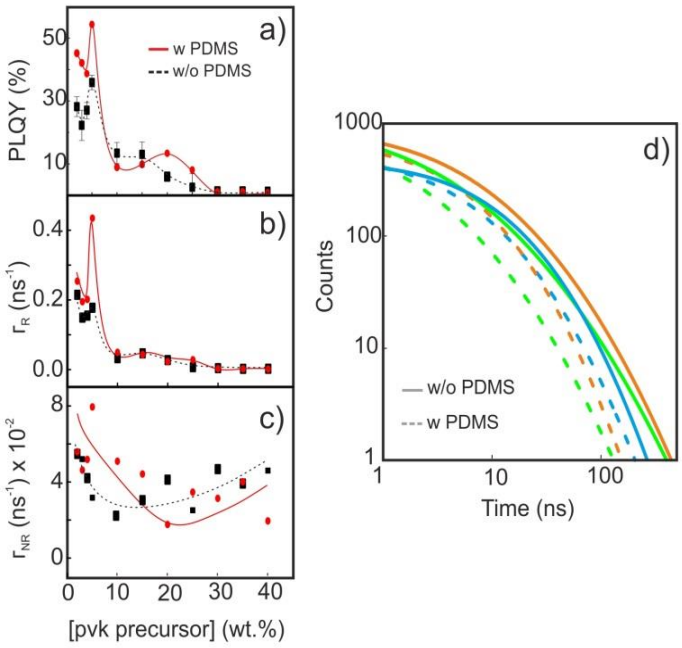

Figure 3.2.3 Concentration dependence of a) PLQY, b) radiative decay and c) non-radiative decay rates values measured for $MAPbBr_3@SiO_2$ samples prepared with (red dots) and without (black dots) PDMS polymer infiltration. Solid and dashed lines are just guidelines used to draw attention to the trend. d) Decay curves from $MAPbBr_3@SiO_2$ samples prepared with (dashed lines) and without (solid lines) PDMS from precursors solution concentrated at 2 wt.% (blue curve), 5 wt.% (orange curves) and 10 wt.% (green curves).

Our analysis indicates that non-radiative decay pathways are not altered significantly by PDMS infiltration consequently the improvement of QY observed is due to the enhancement of radiative pathways. This feature occurs when the refractive index of the environment of an emitter is increased.[30] The decay rate, $\Gamma(r)$, corresponding to the transition of the direct gap depends on the local density of states (LDOS) according to the expression:

$$\Gamma(r) = \frac{2\omega_g}{3\hbar\varepsilon_0}|\mu|^2\rho(r,\omega_g) \qquad (3)$$

where ω_g is the angular frequency, ε_0 the permittivity in vacuum, μ the dipole moment and $\rho(r, \omega_g)$ the LDOS. More precisely, we find that nanocrystals prepared at the lower concentrations (2 wt% < [PVK] <5 wt%) show Γ_{R1} = 0.0177 ns^{-1} without

PDMS and Γ_{R2} = 0.0434 ns^{-1} with PDMS infiltration. Hence, Γ_{R1} / Γ_{R2} = 0.408, which is very close to the fifth power of the ratio of the refractive indexes of the two optical environments (porous SiO_2 and PDMS), as predicted by the theory.[31]

3.2.4 Manipulation of decay pathways

As a complement to the structural versatility of the method in terms of materials employed for the fabrication of porous matrices, we also studied their effects on the photoluminescence of the nanocrystals. In particular, systems composed of SiO_2 nanoparticles of different diameters, TiO_2 and SnO_2 nanoparticles were examined. As previously noted (chapter 2), the variation in the diameter of the silica particles leads to a reduction in the inter-particle spaces (if the aggregation state remains constant in both cases). The direct consequence is a reduction in the size of the nanocrystals and a more pronounced displacement of the PL from the bulk emission.

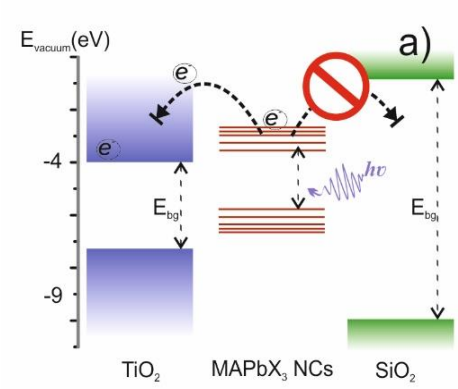

Figure 3.2.4 a) Electrons injection scheme of a TiO_2 or SiO_2@perovskite ($MAPbX_3$) structure.

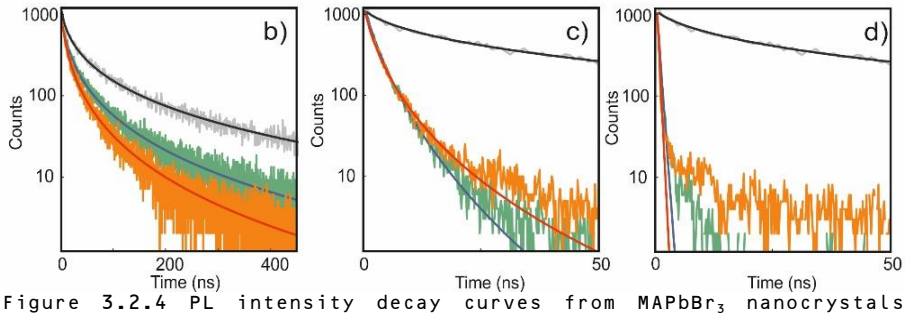

Figure 3.2.4 PL intensity decay curves from $MAPbBr_3$ nanocrystals synthesized inside a scaffold of silica nanoparticles with a 10 nm diameter a), tin dioxide nanoparticles b), titanium dioxide nanoparticles from a 20% concentrated precursors solution (green plot) and the same system infiltrated with PDMS (orange plot). Solid lines represent the best fitting curves for the structures with (red) and without (green) PDMS. Data and fitting (grey plots and black solid lines) from a bulk polycrystalline $MAPbBr_3$ film are also presented as a comparison.

The use of a titanium dioxide-based matrix is highly desirable for any optoelectronic applications and in the same way tin oxide is a very interesting candidate both as a compact layer and as a mesoporous scaffold in solar cells.[32] Both are mainly used as electron transporting material thanks to the high optical transparency, the property of collecting electrons and blocking holes and high electronic mobility. As for the combination with perovskites both present an ideal band alignment for the extraction of charges from perovskites.

The injection of electrons from the perovskite to the conduction band to the metal oxides implies, at the same time, an additional non-radiative decay path of the excitons and therefore a quenching of the PL. Both phenomena translate into a shortening of the life time, compared to the same film of nanocrystals grown in the SiO_2 matrices as can be seen in figure 3.2.4b-d where the decay curves of the nc-$MAPbBr_3$ emission in the three types of matrices are collected.

3.3 COLOR CONVERTING LAYER

Among the most important applications for the aforementioned perovskite emission properties in new generation solid state lighting technologies, a prominent place is reserved for LED devices for the production of white light, WLED.[33] There are basically two approaches for the fabrication of these systems: the composition of emitters in the frequencies of blue, green and red (RGB)[34] or the conversion of the part of a UV or blue emitter into longer wavelengths.[35] The first case is particularly complex in terms of uniformity, and as far as perovskites are concerned, we have already mentioned in the previous chapter the low efficiency in blue and the so-called "red wall".[36] While regarding the layers for a colour conversion, perovskites nanocrystals are an interesting alternative to systems based on nanophosphors. One of the most common configurations includes a blue LED chip covered with a yellow phosphor (YAG:Ce^{3+}).[37] To obtain the WLED, the alternatives are to integrate a red emitter or directly replace the YAG: Ce^{3+} with green emitting perovskites. Several examples are already present in the literature, for both cases, mainly using colloidal nanocrystals of both inorganic and hybrid perovskites.[38,39] But one of the challenges still open concerns stability towards environmental conditions and in particular humidity. In this section we will illustrate how the SiO_2-pvk composite film synthesis method can allow a very interesting and attractive functionalization for solutions to the colour conversion issue.

3.3.1 Flexible thin film preparation

In order to create an ideal film to be used as an adaptable colour-converting coating, we took advantage of the pore volume that remained empty after embedding nc-$MAPbBr_3$ and loaded it with PDMS. The general scheme of the process is disclosed in figure 3.3.1.

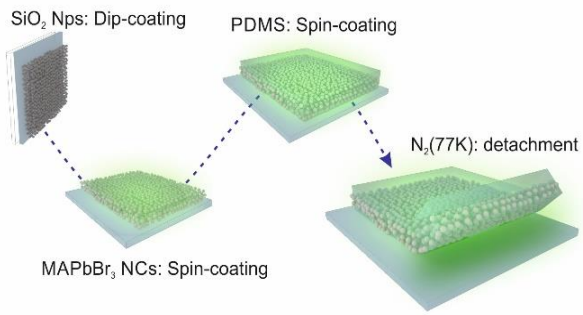

Figure 3.3.1 Graphical representation of PDMS@$MAPbBr_3$@SiO_2 flexible films preparation. The arrow follows the sequence of fabrication steps.

A mix containing a silicone elastomer precursors (olygomers) and a cross-linker (Sylgard184 elastomer kit, Dow Corning) in a mass ratio of 8: 1 was dispersed over the porous silicon oxide matrix that contains the perovskite nanocrystals with a roller blade, then spin-coated at 700 rpm for 60s, and eventually heated at 90°C for 1 h to promote the polymerization. Subsequently, it is necessary to realize incisions in the edges of the sample and after cooling these hybrid PDMS@nc-$MAPbBr_3$@SiO_2 films below the glass transition temperature of the polymer, using liquid nitrogen, it is possible to easily detach exactly the area of the film cut previously and attain a self-standing flexible film. The whole process starting with the infiltration of PDMS and ending with lifting-off the flexible film is conducted outside the glovebox. It is worth mentioning that this method overcomes the incompatibility between solvents used to dissolve PDMS oligomers and ABX_3 perovskite precursors because the process herein proposed do not require the dispersion of the perovskite precursors or pre-synthesized nanocrystals.

3.3.2 Colour conversion

The encapsulation of nc-$MAPbBr_3$@SiO_2 in PDMS has an advantageous effect over the photo-stability of the films. The origin of this instability in air is linked to the adsorption of negatively charged oxygen species at the materials surface, which triggers the migration of anions away from illuminated areas and through the perovskite lattice.[40,41] The time evolution of the photoemission maximum intensity is plotted in figure 3.3.2a. After 10 min, the film infiltrated with PDMS preserves a

bright photoluminescence, whereas that of bare films drops by 80% of its initial value. Remarkably, flexible films maintain both transparency and bright emission (see figure 3.3.2 b and c) after immersion in liquid nitrogen and their subsequent lift-off. Not only PDMS provides protection against environmental agents but also allows immersing the films in water, which has a highly deleterious effect on organic metal halide compounds.[42]

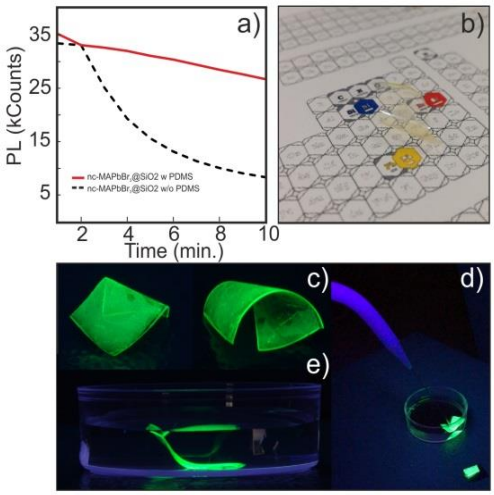

Figure 3.3.2 a) Time evolution of PL emission measured for $MAPbBr_3@SiO_2$ samples with (red line) and without (black line) PDMS infiltration; Camera pictures of a $PDMS@MAPbBr_3@SiO_2$ self-standing transparent flexible film exposed to daylight b) and UV light c); Same sample emitting light when exposed to UV radiation while subject to a water jet d) and immersed in water e)

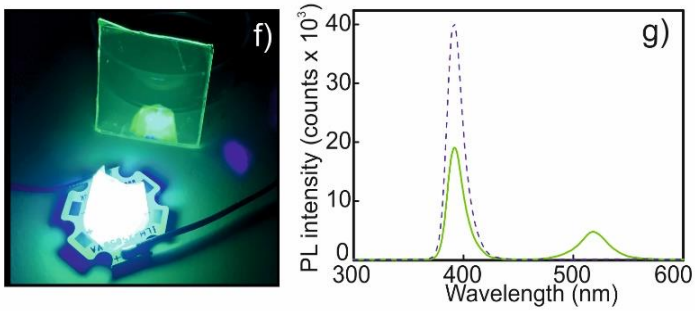

Figure 3.3.2 f) Photograph of a flexible $PDMS@MAPbBr_3@SiO_2$ film covering a 390 nm LED in darkness together with a glass supported $nc\text{-}MAPbBr_3@SiO_2$ sample in the back. g) PL spectra of GaN LED before (blue dashed line) and after the envelopment of flexible $nc\text{-}MAPbBr_3$-based film (green solid line).

We monitored by the naked eye the emission of the self-standing PDMS@nc-$MAPbBr_3@SiO_2$ films when they were fully immersed in water or subject to a water-jet, as reported in figures 3.3.2d and e. It can be clearly seen that the bright emission of nc-$MAPbBr_3$ under UV photo-excitation is kept unchanged while water

3.6 BIBLIOGRAPHY

1 ERBE, ANDREAS, ET AL. HOW TO PROBE STRUCTURE, KINETICS, AND DYNAMICS AT COMPLEX INTERFACES IN SITU AND OPERANDO BY OPTICAL SPECTROSCOPY. ENCYCLOPEDIA OF INTERFACIAL CHEMISTRY, 2018, 199-219.

2 DAVIES, A. GILES, ET AL. TERAHERTZ SPECTROSCOPY OF EXPLOSIVES AND DRUGS. MATERIALS TODAY, 2008, 11.3: 18-26.

3 PERKOWITZ, SIDNEY. OPTICAL CHARACTERIZATION OF SEMICONDUCTORS: INFRARED, RAMAN, AND PHOTOLUMINESCENCE SPECTROSCOPY. ELSEVIER, 2012.

4 LANG, D. V. DEEP-LEVEL TRANSIENT SPECTROSCOPY: A NEW METHOD TO CHARACTERIZE TRAPS IN SEMICONDUCTORS. JOURNAL OF APPLIED PHYSICS, 1974, 45.7: 3023-3032.

5 MIĆIĆ, O. I., ET AL. SIZE-DEPENDENT SPECTROSCOPY OF INP QUANTUM DOTS. THE JOURNAL OF PHYSICAL CHEMISTRY B, 1997, 101.25: 4904-4912.

6 GAPONENKO, SERGEY V. OPTICAL PROPERTIES OF SEMICONDUCTOR NANOCRYSTALS. CAMBRIDGE UNIVERSITY PRESS, 1998.

7 QUINTEN, MICHAEL. OPTICAL PROPERTIES OF NANOPARTICLE SYSTEMS: MIE AND BEYOND. JOHN WILEY & SONS, 2010.

8 HUANG, HE, ET AL. GROWTH MECHANISM OF STRONGLY EMITTING CH 3 NH 3 PBBR 3 PEROVSKITE NANOCRYSTALS WITH A TUNABLE BANDGAP. NATURE COMMUNICATIONS, 2017, 8.1: 1-8.

9 MAES, JORICK, ET AL. LIGHT ABSORPTION COEFFICIENT OF CSPBBR3 PEROVSKITE NANOCRYSTALS. THE JOURNAL OF PHYSICAL CHEMISTRY LETTERS, 2018, 9.11: 3093-3097.

10 MALGRAS, VICTOR, ET AL. OBSERVATION OF QUANTUM CONFINEMENT IN MONODISPERSE METHYLAMMONIUM LEAD HALIDE PEROVSKITE NANOCRYSTALS EMBEDDED IN MESOPOROUS SILICA. JOURNAL OF THE AMERICAN CHEMICAL SOCIETY, 2016, 138.42: 13874-13881.

11 LIU, FENG, ET AL. HIGHLY LUMINESCENT PHASE-STABLE CSPBI3 PEROVSKITE QUANTUM DOTS ACHIEVING NEAR 100% ABSOLUTE PHOTOLUMINESCENCE QUANTUM YIELD. ACS NANO, 2017, 11.10: 10373-10383.

12 DIRIN, DMITRY N., ET AL. HARNESSING DEFECT-TOLERANCE AT THE NANOSCALE: HIGHLY LUMINESCENT LEAD HALIDE PEROVSKITE NANOCRYSTALS IN MESOPOROUS SILICA MATRIXES. NANO LETTERS, 2016, 16.9: 5866-5874.

13 PARVEEN, SUMAIYA, ET AL. LARGE EXCITON BINDING ENERGY, HIGH PHOTOLUMINESCENCE QUANTUM YIELD AND IMPROVED PHOTOSTABILITY OF ORGANO-METAL HALIDE HYBRID PEROVSKITE QUANTUM DOTS GROWN ON A MESOPOROUS TITANIUM DIOXIDE TEMPLATE. JOURNAL OF COLLOID AND INTERFACE SCIENCE, 2019, 539: 619-633.

14 YAN, FEI, ET AL. LIGHT GENERATION IN LEAD HALIDE PEROVSKITE NANOCRYSTALS: LEDS, COLOR CONVERTERS, LASERS, AND OTHER APPLICATIONS. SMALL, 2019, 15.47: 1902079.

15 YUAN, SHUO, ET AL. IN SITU CRYSTALLIZATION SYNTHESIS OF CSPBBR3 PEROVSKITE QUANTUM DOT-EMBEDDED GLASSES WITH IMPROVED STABILITY FOR SOLID-STATE LIGHTING AND RANDOM UPCONVERTED LASING. ACS APPLIED MATERIALS & INTERFACES, 2018, 10.22: 18918-18926.

16 HUANG, HE, ET AL. LEAD HALIDE PEROVSKITE NANOCRYSTALS IN THE RESEARCH SPOTLIGHT: STABILITY AND DEFECT TOLERANCE. ACS ENERGY LETTERS, 2017, 2.9: 2071-2083.

17 GERHARD, MARINA, ET AL. MICROSCOPIC INSIGHT INTO NON-RADIATIVE DECAY IN PEROVSKITE SEMICONDUCTORS FROM TEMPERATURE-DEPENDENT LUMINESCENCE BLINKING. NATURE COMMUNICATIONS, 2019, 10.1: 1-12.

18 YAVARI, MOZHGAN, ET AL. HOW FAR DOES THE DEFECT TOLERANCE OF LEAD-HALIDE PEROVSKITES RANGE? THE EXAMPLE OF BI IMPURITIES INTRODUCING EFFICIENT RECOMBINATION CENTERS. JOURNAL OF MATERIALS CHEMISTRY A, 2019, 7.41: 23838-23853.

19 PAN, JUN, ET AL. BIDENTATE LIGAND-PASSIVATED CSPBI3 PEROVSKITE NANOCRYSTALS FOR STABLE NEAR-UNITY PHOTOLUMINESCENCE QUANTUM YIELD AND EFFICIENT RED LIGHT-EMITTING DIODES. JOURNAL OF THE AMERICAN CHEMICAL SOCIETY, 2017, 140.2: 562-565.

20 SHAMSI, JAVAD, ET AL. METAL HALIDE PEROVSKITE NANOCRYSTALS: SYNTHESIS, POST-SYNTHESIS MODIFICATIONS, AND THEIR OPTICAL PROPERTIES. CHEMICAL REVIEWS, 2019, 119.5: 3296-3348.

21 HA, SEUNG KYUN; MAUCK, CATHERINE M.; TISDALE, WILLIAM A. TOWARD STABLE DEEP-BLUE LUMINESCENT COLLOIDAL LEAD HALIDE PEROVSKITE NANOPLATELETS: SYSTEMATIC PHOTOSTABILITY INVESTIGATION. CHEMISTRY OF MATERIALS, 2019, 31.7: 2486-2496.

22 MALGRAS, VICTOR, ET AL. STABLE BLUE LUMINESCENT CSPBBR3 PEROVSKITE NANOCRYSTALS CONFINED IN MESOPOROUS THIN FILMS. ANGEWANDTE CHEMIE, 2018, 130.29: 9019-9023.

23 SWARNKAR, ABHISHEK, ET AL. COLLOIDAL CSPBBR3 PEROVSKITE NANOCRYSTALS: LUMINESCENCE BEYOND TRADITIONAL QUANTUM DOTS. ANGEWANDTE CHEMIE, 2015, 127.51: 15644-15648.

24 PROTESESCU, LOREDANA, ET AL. NANOCRYSTALS OF CESIUM LEAD HALIDE PEROVSKITES (CSPBX3, X= CL, BR, AND I): NOVEL OPTOELECTRONIC MATERIALS SHOWING BRIGHT EMISSION WITH WIDE COLOR GAMUT. NANO LETTERS, 2015, 15.6: 3692-3696.

25 TONG, YU, ET AL. SPONTANEOUS SELF-ASSEMBLY OF PEROVSKITE NANOCRYSTALS INTO ELECTRONICALLY COUPLED SUPERCRYSTALS: TOWARD FILLING THE GREEN GAP. ADVANCED MATERIALS, 2018, 30.29: 1801117.

26 BARANOV, DMITRY, ET AL. INVESTIGATION INTO THE PHOTOLUMINESCENCE RED SHIFT IN CESIUM LEAD BROMIDE NANOCRYSTAL SUPERLATTICES. THE JOURNAL OF PHYSICAL CHEMISTRY LETTERS, 2019, 10.3: 655-660.

27 QU, LIANHUA; PENG, XIAOGANG. CONTROL OF PHOTOLUMINESCENCE PROPERTIES OF CDSE NANOCRYSTALS IN GROWTH. JOURNAL OF THE AMERICAN CHEMICAL SOCIETY, 2002, 124.9: 2049-2055.

28 SU, YING, ET AL. HIGHLY CONTROLLABLE AND EFFICIENT SYNTHESIS OF MIXED-HALIDE CSPBX3 (X= CL, BR, I) PEROVSKITE QDS TOWARD THE TUNABILITY OF ENTIRE VISIBLE LIGHT. ACS APPLIED MATERIALS & INTERFACES, 2017, 9.38: 33020-33028.

29 GIANSANTE, CARLO; INFANTE, IVAN. SURFACE TRAPS IN COLLOIDAL QUANTUM DOTS: A COMBINED EXPERIMENTAL AND THEORETICAL PERSPECTIVE. THE JOURNAL OF PHYSICAL CHEMISTRY LETTERS, 2017, 8.20: 5209-5215.

30 JIMÉNEZ-SOLANO, ALBERTO; GALISTEO-LOPEZ, JUAN F.; MÍGUEZ, HERNÁN. ABSORPTION AND EMISSION OF LIGHT IN OPTOELECTRONIC NANOMATERIALS: THE ROLE OF THE LOCAL OPTICAL ENVIRONMENT. THE JOURNAL OF PHYSICAL CHEMISTRY LETTERS, 2018, 9.8: 2077-2084.

31 YABLONOVITCH, E.; GMITTER, T. J.; BHAT, R. INHIBITED AND ENHANCED SPONTANEOUS EMISSION FROM OPTICALLY THIN ALGAAS/GAAS DOUBLE HETEROSTRUCTURES. PHYSICAL REVIEW LETTERS, 1988, 61.22: 2546.

32 CHEN, YICHUAN, ET AL. SNO2-BASED ELECTRON TRANSPORTING LAYER MATERIALS FOR PEROVSKITE SOLAR CELLS: A REVIEW OF RECENT PROGRESS. JOURNAL OF ENERGY CHEMISTRY, 2019, 35: 144-167.

33 STEIGERWALD, DANIEL A., ET AL. ILLUMINATION WITH SOLID STATE LIGHTING TECHNOLOGY. IEEE JOURNAL OF SELECTED TOPICS IN QUANTUM ELECTRONICS, 2002, 8.2: 310-320.

34 KUBOTA, HIROFUMI, ET AL. ORGANIC LED FULL COLOR PASSIVE-MATRIX DISPLAY. JOURNAL OF LUMINESCENCE, 2000, 87: 56-60.

35 LIN, CHUN CHE; LIU, RU-SHI. ADVANCES IN PHOSPHORS FOR LIGHT-EMITTING DIODES. THE JOURNAL OF PHYSICAL CHEMISTRY LETTERS, 2011, 2.11: 1268-1277.

36 PROTESESCU, LOREDANA, ET AL. DISMANTLING THE "RED WALL" OF COLLOIDAL PEROVSKITES: HIGHLY LUMINESCENT FORMAMIDINIUM AND FORMAMIDINIUM–CESIUM LEAD IODIDE NANOCRYSTALS. ACS NANO, 2017, 11.3: 3119-3134.

37 KASUYA, R., ET AL. CHARACTERISTIC OPTICAL PROPERTIES OF TRANSPARENT COLOR CONVERSION FILM PREPARED FROM YAG: CE 3+ NANOPARTICLES. APPLIED PHYSICS LETTERS, 2007, 91.11: 111916.

38 ZHANG, CAICAI, ET AL. LIGHT DIFFUSING, DOWN-CONVERTING PEROVSKITE-ON-POLYMER MICROSPHERES. JOURNAL OF MATERIALS CHEMISTRY C, 2019, 7.22: 6527-6533.

39 GUNER, TUGRUL; DEMIR, MUSTAFA M. A REVIEW ON HALIDE PEROVSKITES AS COLOR CONVERSION LAYERS IN WHITE LIGHT EMITTING DIODE APPLICATIONS. PHYSICA STATUS SOLIDI (A), 2018, 215.13: 1800120.

40 JACOBSSON, T. JESPER, ET AL. UNREACTED PBI2 AS A DOUBLE-EDGED SWORD FOR ENHANCING THE PERFORMANCE OF PEROVSKITE SOLAR CELLS. JOURNAL OF THE AMERICAN CHEMICAL SOCIETY, 2016, 138.32: 10331-10343.

41 ANAYA, MIGUEL, ET AL. ORIGIN OF LIGHT-INDUCED PHOTOPHYSICAL EFFECTS IN ORGANIC METAL HALIDE PEROVSKITES IN THE PRESENCE OF OXYGEN. THE JOURNAL OF PHYSICAL CHEMISTRY LETTERS, 2018, 9.14: 3891-3896.

42 BOYD, CALEB C., ET AL. UNDERSTANDING DEGRADATION MECHANISMS AND IMPROVING STABILITY OF PEROVSKITE PHOTOVOLTAICS. CHEMICAL REVIEWS, 2018, 119.5: 3418-3451.

43 DURSUN, IBRAHIM, ET AL. PEROVSKITE NANOCRYSTALS AS A COLOR CONVERTER FOR VISIBLE LIGHT COMMUNICATION. ACS PHOTONICS, 2016, 3.7: 1150-1156.

44 PANT, ANUPUM, ET AL. FUNDAMENTALS OF LATERAL AND VERTICAL HETEROJUNCTIONS OF ATOMICALLY THIN MATERIALS. NANOSCALE, 2016, 8.7: 3870-3887.

45 GLYNN, COLM; O'DWYER, COLM. SOLUTION PROCESSABLE METAL OXIDE THIN FILM DEPOSITION AND MATERIAL GROWTH FOR ELECTRONIC AND PHOTONIC DEVICES. ADVANCED MATERIALS INTERFACES, 2017, 4.2: 1600610.

46 ANAYA, MIGUEL, ET AL. OPTICAL DESCRIPTION OF MESOSTRUCTURED ORGANIC–INORGANIC HALIDE PEROVSKITE SOLAR CELLS. THE JOURNAL OF PHYSICAL CHEMISTRY LETTERS, 2015, 6.1: 48-53.

47 JIMÉNEZ-SOLANO, ALBERTO; GALISTEO-LOPEZ, JUAN F.; MÍGUEZ, HERNÁN. ABSORPTION AND EMISSION OF LIGHT IN OPTOELECTRONIC NANOMATERIALS: THE ROLE OF THE LOCAL OPTICAL ENVIRONMENT. THE JOURNAL OF PHYSICAL CHEMISTRY LETTERS, 2018, 9.8: 2077-2084.

48 ASPNES, D. E. ANALYSIS OF MODULATION SPECTRA OF STRATIFIED MEDIA. JOSA, 1973, 63.11: 1380-1390.

49 RAJA, ARCHANA, ET AL. DIELECTRIC DISORDER IN TWO-DIMENSIONAL MATERIALS. NATURE NANOTECHNOLOGY, 2019, 14.9: 832-837.

50 CISNEROS, JORGE I. OPTICAL CHARACTERIZATION OF DIELECTRIC AND SEMICONDUCTOR THIN FILMS BY USE OF TRANSMISSION DATA. APPLIED OPTICS, 1998, 37.22: 5262-5270.

51 LUNKENHEIMER, PETER, ET AL. ORIGIN OF APPARENT COLOSSAL DIELECTRIC CONSTANTS. PHYSICAL REVIEW B, 2002, 66.5: 052105.

52 LEGUY, AURÉLIEN MA, ET AL. EXPERIMENTAL AND THEORETICAL OPTICAL PROPERTIES OF METHYLAMMONIUM LEAD HALIDE PEROVSKITES. NANOSCALE, 2016, 8.12: 6317-6327.

53 CALVO, MAURICIO E. MATERIALS CHEMISTRY APPROACHES TO THE CONTROL OF THE OPTICAL FEATURES OF PEROVSKITE SOLAR CELLS. JOURNAL OF MATERIALS CHEMISTRY A, 2017, 5.39: 20561-20578.

54 HE, CHONGJUN, ET AL. REFRACTIVE INDEX DISPERSION OF ORGANIC–INORGANIC HYBRID HALIDE PEROVSKITE CH3NH3PBX3 (X= CL, BR, I) SINGLE CRYSTALS. CRYSTAL RESEARCH AND TECHNOLOGY, 2019, 54.5: 1900011.

55 MOREELS, IWAN, ET AL. COMPOSITION AND SIZE-DEPENDENT EXTINCTION COEFFICIENT OF COLLOIDAL PBSE QUANTUM DOTS. CHEMISTRY OF MATERIALS, 2007, 19.25: 6101-6106.

56 MOREELS, IWAN, ET AL. SIZE-DEPENDENT OPTICAL PROPERTIES OF COLLOIDAL PBS QUANTUM DOTS. ACS NANO, 2009, 3.10: 3023-3030.

57 HENS, Zeger; MOREELS, Iwan. Light absorption by colloidal semiconductor quantum dots. Journal of Materials Chemistry, 2012, 22.21: 10406-10415.

58 NIKLASSON, Goran A.; GRANQVIST, C. G.; HUNDERI, O. Effective medium models for the optical properties of inhomogeneous materials. Applied Optics, 1981, 20.1: 26-30.

59 LEYDEN, Matthew R., et al. Methylammonium lead bromide perovskite light-emitting diodes by chemical vapor deposition. The Journal of Physical Chemistry Letters, 2017, 8.14: 3193-3198.

60 STOUMPOS, Constantinos C.; MALLIAKAS, Christos D.; KANATZIDIS, Mercouri G. Semiconducting tin and lead iodide perovskites with organic cations: phase transitions, high mobilities, and near-infrared photoluminescent properties. Inorganic chemistry, 2013, 52.15: 9019-9038.

61 TAUC, J.; GRIGOROVICI, Radu; VANCU, Anina. Optical properties and electronic structure of amorphous germanium. physica status solidi (b), 1966, 15.2: 627-637.

62 VIEZBICKE, Brian D., et al. Evaluation of the Tauc method for optical absorption edge determination: ZnO thin films as a model system. physica status solidi (b), 2015, 252.8: 1700-1710.

63 LEVY, Ohad; CHERKAEV, Elena. Effective medium approximations for anisotropic composites with arbitrary component orientation. Journal of Applied Physics, 2013, 114.16: 164102.

64 FOROUHI, A. R.; BLOOMER, I. Optical dispersion relations for amorphous semiconductors and amorphous dielectrics. Physical review B, 1986, 34.10: 7018.

65 JobinYvon New Amorphous Dispersion Formula. http://fileadmin/uploads/Scientific/Downloads/OpticalSchool_CN/TN/ellipsometer/New_Amorphous_Dispersion_Formula.pdf

66 LÖPER, Philipp, et al. Complex refractive index spectra of CH3NH3PbI3 perovskite thin films determined by spectroscopic ellipsometry and spectrophotometry. The journal of physical chemistry letters, 2015, 6.1: 66-71.

67 ALIAS, Mohd Sharizal, et al. Optical constants of CH 3 NH 3 PbBr 3 perovskite thin films measured by spectroscopic ellipsometry. Optics express, 2016, 24.15: 16586-16594.

68 VOSSMEYER, T., et al. CdS nanoclusters: synthesis, characterization, size dependent oscillator strength, temperature shift of the excitonic transition energy, and reversible absorbance shift. The Journal of Physical Chemistry, 1994, 98.31: 7665-7673.

69 ANGELONI, Ilaria, et al. Disentangling the Role of Shape, Ligands, and Dielectric Constants in the Absorption Properties of Colloidal CdSe/CdS Nanocrystals. ACS Photonics, 2016, 3.1: 58-67.

70 LIM, Sung Jun, et al. Brightness-equalized quantum dots. Nature communications, 2015, 6.1: 1-10.

71 GEIREGAT, Pieter, et al. Giant and broad-band absorption enhancement in colloidal quantum dot monolayers through dipolar coupling. Acs Nano, 2013, 7.2: 987-993.

72 GIANSANTE, Carlo, et al. "Darker-than-Black" PbS quantum dots: enhancing optical absorption of colloidal semiconductor nanocrystals via short conjugated ligands. Journal of the American Chemical Society, 2015, 137.5: 1875-1886.

73 TAKAGAHARA, Toshihide. Effects of dielectric confinement and electron-hole exchange interaction on excitonic states in semiconductor quantum dots. Physical Review B, 1993, 47.8: 4569.

74 MOREELS, Iwan, et al. The dielectric function of PbS quantum dots in a glass matrix. Optical Materials Express, 2012, 2.5: 496-500.

75 MASI, Sofia, et al. Chemi-Structural Stabilization of Formamidinium Lead Iodide Perovskite by Using Embedded Quantum Dots. ACS Energy Letters, 2020, 5.2: 418-427.

76 XU, JUNWEI, ET AL. IMBEDDED NANOCRYSTALS OF CSPBBR3 IN CS4PBBR6: KINETICS, ENHANCED OSCILLATOR STRENGTH, AND APPLICATION IN LIGHT-EMITTING DIODES. ADVANCED MATERIALS, 2017, 29.43: 1703703.

5 PEROVSKITE NANOCRYSTALS NONLINEAR OPTICS

5.1 INTRODUCTION

In the tenacious, but also targeted scientific exploration of the technological potential unveiled by perovskite materials, the investigation of their optical behaviour finds an extension as interesting, as it is still underexplored, in the field of nonlinear optics.[1] Also in this case the study of the characteristic phenomena of this so-called regime makes a significant contribution both to the fundamental analysis and to the technological development of these materials. From the fundamental point of view, the next step with respect to the analysis of the linear properties concerns the phenomena induced by the interaction with a light or electromagnetic field sufficiently intense to modify the optical behaviour of a material.[2] The term "nonlinear" refers to the nonlinear dependence on the optical response of the system under examination, with respect to the force of the applied field.[3] In order to describe these phenomena, the more general definition of the polarization (P) of a system induced by an electric field expressed as a function of the force of the field (E) is normally taken into consideration, since the variation of the polarization can be the source of new components of the electromagnetic field.[4] The equation known to be adopted expresses this polarization as a series of powers:

$$P(t) = \varepsilon_0\left(\chi^{(1)}E(t) + \chi^{(2)}E^2(t) + \chi^{(3)}E^3(t) + \cdots\right) \qquad (1)$$

in which ε_0 is the permittivity in a vacuum, and the term χ is a constant of proportionality defined as susceptibility which, as can be seen in the relationship between polarizability and applied field, χ term assumes an increasing order. In this way, the optical response of a material can be described, taking into consideration, in addition to the first order linear susceptibility, all the higher order nonlinear susceptibilities that can dominate the behaviour of the system according to the excitation conditions, for example intensity and frequency, but also depending on the type of material and the geometric conditions. In the latter case, symmetry is, in fact, a crucial factor for the assignment of the type of susceptibility coefficient, or of the order n of the powers that can describe the series expressed in the relation (1). In particular, even-order susceptibilities that can contribute to the nonlinear response do not appear in the description of the centrosymmetric materials.[4,5] The odd-order susceptibilities are always present in the nonlinear optical response

regardless of the presence or absence of an inversion centre in the symmetry of the crystal. Nonlinear behaviour implies a modification of the way in which a material can interact with light and consequently can lead to the generation of new optical phenomena, including the processes for generating new frequencies,[6] the modification of the refractive index with consequent modulation of the wave phase[7] or even multi-photon absorption.[8] From the point of view of technological applications, however, novel nonlinear material with easy photonic integration capability are of vital importance for optoelectronic devices - e.g. for optical storage, routing, and switching,[9-11] nano-medicine,[12] and quantum optics.[13] Critical requirements are high nonlinear interaction strength, as quantified by the nonlinear susceptibility, together with easy synthesis and integration. Recently, a broad range of materials with high nonlinear susceptibility have been explored, ranging from epsilon near- zero (ENZ) materials,[14-16] to 2D materials which are novel and easy to integrate as graphene,[17] black phosphorus[18] and TMDs such as MoS_2,[19] WSe_2.[20] More recently, the optical response of perovskites in the nonlinearity regimes has also started to be investigated.[21-23]

5.2 2ND AND 3RD ORDER NONLINEAR OPTICS IN PEROVSKITES

In general, perovskites offer a wide range of optoelectronic properties such as strong absorption,[24] high dielectric constant,[25] a reversible bandgap tunability[26] and strong excitonic resonance, in particular in the case of high bandgap perovskites[27,28] and in systems confined with a high binding energy[29] and large oscillator strength,[30] which promote excellent non-linear performance. More specifically, due to the centrosymmetric structure typical of perovskite crystals, the second order optical response is not the main nonlinear contribution. In any case it was possible, in some examples, to generate a second harmonic signal[31] attributable on the one hand to a certain propensity to electronic polarization (ferroelectricty).[32-34] Second order phenomena have also been reported, since these systems can be synthesized in such a way that it is possible to break the centrosymmetric structure of the crystalline perovskite phases (for example introducing larger organic cations).[35] The nonlinear effects of the third order are, however, predominant and to date some interesting studies have been reported both in the case of single crystals of bulk material,[36] polycrystalline thin films[37] and especially in the case of 2D perovskites harmonic generation.[38] A final aspect that makes these materials particularly interesting for future applications in technology based on nonlinear systems is manufacturing. As we know, perovskites can be easily obtained in the form of single

crystals, but above all as thin films through liquid phase and low temperature processes (see chapter 1). The convenience is already in the low fabrication costs for direct use of these materials, but, especially in the field of nonlinear photonics, it is advantageous to have materials that can be easily integrated into more complex architectures that can for example refine the control on optical properties or amplify effects specific.[39] In this perspective, the picture is obviously enriched by the possibility of synthesis of low-dimensional perovskites in different shapes and in the liquid and solid phase, with further expansion of the range of properties available for light manipulation.

In this chapter, we report the first evidence of a third order nonlinear effect which is the third harmonic generation (THG) from formamidinium lead bromide ($FAPbBr_3$) perovskite nanocrystals obtained through the templated synthesis. We further characterize the spectral dependence of the generated third harmonic and extract the spectral shape and value of the nonlinear susceptibility χ^3. Formamidinium-based perovskites have already demonstrated greater stability at high temperatures with respect to the best known methylammonium-based counterparts,[40] while the use of nanocrystals (as we already discussed in chapter 1) makes it possible to tune the spectral position of the third harmonic without changing the chemical composition and thus avoiding the problems related to the phase segregation.[41] Plus the systems here presented offer the right versatility and ease of fabrication, as we already discussed in this thesis (see chapter 2), which meet and perfectly adapt to the necessary requirements for the above mentioned technological implementation, like transparency and a laminar structure for device integration.

5.3 $FAPBBR_3$ NCS PREPARATION AND CHARACTERIZATION

In this case, the synthesis of the nanocrystals were made through a solution of precursors with formamidinium bromide (FABr) and lead bromide ($PbBr_2$) in molar ratio 1: 1 and at 20wt% in DMSO. The high-resolution micrograph with further zoom, presented in figure 5.3, illustrates that the size of the $FAPbBr_3$ nanocrystal reach a diameter of 9 nm. Also in this case we prepared a polycrystalline film starting from the same precursor solution spin coated directly on a glass substrate in order to have a bulk reference. X-ray diffraction analysis was already presented in chapter 2 (see figure 2.3.2q). The bulk film forms a layer of 300 nm while the nanocrystals are encapsulated in a matrix of 1300 nm. Finally, also in this case, as already seen in chapter 3, we did the quantitative analysis by means of ICP-OES. Considering the

ppm of lead obtained and the $FAPbBr_3$ density[42] of 3.777 gr/cm^3 we calculated a percentage by volume of $FAPbBr_3$ NCs of 6.7% with respect to the whole volume of the composite material (same procedure as described in chapter 3).

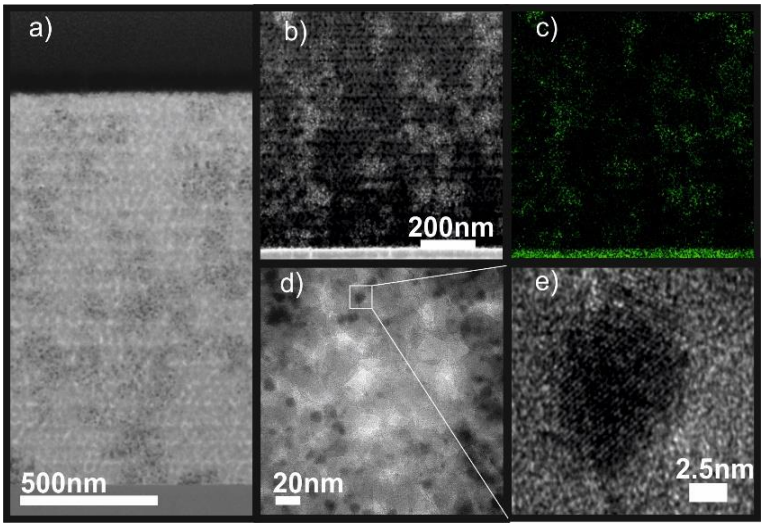

Figure 5.3 T.E.M. characterisation: a) complete cross section of a SiO_2@$FAPbBr_3$ sample; b) HAADF-STEM image; c) Pb elemental mapping (green) of sample area presented in b) using EDX; d) High Resolution TEM micrograph; e) zoom-in of $FAPbBr_3$ NC within the white square in figure in d).

5.3.1 Linear characterization

It can be seen in figure 5.3.1a that the photoluminescence emission of the perovskite nanocrystals within the porous structure is shifted to shorter wavelengths compared to the emission from the bulk polycrystalline film, considering also that both these samples have been synthesized by the same $FAPbBr_3$ precursor solution.

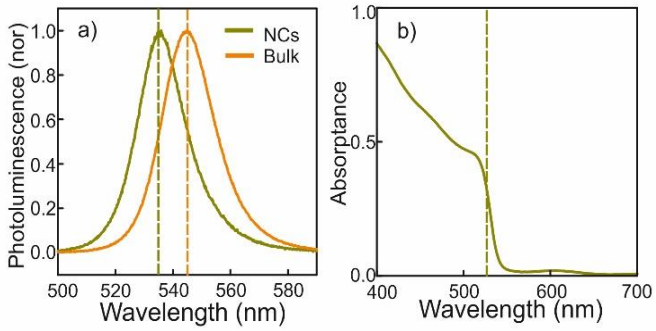

Figure 5.3.1 a) PL Normalised photoluminescence spectra of the 9 nm $FAPbBr_3$ NCs embedded in the porous SiO_2 matrix (green line) and a bulk thin film made of the same perovskites composition (orange line). The dotted lines denote the spectral shift of the PL peaks. b) Normalized absorptance obtained from the $FAPbBr_3$ NCs-based film.

While the luminescence peak of the bulk film has the maximum at 545 nm, the peak relative to the film consisting of nanocrystals of the same perovskites in a SiO_2 matrix is clearly shifted by 10 nm with a narrow emission (FWHM=22 nm). In parallel, figure 5.3.1b shows the characteristic absorptance (A) of the nanocrystal-based film, which has been obtained from measurements of total reflection (R) and total transmission (T) of light within an integrating sphere (A=1-R-T). In addition, through ballistic transmittance and specular reflectance measurements at different incidence angles, we extrapolated the real and imaginary part of the effective complex refractive index of the $FAPbBr_3@SiO_2$ composite material using the Forouhi-Bloomer model,[43] similar to what was already seen in the chapter 3. Figure 5.3.1c shows the optical constants obtained from this model fitting to the transmittance and reflectance values obtained experimentally. The refractive index (n) and the extinction coefficient (k) both increase sharply for energies increasing beyond the band-edge energy. For wavelengths larger than the E_{bg}, k is almost zero, while the n is close to 1.31.

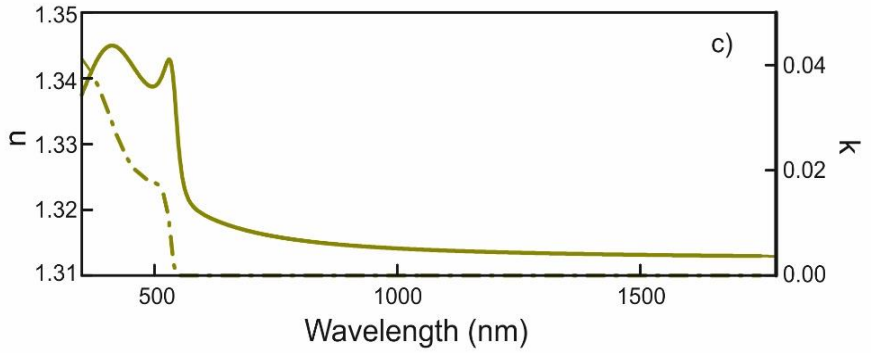

Figure 5.3.1 c) Spectral dependence of refractive index, n, (solid line) and extinction coefficient, k, (dashed line) the $FAPbBr_3@SiO_2$ composite thin film.

5.4 THIRD ORDER EFFECTS

5.4.1 Third Harmonic Generation

Third harmonic generation (THG) is the emission of a wave of frequency 3ω, after excitation by an incident field of frequency ω (the pump), and it is mediated by the induced non-linear polarisability, the strength of which is quantified by χ^3.[44] For THG measurements an optical set-up was used, in which the third harmonic from $FAPbBr_3$ nanocrystal film is excited by a normal-incident excitation laser beam (Yb:KGW PHAROS, Light Conversion laser system) of 200 fs duration, at a repetition rate of 100 kHz, 1 μJ pulse energy, tuned from 1340 nm to 1740 nm, emerging from

an optical parametric amplifier (Orpheus, Light-Conversion). The ensuing third harmonic spectrum was measured, incrementally at 20 nm in the aforementioned wavelength range, by transmission coupling to a spectrometer. The laser power was maintained at 15 mW (~7 GW/cm^2) throughout the measurements. As a reference, the third harmonic spectra of a glass microscope slide were also measured, to factor out the fluctuations in intensity and beam-diameter of the laser pump beam. Besides, glass presents a spectrally flat nonlinear susceptibility,[45] $\chi^{(3)glass}$=1.6±0.2x10^{-22} (m/V)^2.

Some of the spectra taken from $FAPbBr_3$ nanocrystal film at different pump wavelengths between 1300-1740 nm are plotted in figure 5.4.1a (shaded areas). All spectra show sharp peaks at the third harmonic wavelength. These peaks have an intensity that depends on the wavelength of the pump field, as shown by the green circles. The value of third harmonic maximum intensity at each measured wavelength normalized by the value of THG intensity of the glass is shown in the figure. The same nonlinear characterization has been carried out also in the case of polycrystalline film, for comparison. As illustrated in figure 5.4.1b, from the combination of the two spectral behaviours (NCs and bulk) it can be seen how it is possible to tune the maximum emission of the third harmonic on different frequencies. Because of the quantum confinement effect, the band gap moves as we already seen in the photoluminescence and therefore the same happens to the relative resonant effect that generates the enhancement in the nonlinear response.

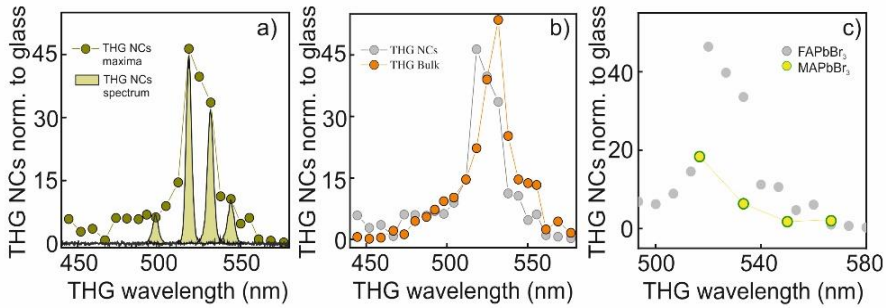

Figure 5.4.1 a) Spectral evolution of the intensity of the THG from the $FAPbBr_3$ NCs is shown normalised to the THG intensity of the glass sample after the background glass intensity is subtracted. The THG intensity is taken at the maxima of measured spectrum at each experimental wavelength. Green shaded peaks correspond to THG spectra recorder for $FAPbBr_3$ nanocrystals film from a few experimental wavelengths between 1340-1740 nm. b) Comparison between THG spectral dependence of $FAPbBr_3$ NCs and bulk film with the two maximum values shifted according to the different band gaps. THG values are normalised as in a). c) THG maxima values obtained for a $MAPbBr_3$ NCs-based film at four different wavelengths normalized to the glass and compared to THG from $FAPbBr_3$ NCs sample.

As a further test, we also tested a sample composed of $MAPbBr_3$ nanocrystals embedded in same SiO_2 nanoparticles porous film which in turn revealed a THG

signal with a maximum pointing to the characteristic MA-based perovskite bandgap, as shown in figure 5.4.1c. This corroborates the possibility of tuning the generation of the third harmonic throughout the band gap range of the perovskites changing chemical composition. Despite the encouraging results, we have chosen to focus the study only on the $FAPbBr_3$ nanocrystals which revealed a more intense THG response than the methylammonium-based ones. As far as the bulk material is concerned, however, we have already pointed out the complications related to the analysis of optical constants which therefore make it more difficult to face the study of non-linear susceptibility.

Figure 5.4.1d reports the absolute efficiency of generated third harmonic from the $FAPbBr_3$ nanocrystal film. The absolute efficiency, η, is measured from $\eta = P_3^{NC}/P_1^{laser}$ where P_3^{NC} and P_1^{laser} are the measured power of the third harmonic signal of the $FAPbBr_3$ nanocrystal film and of the laser pump beam, respectively. In addition, the nature of the THG signal transmitted through the film is verified by recording the polarization of the generated third harmonic from the $FAPbBr_3$ nanocrystal film, as shown in figure 5.4.1e, which, as expected, preserves the same linear polarization as the incident beam. Furthermore, by measuring the intensity of this generated third harmonic signal as a function of the excitation power, the characteristic cubic-dependence of a third-order effect such as THG is confirmed, as shown in figure 5.4.1f.

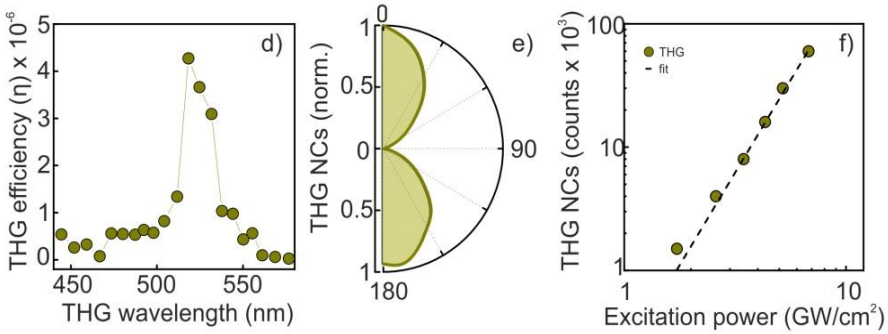

Figure 5.4.1 d) Absolute THG efficiency from a $ncFAPbBr_3@SiO_2$ film. e) Polarization analysis of the third harmonic beam (λ_1=1542nm, λ_3=514nm) f Log-log plot of the third harmonic beam intensity versus pump power at λ_1=1542 nm for the $ncFAPbBr_3@SiO_2$ film. The fitting (dotted line) demonstrates a linear dependence with slope 3 taken at wavelength 1500 nm.

5.4.2 Two-photon Absorption

As a cumulative evidence of the strong nonlinear character, these materials have also demonstrated an interesting nonlinear absorption as observable from the two-photon induced photoluminescence measured when exciting the sample with laser wavelengths in the range 840-1360 nm (see figure 5.4.2a) with a quadratic dependence of the photoluminescence intensity with the excitation power.

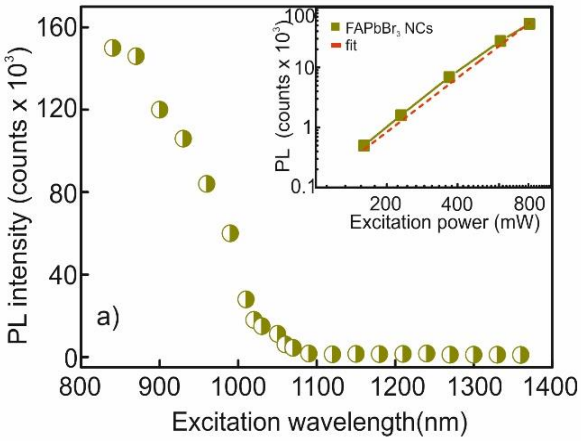

Figure 5.4.2 a) Spectral dependence of the Two Photon Emission intensity (maximum of each photoluminescence peak).The inset shows the log-log plot of the TPE induced luminescence intensity versus the excitation power. Dotted red line corresponds to the linear fitting with slope 2.

5.5 THIRD ORDER SUSCEPTIBILITY

From the spectra of the THG signal in the wavelength range 1340-1740 nm (Fig 5.4.1a), the spectral behaviour of $\chi^{(3)NC}$, the third-order susceptibility of the $FAPbBr_3$ nanocrystal, can be extracted by fitting the experimental data with a length-dependant, L, function $f(\lambda, L)$, which is proportional to the predicted third harmonic intensity of the nanocrystal I_3, as calculated by an analytical solution of nonlinear Maxwell's equations[46] assuming a non-depleting pump wave in the film:

$$I_3 = f(\lambda, L)\left|\chi^{(3)}\right|^2 I_1^3 \qquad (2)$$

Where $\chi^{(3)}$ is the third-order nonlinear susceptibility, I_1 is the pump intensity and the function

$$f(\lambda, L) = \frac{9\omega^2}{16|\tilde{n}_3|n_1^3\varepsilon_0^2c^4}\left(\frac{e^{-2\alpha_3 L} - 2\cos(\Delta kL)\, e^{-\alpha_3 L} + 1}{{\alpha_3}^2 + \Delta k^2}\right)e^{-2\alpha_3 L}, \qquad (3)$$

includes the refractive indices of the material at the pump and third harmonic wavelength as well as the frequency at the pump wavelength and the film thickness (L). Δk is the phase mismatch between the pump and third harmonic wave, and α_3 the absorption coefficient of the third harmonic wave, which both influence the generated third harmonic intensity, I_3. Also, in equation (3), ω is the angular frequency of the pump, $|\tilde{n}_3|$ is the complete refractive index of the composite film made of $FAPbBr_3$ nanocrystals at the third harmonic wavelength while ε_0 and c constants maintain the usual definition.

α_3 and Δk can be calculated from the linear optical properties of the $FAPbBr_3$ nanocrystal composite film plotted in the figure 5.3.1c, as α_3 is dependent upon the extinction coefficient (k_3), at the third harmonic wavelength (λ_3), and $\Delta k(\lambda)$ is proportional to the difference in the refractive index between at the pump wavelength (n_1) and third harmonic wavelength (n_3) and dependent upon the pump wavelength (λ_1).

$$\alpha_3 = \frac{2\pi k_3}{\lambda_3} \qquad \textbf{(4)}$$

$$\Delta k = \frac{2\pi(n_1 - n_3)}{\lambda_1} \qquad \textbf{(5)}$$

$\Delta k(\lambda)$ and $\alpha(\lambda)$ are plotted in figure 5.5a: $\alpha(\lambda)$ (green solid line) falls off after the band-edge at 520 nm (THG) where the absorbance of the $FAPbBr_3$ nanocrystal film reduces drastically while $\Delta k(\lambda)$ (grey dashed line) follows the same spectral behaviour of the real part of the linear refractive index of $FAPbBr_3$ nanocrystal film (figure 5.3.1c). The spectrum discloses a sharp increase for energies above the bandgap. For a fixed pump wavelength of 1560 nm, where the maximum THG intensity is experimentally observed, the predicted length-dependency $f(\lambda, L)$ is shown (figure 5.5b). This function presents a maximum and the green dotted line indicates the sample thickness used in our experiments. At this wavelength, absorption dominates the model, as the absorption length ($1/\alpha$) is much shorter than the coherence length ($2\pi/\Delta k$), and therefore THG oscillations with film thickness are exponentially attenuated. Moreover, it is clear that the length of the nanocrystal used here, which is 1300 nm, resides on the positive gradient of the graph. The efficiency of the third harmonic generation could be increased by a factor of around 2 by fine tuning the film thickness.

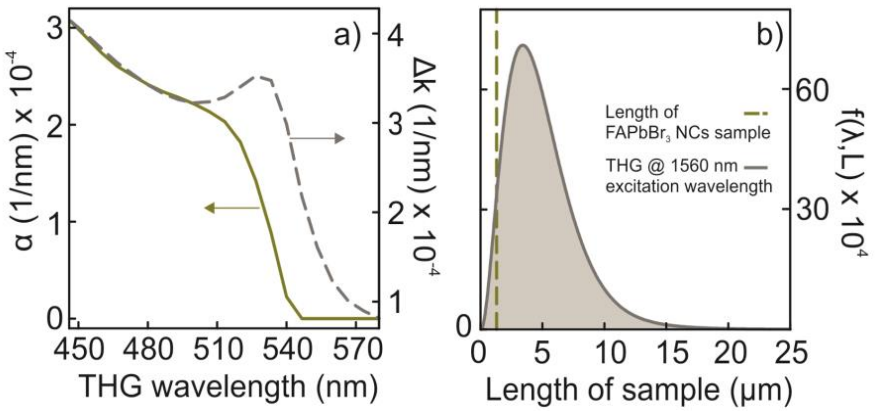

Figure 5.5 a) Spectral absorption coefficient of the third harmonic wave and the phase mismatch between pump and third harmonic wave in the wavelength range of 1340-1740 nm; b) length-dependant function f(λ,L) versus ncFAPbBr3@SiO2 film thickness (λ_1=1560nm, λ_3=520nm). The vertical dotted line indicates the actual thickness of the composite film (1300 nm)

Finally, as anticipated, it is possible to extract the third order susceptibility of the perovskite nanocrystals contained in the porous film. For this calculus it is necessary knowing the experimental value of I_3, in equation (2), for the composite system and for the glass, or $I_3^{NC/glass}$. Both values are obtained from spectra measured at every 20 nm from $FAPbBr_3$ nanocrystal (NC) film and glass in the wavelength range 1340-1740 nm. The model described in equation (2), therefore, becomes

$$I_3^{NC/glass} = f^{NC/glass}(\lambda, L)\left|\chi^{(3)NC/glass}\right|^2 I_1^3 \qquad \textbf{(4)}$$

By simulating the function $f^{NC/glass}(\lambda)$ at the length L of 1300 nm and 1mm, respectively, for the nanocrystals and the glass it is possible then to isolate the $\chi^{(3)NC}$ in equation (4) by splitting the system as the ratio between the susceptibility of the composite film and that of the glass. In this way we cancel out the fluctuations of the pump intensity I_1:

$$\frac{\left|\chi^{(3)NC}(\lambda)\right|}{\left|\chi^{(3)glass}\right|} = \left(\frac{I_3^{NC}}{I_3^{glass}}\frac{f^{glass}(\lambda)}{f^{NC}(\lambda)}\right)^{\frac{1}{2}} \qquad \textbf{(5)}$$

In the end, taking into account the contribution, in volume, of the nanocrystals with respect to the porous matrix and the spectrally flat third order non-linearity of the glass[45], we were able to derive the spectral dependence of $\chi^{(3)}$ of the $FAPbBr_3$ nanocrystals as shown in figure 5.5c.

$$\chi^{(3)NC}(\lambda) = \left(\frac{I_3^{NC}}{I_3^{glass}}\frac{f^{glass}(\lambda)}{f^{NC}(\lambda)}\right)^{\frac{1}{2}}\frac{\left|\chi^{(3)glass}\right|}{V} \qquad \textbf{(6)}$$

A clear peak in $\chi^{(3)NC}(\lambda)$ is evident for wavelengths around 520 nm, which is also close to the frequency of the excitonic resonance of the nanocrystals as show in the linear results (figure 2). This can be confirmed when comparing to the plot of Re(n) (green line) which is over-imposed in the same figure.

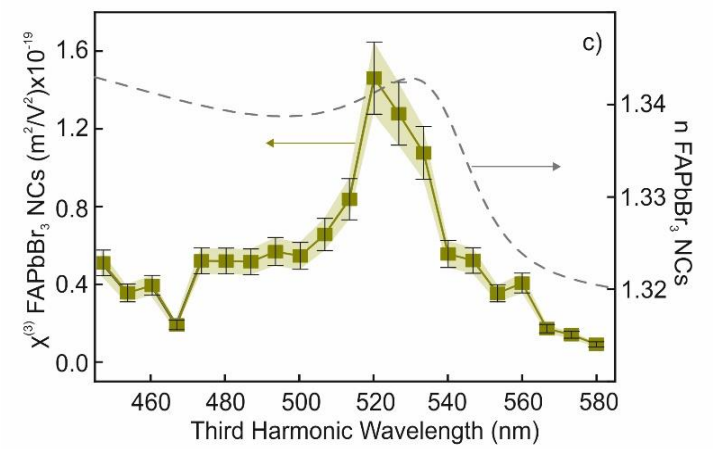

Figure 5.5 c) Spectral shape of the third order nonlinear susceptibility for the $FAPbBr_3$ nanocrystal encapsulated in the SiO_2 NPs porous film, compared with the spectral dependence of real part of the linear refractive index of the $FAPbBr_3$ nanocrystal film in the experimental wavelength range.

The maximum absolute value of $\chi^{(3)NC}(\lambda)$ obtained at 1560 nm pump wavelength is $1.46\pm0.2 \times 10^{-19} m^2/V^2$, which is in the order of magnitude of few other examples of low dimensional perovskite systems reported so far like two-dimensional layered system[38,47] and cesium-based perovskite colloidal nanocrystals[48] (in this case, $\chi^{(3)}$ values are extracted from Z-scan technique). In general, however, the calculated susceptibility shows a nonlinear character of the third order similar to organic materials currently employed in this field[49] and to some more similar system, which are nanocrystalline semiconductors infiltrated in glass matrices (normally Si- or Al-based).[50,51]

5.6 CONCLUSIONS

In conclusion, this analysis has allowed, in the first place, to investigate an aspect of the fundamental properties of perovskite nanocrystals that is still underexplored and a nonlinear phenomenon rarely reported in the case of perovskites. The optical response of the third order in the form of a third harmonic generation, although rather common with the adequate field intensity applied, was demonstrated here for the first time in the case of perovskite $FAPbBr_3$ nanocrystals. We further characterise the spectral dependence of the generated third harmonic and extract the spectral shape and value of the nonlinear susceptibility of the ($FAPbBr_3$) nanocrystals film, $\chi^{(3)NC}=1.46\pm0.2 \times 10^{-19} m^2/V^2$. Obviously it is necessary to keep in mind the limitations of the third order susceptibility extraction method related to

the approximations already known also in the calculation of the linear properties and which depend above all on the description of the components of the composite system (for example exact quantity and dispersion of the nanocrystals inside the porous matrix) together with the fact that the model used for the $\chi^{(3)NC}$ simulation[46] assumes a non-depleting pump wavelength. In any case, the templated synthesis in porous matrices in the form of optically transparent films demonstrates again an indisputable advantage in the possibility of adapting to more sophisticated and sensitive experimental analysis set ups in terms of the optical quality of the samples (consider, for example, as the susceptibility spectral dependence is a result that is already quite interesting beyond the values obtained). From the point of view of the result, however, it should be noted that compared to, for example, 2D materials, the composite systems presented in this work are certainly easier to fabricate, while the structure, as we have already discussed previously, can be very advantageous when integrating the perovskites in more complex architectures and improve or control their properties. The same consideration, of course, becomes valid in the assembly of new devices for the technological application. Furthermore, as can be deduced from the phase mismatch analysis, there is the possibility of optimizing the structure in terms of thickness, but also in terms of volume ratio as well as from the point of view of the composition of the perovskites. Considering, then, what has already been observed in chapter 3, it is also possible to improve the stability problems in particular with respect to the humidity of the environment which is one of the factors notoriously slowing down the development of technologies based on perovskites.

5.7 NOTES

THG measurements were performed during a secondment at the Complex Nanophotonics group (Imperial College London) led by Dr. Riccardo Sapienza. I would like to thank the group for the support in the nonlinear optics analysis and the collaboration for the extracting of $\chi^{(3)}$ (section 5.5).

5.8 BIBLIOGRAPHY

1 GARMIRE, Elsa. Nonlinear optics in daily life. Optics express, 2013, 21.25: 30532-30544.

2 MAIER, M.; KAISER, W.; GIORDMAINE, J. A. Intense light bursts in the stimulated Raman effect. Physical review letters, 1966, 17.26: 1275.

3 BRAUNSTEIN, Rubin. Nonlinear optical effects. Physical Review, 1962, 125.2: 475.

4 BOYD, Robert W. Nonlinear optics. Academic press, 2019.

5 SIONCKE, Sonja; VERBIEST, Thierry; PERSOONS, André. Second-order nonlinear optical properties of chiral materials. Materials Science and Engineering: R: Reports, 2003, 42.5-6: 115-155.

6 FEJER, Martin M. Nonlinear optical frequency conversion. Physics today, 1994, 47.5: 25-33.

7 ALFANO, Robert R.; SHAPIRO, S. L. Observation of self-phase modulation and small-scale filaments in crystals and glasses. Physical Review Letters, 1970, 24.11: 592.

8 BHAWALKAR, J. D.; HE, G. S.; PRASAD, P. N. Nonlinear multiphoton processes in organic and polymeric materials. Reports on Progress in Physics, 1996, 59.9: 1041.

9 LEUTHOLD, Juerg; KOOS, Christian; FREUDE, Wolfgang. Nonlinear silicon photonics. Nature photonics, 2010, 4.8: 535-544.

10 GRINBLAT, Gustavo, et al. Ultrafast all-optical modulation in 2D hybrid perovskites. ACS nano, 2019, 13.8: 9504-9510.

11 WU, Leiming, et al. Perovskite CsPbX3: a promising nonlinear optical material and its applications for ambient all-optical switching with enhanced stability. Advanced Optical Materials, 2018, 6.19: 1800400.

12 BONACINA, Luigi. Nonlinear nanomedecine: harmonic nanoparticles toward targeted diagnosis and therapy. Molecular Pharmaceutics, 2013, 10.3: 783-792.

13 CHANG, Darrick E.; VULETIĆ, Vladan; LUKIN, Mikhail D. Quantum nonlinear optics—photon by photon. Nature Photonics, 2014, 8.9: 685-694.

14 ALAM, M. Zahirul; DE LEON, Israel; BOYD, Robert W. Large optical nonlinearity of indium tin oxide in its epsilon-near-zero region. Science, 2016, 352.6287: 795-797.

15 CASPANI, Lucia, et al. Enhanced nonlinear refractive index in ε-near-zero materials. Physical review letters, 2016, 116.23: 233901.

16 RESHEF, Orad, et al. Nonlinear optical effects in epsilon-near-zero media. Nature Reviews Materials, 2019, 4.8: 535-551.

17 HENDRY, Euan, et al. Coherent nonlinear optical response of graphene. Physical review letters, 2010, 105.9: 097401.

18 LU, S. B., et al. Broadband nonlinear optical response in multi-layer black phosphorus: an emerging infrared and mid-infrared optical material. Optics express, 2015, 23.9: 11183-11194.

19 YIN, Xiaobo, et al. Edge nonlinear optics on a MoS2 atomic monolayer. Science, 2014, 344.6183: 488-490.

20 BIKORIMANA, S., et al. Nonlinear optical responses in two-dimensional transition metal dichalcogenide multilayer: WS2, WSe2, MoS2 and Mo0.5W0.5S2. Optics Express, 2016, 24.18: 20685-20695.

21 FERRANDO, Albert; MARTINEZ PASTOR, Juan P.; SUÁREZ, Isaac. Toward metal halide perovskite nonlinear photonics. The journal of physical chemistry letters, 2018, 9.18: 5612-5623.

22 XU, Jialiang, et al. Halide perovskites for nonlinear optics. Advanced Materials, 2020, 32.3: 1806736.

23 HAN, XIAO, ET AL. 2D ORGANIC-INORGANIC HYBRID PEROVSKITE MATERIALS FOR NONLINEAR OPTICS. NANOPHOTONICS, 2020, 1.AHEAD-OF-PRINT.

24 WENGER, BERNARD, ET AL. CONSOLIDATION OF THE OPTOELECTRONIC PROPERTIES OF CH3NH3PBBR3 PEROVSKITE SINGLE CRYSTALS. NATURE COMMUNICATIONS, 2017, 8.1: 1-10.

25 JUAREZ-PEREZ, EMILIO J., ET AL. PHOTOINDUCED GIANT DIELECTRIC CONSTANT IN LEAD HALIDE PEROVSKITE SOLAR CELLS. THE JOURNAL OF PHYSICAL CHEMISTRY LETTERS, 2014, 5.13: 2390-2394.

26 JANG, DONG MYUNG, ET AL. REVERSIBLE HALIDE EXCHANGE REACTION OF ORGANOMETAL TRIHALIDE PEROVSKITE COLLOIDAL NANOCRYSTALS FOR FULL-RANGE BAND GAP TUNING. NANO LETTERS, 2015, 15.8: 5191-5199.

27 CHEN, XIHAN, ET AL. EXCITONIC EFFECTS IN METHYLAMMONIUM LEAD HALIDE PEROVSKITES. THE JOURNAL OF PHYSICAL CHEMISTRY LETTERS, 2018, 9.10: 2595-2603.

28 LOZHKINA, OLGA A., ET AL. LOW INHOMOGENEOUS BROADENING OF EXCITONIC RESONANCE IN MAPBBR3 SINGLE CRYSTALS. THE JOURNAL OF PHYSICAL CHEMISTRY LETTERS, 2018, 9.2: 302-305.

29 MARONGIU, DANIELA, ET AL. THE ROLE OF EXCITONS IN 3D AND 2D LEAD HALIDE PEROVSKITES. JOURNAL OF MATERIALS CHEMISTRY C, 2019, 7.39: 12006-12018.

30 CHEN, XIAOXUAN, ET AL. TEMPERATURE DEPENDENT REFLECTANCE AND ELLIPSOMETRY STUDIES ON A CSPBBR3 SINGLE CRYSTAL. THE JOURNAL OF PHYSICAL CHEMISTRY C, 2019, 123.16: 10564-10570.

31 POPKOVA, ANNA A., ET AL. SECOND HARMONIC GENERATION IN CH3NH3PBI3 THIN FILMS. IN: FRONTIERS IN OPTICS. OPTICAL SOCIETY OF AMERICA, 2018. P. JW3A. 49.

32 GOVINDA, SHARADA, ET AL. CAN SHG MEASUREMENTS DETERMINE THE POLARITY OF HYBRID LEAD HALIDE PEROVSKITES?. ACS ENERGY LETTERS, 2018, 3.8: 1887-1891.

33 STRELCOV, EVGHENI, ET AL. CH3NH3PBI3 PEROVSKITES: FERROELASTICITY REVEALED. SCIENCE ADVANCES, 2017, 3.4: E1602165.

34 WEI, TZU-CHIAO, ET AL. NONLINEAR ABSORPTION APPLICATIONS OF CH3NH3PBBR3 PEROVSKITE CRYSTALS. ADVANCED FUNCTIONAL MATERIALS, 2018, 28.18: 1707175.

35 WEI, WEN-JUAN, ET AL. REGULATING SECOND-HARMONIC GENERATION BY VAN DER WAALS INTERACTIONS IN TWO-DIMENSIONAL LEAD HALIDE PEROVSKITE NANOSHEETS. JOURNAL OF THE AMERICAN CHEMICAL SOCIETY, 2019, 141.23: 9134-9139.

36 CLARK, D. J., ET AL. POLARIZATION-SELECTIVE THREE-PHOTON ABSORPTION AND SUBSEQUENT PHOTOLUMINESCENCE IN CSPBBR 3 SINGLE CRYSTAL AT ROOM TEMPERATURE. PHYSICAL REVIEW B, 2016, 93.19: 195202.

37 JOHNSON, JUSTIN C., ET AL. THIRD-ORDER NONLINEAR OPTICAL PROPERTIES OF METHYLAMMONIUM LEAD HALIDE PEROVSKITE FILMS. JOURNAL OF MATERIALS CHEMISTRY C, 2016, 4.22: 4847-4852.

38 ABDELWAHAB, IBRAHIM, ET AL. HIGHLY ENHANCED THIRD-HARMONIC GENERATION IN 2D PEROVSKITES AT EXCITONIC RESONANCES. ACS NANO, 2018, 12.1: 644-650.

39 BERESTENNIKOV, ALEXANDER S., ET AL. ACTIVE META-OPTICS AND NANOPHOTONICS WITH HALIDE PEROVSKITES. APPLIED PHYSICS REVIEWS, 2019, 6.3: 031307.

40 EPERON, GILES E., ET AL. FORMAMIDINIUM LEAD TRIHALIDE: A BROADLY TUNABLE PEROVSKITE FOR EFFICIENT PLANAR HETEROJUNCTION SOLAR CELLS. ENERGY & ENVIRONMENTAL SCIENCE, 2014, 7.3: 982-988.

41 BRENNAN, MICHAEL C., ET AL. LIGHT-INDUCED ANION PHASE SEGREGATION IN MIXED HALIDE PEROVSKITES. ACS ENERGY LETTERS, 2017, 3.1: 204-213.

42 SCHUELLER, EMILY C., ET AL. CRYSTAL STRUCTURE EVOLUTION AND NOTABLE THERMAL EXPANSION IN HYBRID PEROVSKITES FORMAMIDINIUM TIN IODIDE AND FORMAMIDINIUM LEAD BROMIDE. INORGANIC CHEMISTRY, 2018, 57.2: 695-701.

43 ÁVILA, JORGE, ET AL. HIGH VOLTAGE VACUUM-DEPOSITED CH3NH3PBI3–CH3NH3PBI3 TANDEM SOLAR CELLS. ENERGY & ENVIRONMENTAL SCIENCE, 2018, 11.11: 3292-3297.

44 BREDAS, J. L_, ET AL. "THIRD-ORDER NONLINEAR OPTICAL RESPONSE IN ORGANIC MATERIALS: THEORETICAL AND EXPERIMENTAL ASPECTS." CHEMICAL REVIEWS 94.1 (1994): 243-278.

45 GUBLER, ULRICH; BOSSHARD, CHRISTIAN. OPTICAL THIRD-HARMONIC GENERATION OF FUSED SILICA IN GAS ATMOSPHERE: ABSOLUTE VALUE OF THE THIRD-ORDER NONLINEAR OPTICAL SUSCEPTIBILITY X (3). PHYSICAL REVIEW B, 2000, 61.16: 10702.

46 YOUNGBLOOD, NATHAN, ET AL. LAYER-TUNABLE THIRD-HARMONIC GENERATION IN MULTILAYER BLACK PHOSPHORUS. ACS PHOTONICS, 2017, 4.1: 8-14.

47 SAOUMA, F. O., ET AL. SELECTIVE ENHANCEMENT OF OPTICAL NONLINEARITY IN TWO-DIMENSIONAL ORGANIC-INORGANIC LEAD IODIDE PEROVSKITES. NATURE COMMUNICATIONS, 2017, 8.1: 1-8.

48 SZEREMETA, JANUSZ, ET AL. THE TWO-PHOTON ABSORPTION CROSS-SECTION STUDIES OF CSPBX3 (X= I, BR, CL) NANOCRYSTALS. NANOMATERIALS, 2020, 10.6: 1054.

49 BLOM, FREEK C., ET AL. THIRD HARMONIC GENERATION AS A RAPID SELECTION TOOL FOR ORGANIC MATERIALS FOR NONLINEAR INTEGRATED OPTICS DEVICES. OPTICAL MATERIALS, 1999, 12.2-3: 327-331.

50 LU, S. G., ET AL. NONLINEAR OPTICAL PROPERTIES IN CDS/SILICA NANOCOMPOSITES. MICROELECTRONIC ENGINEERING, 2003, 66.1-4: 171-179.

51 NASU, HIROYUKI, ET AL. INFLUENCE OF MATRIX ON THIRD ORDER OPTICAL NONLINEARITY FOR SEMICONDUCTOR NANOCRYSTALS EMBEDDED IN GLASS THIN FILMS PREPARED BY RF-SPUTTERING. JOURNAL OF NON-CRYSTALLINE SOLIDS, 2005, 351.10-11: 893-899.

APPENDIX I: SPECULAR REFLACTANCE POROSIMETRY

The study through specular reflectance when the vapour pressure of a solvent increases (or decreases) within the pores of the matrix composed of SiO_2 particles, allows to obtain useful information to quantify the total volume of the pores and their size. The reflectance spectra are recorded at each variation of the relative pressure of the introduced vapour (IpOH), from 0 to 1 (considering a minimum waiting time to allow the system to reach the equilibrium, before each measurement). So the pressure range extends from the minimum value obtained in the chamber with the porous matrix under vacuum, P_0, up to the saturation pressure of the solvent, P_s.

The specular reflectance presents the typical oscillating shape resulting from the optical interference characteristic of a thin film. But the increase in vapour pressure, as can be seen in the figure 2.3.1c, causes a spectral translation towards longer wavelengths. The spectral separation between one curve and the next recorded at a higher vapour pressure is, in fact, due to a change in the optical thickness of the film. Considering the latter as the product between the effective refractive index of the film and its geometric thickness, the evolution of reflectance, as a function of pressure, can be related to the variation of the effective index caused by the adsorption and condensation of the vapour inside the pores of the matrix.

Reflectance fitting

So, for the calculation of the effective refractive index, as already mentioned in chapter 2, a MatLab code written on the basis of the transfer matrix method was used.[1] Given the uniformity of the sample, the system, in this calculation, is described by a dielectric layer between two semi-infinite media, assuming an isotropic and homogeneous refractive index for each. According to the formalism of the transfer matrix, a series of equations are solved to obtain the reflection and transmission coefficients, imposing a condition of continuity of the electric and magnetic field at the two interfaces present in the system.

The thickness and the effective refractive index of the porous film are then included in the calculation as parameters for fitting the experimental reflectance data with the calculated function, using the least squares method. For each fitting relative to

the distinct reflectance spectra, the effective refractive index is adjusted as the vapour pressure varies.

Pore volume fraction

The variation with respect to the pressure increase can, then, be related to the occupation of a fraction of the pores volume by the solvent. For the volumetric description of the porous film, in this case, the Bruggemann approximation of the effective medium was applied[2]. In this picture the porous material is composed of three elements: silica, with a known refractive index (n_{SiO2}=1.45, at 1µm); the solvent (in our case IpOH) with index n_{IpOH}=1.37 (at 1µm) and a homogeneous medium with a refractive index, n_{medium}, equal to 1 when the vapour has not yet started to enter the pores. So, the effective index of the material thus composed can be defined by the following equation:

$$f_{SiO2}\frac{n_{SiO2}^2-n^2}{n_{SiO2}^2+2n^2}+f_{IpOH}\frac{n_{IpOH}^2-n^2}{n_{IpOH}^2+2n^2}+f_{medium}\frac{n_{medium}^2-n^2}{n_{medium}^2+2n^2}=0 \quad (1)$$

where $f_{SiO2}, f_{IpOH}, f_{medium}$ indicate the volume fractions of the corresponding elements indicated above.

Having therefore extrapolated the value of the effective refractive index through the fitting of the reflectance spectra of the system under vacuum (without any f_{IpOH}), it is possible to find the total fraction of the pore volume:

$$f_{medium}=f_{pore}=1-f_{SiO2} \quad (2)$$

Subsequently, in the same way, the fraction of pores volume occupied by the adsorbed and/or condensed vapour of the solvent, f_{IpOH}, can be found according to the evolution of the effective refractive index, as the solvent vapour pressure increase:

$$f_{medium}=1-f_{SiO2}-f_{IpOH} \quad (3)$$

The characteristic adsorption isothermal curve shown in the figure 2.3.1d is obtained from the variation of the f_{IpOH}/f_{pore} (that is V_{ads}/V_{pore} volume ratio) as a function of the solvent partial pressure. The observed behaviour can generally be traced back to that of a structure with accessible and interconnected porosity[3].

Pore size distribution

Finally, to obtain the Pore Size Distribution, through the measurements obtained so far, it is possible to recall the Kelvin's law which governs the condensation phenomenon of the solvent adsorbed inside the pores in the condition of low partial pressure[4]:

$$ln\left(\frac{P}{P_s}\right)=-\frac{2\gamma V_L}{RT}\frac{1}{r_k} \quad (4)$$

In this formalism the term P/P_s refers to the ratio between the pressure inside a pore and the saturation pressure of the solvent. r_k is the radius of the aforementioned pore (Kelvin radius), V_L and γ are the molar volume and surface tension of the solvent, respectively, while R and T refer to the gas constant and temperature. Considering this law, at each relative pressure value, the corresponding pores (i.e. those with radius r_k) will be filled with condensed isopropanol. Therefore, a variation of the pore volume fraction occupied by the adsorbed solvent V_{ads} is related to the presence of a greater fraction of pores with radius r_k, corresponding to that value of P/P_s.

More precisely, however, the radius of the real pore is obtained by adding to the value of r_k the thickness t of a layer of solvent molecules adsorbed on the pore walls and calculated according to the Brunauer, Emmet, and Teller expression[5]:

$$t = -\frac{d_0 KC\left(\frac{P}{P_s}\right)}{\left[1 - KC\left(\frac{P}{P_s}\right)\right]\left[1 + K(C-1)\left(\frac{P}{P_s}\right)\right]} \quad \textbf{(5)}$$

The parameter K depends on the solvent, C is the BET constant and d_0 the thickness of a single monolayer of molecules (approximately the diameter of a gas molecule of the solvent used). The constant C can be obtained through the following equation

$$\frac{P}{V_{ads}(P - P_s)} = \frac{1}{V_m} + \frac{C-1}{V_m C}\frac{P}{P_s} \qquad \frac{P}{V_{ads}(P - P_s)} = \frac{1}{V_m} + \frac{C-1}{V_m C}\frac{P}{P_s} \quad \textbf{(6)}$$

in which V_m indicates the ratio between the volume of the adsorbed monolayer and the total volume of the pores.

1 LOZANO, GABRIEL, ET AL. THEORETICAL ANALYSIS OF THE PERFORMANCE OF ONE-DIMENSIONAL PHOTONIC CRYSTAL-BASED DYE-SENSITIZED SOLAR CELLS. THE JOURNAL OF PHYSICAL CHEMISTRY C, 2010, 114.8: 3681-3687.

2 NAGY, NORBERT, ET AL. ELLIPSOMETRY OF SILICA NANOPARTICULATE LANGMUIR– BLODGETT FILMS FOR THE VERIFICATION OF THE VALIDITY OF EFFECTIVE MEDIUM APPROXIMATIONS. LANGMUIR, 2006, 22.20: 8416-8423.

3 CONDON JB. SURFACE AREA AND POROSITY DETERMINATIONS BY PHYSISORPTION: MEASUREMENT, CLASSICAL THEORIES AND QUANTUM THEORY. ELSEVIER; 2019 OCT 16.

4 GREGG SJ, SING KS, SALZBERG HW. ADSORPTION SURFACE AREA AND POROSITY. JOURNAL OF THE ELECTROCHEMICAL SOCIETY. 1967 NOV 1;114(11):279C.

5 GREGG SJ, SING KS, SALZBERG HW. ADSORPTION SURFACE AREA AND POROSITY. JOURNAL OF THE ELECTROCHEMICAL SOCIETY. 1967 NOV 1;114(11):279C.

7 GENERAL CONCLUSIONS

In this thesis a new synthesis method of $APbX_3$ type perovskites ($A=MA^+, FA^+, Cs^+$; $X=I^-, Br^-$) in the form of nanocrystals was presented. The method allows the preparation of thin films composed of perovskite nanocrystals encapsulated in porous matrices formed by metal oxide nano-particles (in particular SiO_2, but also TiO_2 and SnO_2): pvk@MOx. The effectiveness of the control on the dimensions of the nanocrystals has been demonstrated through the variation of the concentration of the perovskite precursor solutions, infiltrated in the porous layers.

A complete structural characterization of the composite materials (porous matrices and perovskite nanocrystals) has been presented which clearly highlights the formation of perovskite nanocrystals inside the pores of the matrices, avoiding the formation of bulk material but also nanocrystals aggregation.

For the first time, a study of the growth process of perovskite nanocrystals within the matrices and of the effects of factors such as precursor concentration, illumination and temperature was presented.

A linear analysis of the optical properties of films composed of perovskite nanocrystals was presented. In particular, the control over the emission properties (PL and PLQY) has been related to the effects of quantum confinement. We have been able to change the optical environment of the matrix in order to modify the emission properties of perovskite nanocrystals). This modification was also useful to highlight the versatility of the synthetic method both as regards the scaffold and the chemical composition of perovskites. This allowed us to prepare a series of flexible and self-standing films based on the porous system with the perovskite nanocrystals both embedded in a polymer matrix. The materials thus obtained have shown not only mechanical functionality, but also the preservation of perovskites from degradation in extreme humidity conditions (underwater). It has also been demonstrated how such flexible systems can be used as colour converting layer for the new generation of LEDs.

A study on the spectral dependence of the refractive index and extinction coefficient of perovskite nanocrystals together with the variation with respect to the size was presented for the first time. This analysis finds particular relevance in the future design of optoelectronic devices based on such nanocrystals.

A judicious study of the photoluminescence of perovskite nanocrystals at low temperatures (at ambient pressure) and high pressures (at ambient temperature) has been presented. This characterization allowed us to distinguish the contribution of thermal expansion and electron-phonon coupling in the dependence of the band

gap with temperature, highlighting the role of lattice dynamics on the optical and electronic response as perovskite size decreases. We also demonstrated how this dependence varies with the size of the nanocrystals.

In what respect to non-linear optical properties, a characterization of the third order response (in particular the spectral shape of susceptibility χ^3) of $FAPbBr_3$ perovskite nanocrystals was presented, through which the possibility of using perovskite nanocrystals for the effective generation of third harmonics was demonstrated.

The fabrication and characterization of solar cells and LEDs based on perovskite nanocrystals encapsulated in porous SiO_2 matrices was presented. The performance of these devices irrefutably demonstrates the percolation of the charges through the population of nanocrystals inside the isolated matrices, up to the electrodes. In addition, with regard to solar cells, the use of a matrix for the preparation (encapsulation) of the nanocrystals demonstrated to slow down their degradation as well. Such cells revealed an improvement in stability over time compared to the cell with a bulk layer.

Together with the fundamental study, the composite systems developed in this thesis have therefore revealed the possibility of further developments in direct technological applications.

NANOCRISTALES DE PEROVSKITAS ABX_3 EN MATRICES POROSAS: RESUMEN

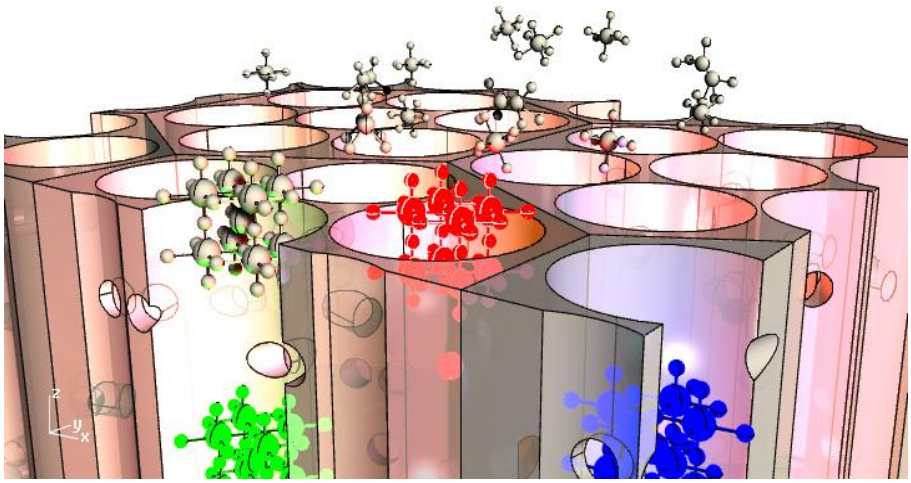

1. Introducción

El término perovskita define una clase de materiales con la estructura cristalina ABX_3 del titanato de calcio (típicamente pseudo-cúbica).[1,2] Aunque esta familia de compuestos es bien conocida desde mediados del siglo XIX, las especies formadas por plomo (catión B), haluros (anión X) y cationes A de tipo orgánico y / o inorgánico (MA, FA, Cs) se han convertido en objetos de un renovado interés en toda la comunidad científica y de un intenso estudio en los últimos veinte años. Las razones de su importancia residen en las propiedades optoelectrónicas que han hecho de estos semiconductores híbridos materiales excelentes, en particular para la tecnología fotovoltaica y para la iluminación.[3,4] Una contribución igualmente importante a su éxito proviene de la facilidad de preparación, mediante procesos en solución. Esto se traduce en unos costes de producción reducidos, que junto con unos rendimientos excelentes hacen que este tipo de perovskitas sea bastante competitivo en el contexto energético actual. Como parte negativa para el avance tecnológico de estos semiconductores encontramos cuestiones relacionadas con la estabilidad a largo plazo. Las perovskitas de haluro de plomo son particularmente sensibles a las condiciones ambientales y pueden degradarse bajo la influencia de agua, oxígeno, temperatura y luz.[5,6] Sin embargo, estos semiconductores son muy

versátiles y, desde su reciente desarrollo, la investigación se dedicó a la exploración de la composición química ideal (perovskitas completamente inorgánicas, perovskitas mixtas, perovskitas sin plomo, etc.) en términos de propiedades y estabilidad, de su morfología, de las técnicas de preparación y en la exploración de estos semiconductores en la nano-escala.

La nanotecnología ha acompañado la investigación en muchos otros campos e incluso en el caso de las perovskitas los resultados hasta ahora han sido sorprendentes. Los materiales de baja dimensionalidad, ya sean nanocristales u otras posibles conformaciones en 0, 1 ó 2 dimensiones, han ampliado el potencial de las perovskitas aumentando la estabilidad de las celdas solares o bien mejorando sus propiedades ópticas de emisión de luz. Además su fabricación es fácilmente integrable en las arquitecturas de dispositivos optoelectrónicos o en nuevas estructuras más complejas (p. ej. ejemplo cristales fotónicos) para su funcionalización adicional.[7-9] Sin embargo, uno de los aspectos más relevantes de los nanocristales de perovskita sigue siendo el efecto del confinamiento cuántico. Para entender esta importancia es necesario recordar que estos semiconductores cuando se fabrican en su forma "*bulk*" pueden variar su *bandgap* a lo largo del espectro visible. Esto se logra a través de la composición química y en particular en la substitución de los halógenos (iodo, bromo, cloro). No obstante una de las consecuencias de la síntesis de perovskitas mixtas (por ejemplo $MAPbBr_xI_{3-x}$) es la migración iónica que conduce fácilmente a una segregación de fases o incluso a la descomposición del material.[10,11] En los nanocristales, en cambio, gracias al fenómeno del confinamiento cuántico, cuando el radio del semiconductor alcanza las dimensiones del radio de Bohr, es posible controlar el *bandgap* a través del tamaño de los cristales.[12,13] Otra ventaja interesante del confinamiento cuántico es la estabilidad del excitón fotogenerado y una mejor eficiencia en términos de emisión. Sin embargo, este último aspecto está fuertemente condicionado por una de las cualidades más interesantes de los nanocristales de perovskita, que es la tolerancia con respecto a la presencia de defectos o trampas para las cargas.[14]

En cuanto a la preparación de nanocristales de perovskita, los métodos más utilizados hasta la fecha involucran procesos mediados por ligandos orgánicos o sea síntesis de tipo coloidal.[15] A pesar de la tolerancia anterior, los ligandos permiten controlar el tamaño y la forma de las perovskitas, pero también actúan como agentes pasivantes de defectos mejorando el rendimiento de los semiconductores.[16] Sin embargo, existen algunos inconvenientes relacionados con el uso de ligandos al momento del depósito de partículas coloidales para la formación de películas. El desprendimiento de los ligandos durante los ciclos de lavado y purificación y los fenómenos de auto-agregación de los nanocristales inducen una pérdida de estabilidad y un empeoramiento de las propiedades ópticas.[17,18] En este contexto, mucho más recientemente se ha presentado una síntesis alternativa, sin ligandos, es decir la preparación de nanocristales de

perovskita mediante moldes o *templates*.[19] Este método consiste generalmente en la infiltración de una solución de precursores de perovskita en una matriz porosa que puede ser de distinta naturaleza (orgánica o inorgánica). El tamaño y/o la forma de los poros fuerzan la cristalización de las perovskitas dentro de los mismos. Por tanto, si se controlan las características microestructurales de la matriz utilizada es posible gobernar, por ejemplo, el confinamiento cuántico de los nanocristales de perovskita, pero también es posible manipular sus propiedades químico-físicas según el tipo de material elegido para la matriz porosa.

Aunque ya se había explorado la posibilidad de confinar espacialmente semiconductores en una matriz, al comienzo de esta tesis aún no se había adaptado al caso de estas "nuevas" perovskitas. En particular, la atención de esta tesis se ha dirigido al uso de matrices porosas en forma de películas delgadas en vista de una aplicación tecnológica directa de estos sistemas compuestos. El potencial de este método, de hecho, también se refiere al uso de una inmensa variedad de estructuras porosas con diferentes composiciones químicas y por lo tanto diferentes propiedades más o menos compatibles con las de las perovskitas. Si bien los primeros trabajos (ca. 2016) se centraron en particular en el fenómeno del confinamiento y en el control espectral del *bandgap* de los nanocristales de perovskita, las matrices utilizadas se procesaron en forma de polvo lo cual no permite su posterior integración en un dispositivo.[20,21] En esta tesis, por otro lado, luego de un estudio inicial sobre el uso de láminas de matrices meso-estructuradas, se trabajó con matrices formadas por estratificaciones de nanopartículas, especialmente adecuadas para la arquitectura de dispositivos optoelectrónicos de nueva generación. Paralelamente al estudio realizado en esta tesis, el método de moldeado para la síntesis de nanocristales de perovskita ha demostrado no solo ser una alternativa válida a la síntesis coloidal, sino que ofrece nuevas ventajas respecto, por ejemplo, a la estabilidad de perovskitas.[22] La naturaleza de las matrices, además, como ya se mencionó, puede influir en la respuesta de las perovskitas con respecto, por ejemplo, a la extracción de portadores de carga. Finalmente, algunos casos reportados, han mostrado la posibilidad de aplicar ciertos sistemas matriz-perovskitas en dispositivos fotovoltaicos y de iluminación.[23,24]

Pero si bien el tema de los nanocristales de perovskita todavía ofrece mucho espacio para la exploración y optimización de sus propiedades optoelectrónicas, el uso de matrices porosas está todavía menos estudiado y el objetivo de esta tesis ha sido investigar esto nuevo método de síntesis y estudiar los nanocristales de perovskita, sus propiedades ópticas y estructurales fundamentales y sus posibles implicaciones tecnológicas.

2. Nanocristales de perovskitas en películas de MOx NPs

La síntesis de nanocristales de perovskita (NCs) desarrollada en esta tesis consiste en un proceso *one-step* en el que una solución que contiene los precursores de perovskita se infiltra en una matriz porosa. La matriz utilizada para este propósito consiste en nanopartículas de óxido metálico (incluído SiO_2 MOx NPs) depositadas por *dip-coating* para formar una estratificación porosa morfológicamente homogénea y ópticamente transparente. Para distribuir uniformemente las especies contenidas en la solución precursora de perovskitas, dentro de la matriz, se utilizó la técnica de deposición *spin-coating*. Una vez impregnada la película porosa, un tratamiento térmico acelera la cristalización de las perovskitas dentro de los poros que actúan como nano-reactores para la síntesis de nanocristales. Para este método se han optimizado diversos parámetros implicados tanto en el propio proceso de síntesis (concentración de precursores, temperatura) como en las deposiciones (velocidad de deposición, espesor y uniformidad de la matriz). Las técnicas de recubrimiento utilizadas son ventajosas, ya que son escalables y de bajo costo y además permiten obtener deposiciones homogéneas (es importante asegurar una buena calidad óptica tanto para no obstaculizar la respuesta de la perovskita y no comprometer el rendimiento de un dispositivo) y controlar con extrema precisión el espesor de la película de nanopartículas y en consecuencia el volumen disponible para la síntesis de perovskitas.

La versatilidad del método se observa tanto a la posibilidad de utilizar, por ejemplo, diferentes tipos de óxidos metálicos, como en la elección de la composición química de las perovskitas según la aplicación específica (por ejemplo, $MAPbI_3$, más adecuado para absorción de la radiación visible o $MAPbBr_3$, más adecuado para la emisión). En esta tesis, sin embargo, la matriz más utilizada se basa en nanopartículas de SiO_2 que, además de la finalidad sintética en sí, permite un buen aislamiento eléctrico de los nanocristales y por tanto un análisis más limpio de su comportamiento. Para una descripción más cuantitativa de la matriz, hemos podido utilizar la técnica de porosimetría por reflectancia especular[25] con la que es posible determinar la porosidad del sistema (alrededor del 50% en el caso de SiO_2) y la distribución del tamaño de poro, PSD (alrededor de 8 nm). De esta manera se confirma que a pesar de que la estructura porosa es relativamente simple, caracterizándose por una PSD bastante estrecha. Esto nos ha permitido utilizar este tipo de matrices para la síntesis homogenénea de nanocristales de perovskita. Aparte del confinamiento espacial dentro de la matriz, con el método desarrollado es posible ejercer un control específico sobre las dimensiones de los nanocristales de perovskita variando la concentración de la solución precursora infiltrada en los poros. A medida que disminuye la concentración, se obtienen cristales más pequeños. Este resultado se evidencia tanto por el desplazamiento espectral de fotoluminiscencia (PL) con respecto a la emisión de una película *bulk* policristalina (consecuencia directa de los efectos del confinamiento cuántico), como por el

análisis estructural a través del microscopio electrónico de transmisión de alta resolución.

El uso de la técnica de preparación *de moldeado* y en particular el uso de matrices porosas en forma de películas homogéneas, nos ha permitido realizar un análisis adicional que es particularmente interesante también porque mucho más complicado en otro tipo de sistemas (coloidales o matrices en polvos), es decir, un estudio de la crecimiento de nanocristales dentro de las matrices. Con estos materiales compuestos fue posible monitorizar la fotoluminiscencia de una misma población de nanocristales y analizar la cinética de crecimiento, evaluando también algunos factores extrínsecos como la iluminación, la temperatura y la concentración de precursores. Considerando, por ejemplo, la posición espectral del pico PL, es posible estimar las dimensiones de los nanocristales en relación con el corrimiento al rojo (mayor tamaño) a partir de las primeras fases de síntesis. Al mismo tiempo, el ancho de pico PL (FWHM) puede proporcionar información sobre un factor de calidad clave para los nanocristales, o sea, la dispersión de tamaño. En concreto, observamos un ensanchamiento de la emisión en el caso en el que se utilizó una solución de precursor más diluida que puede asociarse a un proceso de *defocusing*[26] que implica una mayor dispersión de dimensiones de nanocristales. El estudio del crecimiento en tamaño se realizóutilizando el modelo Lifshitz-Slyozov-Wagner[27]con el cual se aplicó la aproximación de Brus[28], para correlacionar los radios de los nanocristales. . Siguiendo este modelo, se pueden distinguir tres regímenes que pueden interpretarse como fases secuenciales de crecimiento regidas por varios factores limitantes: una fase inicial controlada por las reacciones de fase líquido-sólido; luego, al disminuir la cantidad de reactivos, con el tiempo, la cinética es dominada por la difusión de los precursores y finalmente, con la evaporación del solvente, la disolución de las partículas más pequeñas domina la etapa final. Además, como ya se mencionó, monitoreamos la misma muestra en diferentes condiciones de temperatura e iluminación observando que si bien esta última no parece afectar el crecimiento de los nanocristales, una temperatura alta empeora el mecanismo conduciendo a una mayor dispersión de dimensiones.

3. Óptica lineal de los nanocristales de perovskitas

El estudio realizado sobre las propiedades ópticas lineales de los nanocristales de perovskita sintetizados en matrices porosas de SiO_2 se refiere, en particular, al análisis de fotoluminiscencia y a la extracción de constantes ópticas, es decir, el índice de refracción, n, y el coeficiente de extinción. k. En el primer caso, la fotoluminiscencia también es una herramienta utilizada para evaluar el método de preparación. De la fotoluminiscencia hemos examinado la posición espectral y por tanto el control sobre el confinamiento cuántico de los nanocristales (~160meV), el valor del FWHM y por tanto la homogeneidad del tamaño de los nanocristales (<90

meV), pero también hemos examinado la intensidad, o más bien la eficiencia del emisión a través de medidas de rendimiento cuántico de fotoluminiscencia (PLQY) en función del tamaño de los nanocristales. Los resultados muestran un rendimiento importante (35%), considerando un material ya en forma de película compuesta por nanocristales. El sistema de síntesis desarrollado en esta tesis, sin embargo, otorga una funcionalización adicional que ha traído, en la práctica, dos ventajas. El volumen de poros de la matriz y la interconectividad dan espacio a la posterior infiltración de un polímero (utilizamos polidimetilsiloxano, PDMS) y la primera de las ventajas es la posibilidad de analizar la variación del entorno dieléctrico de los nanocristales (antes SiO_2 y después PDMS). El resultado observado es un aumento en PLQY (54%), gracias a un aumento en los caminos de decaimiento radiativos. Al analizar el decaimiento de la PL también observamos cómo la naturaleza de la matriz puede influir en el comportamiento de los nanocristales. Una matriz basada en nanopartículas de TiO_2 implica, por ejemplo, un apagamiento de la luminiscencia debido a la inyección de electrones de las perovskitas a la banda de conducción del óxido de titanio. La segunda ventaja que aporta la incorporación del polímero está representada por la preparación de una versión flexible y autosoportada de las películas a base de nanocristales de perovskita y nanopartículas de SiO_2 impregnadas con PDMS. Estas películas flexibles ofrecen una protección completa de los nanocristales de perovskita frente a las condiciones de humedad (PL registrada por las muestras directamente sumergidas en agua) manteniendo excelentes propiedades de emisión de luz, por lo que pueden utilizarse como láminas para la conversión de color en LED de nueva generación.[29] Para ello probamos el efecto cubriendo (gracias de nuevo a la naturaleza flexible del film) una bombilla de LED azul, obteniendo la emisión verde de las perovskitas contenidas en el matriz.

Para la extracción de las constantes ópticas (n y k) se ha desarrollado un procedimiento de análisis que incluye la caracterización de la dependencia angular de la luz transmitida (transmitancia, T) y reflejada (reflectancia, R) por los materiales que contienen las perovskitas.De estos dos valores estimamos la cantidad de luz absorbida (absortancia, A). Además se cuantificó la relación volumétrica entre perovskitas y SiO_2. Nuevamente la estructura de los materiales sintetizados en esta tesis posibilita este tipo de análisis, a diferencia de los sistemas coloidales o los propios materiales compuestos en los que las perovskitas se encapsulan en matrices no transparentes a la luz. Los materiales en forma de películas permiten de hecho las medidas espectroscópicas necesarias (a través del espectrómetro Cary + UMA o + esfera integradora) y la presencia de una matriz homogénea y transparente facilita la separación de su comportamiento mediante la aproximación de la medio efectivo[30] (en este caso en particular, usamos Maxwell-Garnett). Además, a partir de las medidas de A, se obtuvo la posición energética del *gap* de los nanocristales de perovskita (útil para el cálculo teórico de n y k)

mediante el método Tauc.[31] Para obtener, en cambio, las cantidades, en volumen, de las perovskitas, utilizamos medidas cuantitativas del plomo contenido en las muestras (a través de ICP-OES). Una vez medido el comportamiento experimental, el cálculo real de n y k se basa en el ajuste de los datos experimentales mediante una función dieléctrica que describe la dependencia espectral de T y R en diferentes ángulos, según un modelo teórico (concretamente utilizamos el modelo de Forouhi-Bloomer[32]). El resultado atestigua un interesante aumento de los valores n y k de los nanocristales en comparación con los de las correspondientes películas *bulk*, tanto en el caso de $MAPbI_3$ como de $MAPbBr_3$, aunque la cantidad de perovskita con respecto a la matriz de SiO_2 es bastante baja y el valor efectivo del índice del material compuesto no presenta grandes cambios. En cualquier caso, los datos relativos a los nanocristales por sí solos son nuevos en comparación con la literatura y, de manera más general, el análisis realizado puede ser útil en el desarrollo y diseño de dispositivos optoelectrónicos basados en nanocristales de perovskita.

4. Dinámica de la red cristalina de los nanocristales

Hay características más relacionadas con la estructura cristalina que han demostrado ser igualmente relevantes para el funcionamiento de dispositivos basados en perovskitas de haluro de plomo. Se destacan las interconexiones entre la movilidad de los portadores de carga y la dinámica de la red.[33] Una cuestión todavía de gran interés se refiere precisamente a los modos colectivos de vibración de la red, es decir, los fonones y su papel en algunos procesos como el transporte de cargas o la relajación de los *hot carriers* y su contribución en algunas propiedades fundamentales como el ancho de línea del excitón y la renormalización del *bangap* respecto a la temperatura.[34] El efecto del cambio de temperatura sobre el gap energético de los semiconductores, en particular, está ligado tanto al movimiento de las bandas de conducción y de valencia como consecuencia de la contracción o expansión de los cristales como a la polarización de las vibraciones de la red y la consiguiente interacción con las bandas electrónicas. Es decir, la derivada del *gap* con respecto a la temperatura contiene dos términos que se refieren a la expansión térmica (TE) y al acoplamiento electrón-fonón (EPC).[35] Las perovskitas son un caso interesante, en comparación con la mayoría de los semiconductores porque el *bandgap* sufre un ensanchamiento con el aumento de temperatura y, en cuanto a los materiales *bulk*, los resultados más recientes atestiguan un peso igual entre TE y EPC sobre la variación del *gap*.[36,37] Pero los nanocristales son todavía bastante nuevos en este tipo de análisis que, es más complicado para los sistemas coloidales. El método más utilizado para investigar el comportamiento de los semiconductores con respecto a la temperatura es el análisis de PL a diferentes temperaturas. Hemos examinado la posición espectral a

medida que varía la temperatura en el caso de nanocristales $MAPbI_3$ de diferentes tamaños, asumiendo como primera aproximación la posición energética del PL cerca de la posición energética del gap. De esta forma es posible obtener la derivada de la energía del *gap* con respecto a la temperatura. Para separar las dos contribuciones (TE y EPC) pudimos medir experimentalmente la primera y obtener la segunda por sustracción. La contribución de la expansión térmica, o el cambio del *gap* con respecto al volumen, se puede obtener mediante medidas de PL al variar de la presión hidrostática aplicada a los nanocristales.[38] Una vez obtenidas las derivados con respecto a temperatura y presión, tanto para los nancristales como para los materiales *bulk* el utilizados para la comparación, pudimos observar un aumento relativo en la contribución de EPC, en comparación con TE, a medida que disminuye el tamaño de los nanocristales. En cualquier caso, en ambos casos experimentales, es decir, tanto con la variación de la presión como con la temperatura, notamos que junto a la reducción de las dimensiones de los nanocristales se observa una especie de aplanamiento de la curva del *gap* en función de la temperatura, es decir, una dependencia mucho menos pronunciada. También se estudiaron las transiciones de fase ortorrómbica-tetragonal que ocurren normalmente en el rango de temperaturas examinado (80K-300K) e inducen un cambio en la curva del *gap* en función de la temperatura.[39] Mediante medidas de difracción de rayos X a baja temperatura hemos observado un posible retraso de la transición de fase, a medida que aumenta la temperatura, en el caso de los nanocristales en comparación con el material *bulk*.

5. Óptica no-lineal de los nanocristales de perovskitas

Una extensión interesante, aunque poco explorada, del comportamiento de las perovskitas, en general, y de los nanocristales en particular, es el estudio de los fenómenos ópticos característicos del régimen no lineal. Se trata de fenómenos inducidos por la interacción con una luz o campo electromagnético suficientemente intenso como para modificar el comportamiento óptico de un material.[40] El término "no lineal" se refiere a la dependencia no lineal de la respuesta óptica del sistema bajo examen, con respecto a la fuerza del campo aplicado.[41] Considerando la estructura centro-simétrica de las perovskitas, la respuesta óptica de segundo orden no es la principal contribución no lineal, aunque en algunos casos se han reportado señales de segundos armónicos.[42] Los efectos de tercer orden son predominantes en estos semiconductores y hasta la fecha existen algunos resultados interesantes en la literatura, en el caso de materiales *bulk*, pero especialmente en el caso de perovskitas de tipo 2D.[43,44] Un último aspecto que hace que estos materiales sean especialmente interesantes para futuras aplicaciones en tecnología basada en sistemas no lineales es la fabricación como películas delgadas mediante procesos en fase líquida y a bajas temperaturas. La

conveniencia ya radica en los bajos costos de producción para un uso directo de estos materiales, pero especialmente en el campo de la fotónica no lineal es ventajoso tener materiales que puedan integrarse fácilmente en arquitecturas más complejas que puedan, por ejemplo, refinar el control sobre las propiedades ópticas o amplificar los efectos específico.[45] En esta perspectiva, el cuadro se enriquece obviamente con la posibilidad de síntesis de perovskitas de baja dimensión en diferentes formas y en fase líquida y sólida, con una mayor expansión de la gama de propiedades disponibles para la manipulación de la luz.

En cuanto a los materiales compuestos preparados en esta tesis, hemos podido profundizar en el comportamiento no lineal de los nanocristales de $FAPbBr_3$ sintetizados en una matriz de SiO_2. Más concretamente, se realizaron medidas de tercer armónico (THG) y los resultados confirman la fuerte dependencia espectral de este fenómeno, con un pico de intensidad correspondiente a la resonancia excitónica de los nanocristales (el análisis no lineal se realizó en paralelo al lineal con PL, A, n y k). Hasta ahora, esta es la primera evidencia de THG de tales semiconductores en forma de nanocristales. Gracias a estas medidas y a la caracterización estructural y de las propiedades lineales fue posible calcular la susceptibilidad de tercer orden de los NCs (χ^3) y su forma espectral, atestiguando un valor máximo (correspondiente al máximo de THG) comparable a los reportados para otras perovskitas de baja dimensión y otros sistemas similares de semiconductores inorgánicos encapsulados en matrices de vidrio.[46] Sin embargo, el método de preparación todavía ofrece espacio para optimizaciones adicionales como lo demuestra también el análisis de *mis-match*, o sea de la eficiencia del THG respecto al espesor de las muestras. Aunque también se demostró un fuerte carácter no lineal mediante medidas de fotoluminiscencia a dos fotones.

6. Aplicaciones de los nanocristales de perovskitas

Teniendo en cuenta el enorme interés tecnológico de las perovskitas nanocristalinas, en este trabajo hemos querido investigar la implementación y comportamiento de los *composites* de película $APbX_3@SiO_2$ como posibles componentes activos en dispositivos de estado sólido tanto para fotovoltaica (PV) como para iluminación. En cuanto a la fotovoltaica, partiendo de los primeros ejemplos de celdas solares a base de perovskita, el éxito de estos semiconductores en la tecnología solar ha sido, además de la excelente función como absorbente con el bandgap adecuado, la capacidad de difusión de las cargas libres que se forman después la excitación, es decir las propiedades de transporte.[47,48] En base a los trabajos ya reportados en la literatura, quisimos analizar el comportamiento de los materiales compuestos, teniendo en cuenta la diferencia con los primeros trabajos que utilizan andamios aislantes,[48,49] como SiO_2 o Al_2O_3, en los que, sin embargo, no hay confinamiento cuántico de perovskitas y la diferencia con el estudio con

perovskita nanocristalina empleada simplemente como material absorbente en céldas solares de colorantes[24,50] (DSSC). La idea es poder utilizar estos materiales basados en perovskitas confinadas para fabricar céldas solares de puntos cuánticos (QDSC) con la posibilidad de mantener el control sobre el *bandgap* variando el tamaño de los nanocristales de perovskita. Hemos podido integrar los materiales constituidos por nanopartículas de SiO_2 y nanocristales de $MAPbI_3$ en la arquitectura de una celda meso-estructurada que normalmente se compone superponiendo los distintos componentes en orden (FTO, TiO_2 compacto, meso-TiO2, perovskitas, Spiro, oro). Básicamente, en la nueva configuración, la lámina de SiO_2 poroso reemplaza la de TiO_2 meso y no hay una capa de perovskita bulk adicional, sino solo los nanocristales encapsulados. Una lámina de TiO_2 compacto y un film de spiro-OMetad se depositan como materiales para el transporte de electrones y huecos respectivamente hacia los dos electrodos. A continuación, examinamos el caso de las céldas solares preparadas con diferentes concentraciones de precursores y, por tanto, nanocristales de diferentes tamaños (siempre confirmado por PL). El resultado más interesante, en general, es el funcionamiento de todos los dispositivos a pesar de que los nanocristales de perovskita están encapsulados en una matriz eléctricamente aislante. Este resultado indica que las cargas pueden viajar directamente a través de los nanocristales y producir la corriente para el funcionamiento de la celda. La diferencia entre las diferentes muestras está principalmente en la cantidad de material activo presente en la matriz porosa y por tanto en la capacidad de absorción pero también en la continuidad del trayecto de las cargas a través del SiO_2. El análisis mediante espectroscopia de impedancia confirma un comportamiento de los dispositivos solares como un electrodo poroso de perovskita similar al de las células solares DSSC (con su "línea de transmisión" constituida por los NCs) que al de las céldas *bulk*, pero con una diferencia de resistencia al transporte (impedancia de Gerischer) y una capacitancia que indica el papel bivalente de los de los nanocristales de perovskita solo, como absorbentes y portadores de carga.

La posibilidad de soportar la transferencia de cargas hacia los electrodos de una celda solar a través de la población de nanocristales distribuidos dentro de la matriz porosa sugiere que el proceso inverso también es posible, es decir, la inyección de cargas a través de una corriente externa hacia los nanocristales con el fin de explotar la recombinación de los pares electrón-hueco dentro de estos últimos y emitir luz de acuerdo con el *bandgap* del perovskitas. Para obtener la electroluminiscencia es posible construir un dispositivo estructuralmente muy similar a una celda solar en el que, sin embargo, la unión de los materiales debe favorecer la transferencia de las cargas al material activo y no la extracción.[51] Como primera aproximación, la composición de la celda solar, como se describió anteriormente, ya contiene unas capas de materiales y una alineación energética de *bandgap* que puede funcionar como un dispositivo de iluminación cuando se conecta

a una corriente. De hecho esta arquitectura se define como LED invertido y es la primera que se ha utilizado para demostrar el funcionamiento de un LED basado en perovskitas.[52] Para el análisis de la electroluminiscencia, se sintetizaron perovskitas totalmente inorgánicas a base de cesio con el mismo método de confinamiento en las matrices de SiO_2 y pudimos observar las emisiones en verde y rojo, cada uno confinado, o separado espectralmente de la emisión de los dispositivos correspondientes con perovskitas *bulk*.

El estudio destaca la capacidad de los nanocristales de perovskita de gestionar la formación y difusión de cargas también a través de la matriz de SiO_2, controlando la distribución volumétrica de estos semiconductores dentro de la matriz porosa. El mecanismo de transporte es posible por la peculiaridad de la estructura compuesta y por la forma en que los nanocristales pueden distribuirse dentro de la matriz porosa. La eficiencia de las celdas solares se acerca a los valores reportados en sistemas con una arquitectura similar,[53,54] pero el método de preparación aún ofrece margen de mejora. Uno de los parámetros más prometedores es la estabilidad a largo plazo de las celdas con nanocristales encapsulados, como se demuestra en este trabajo, en comparación con la celda solar *bulk*.

7. Conclusiones generales

En esta tesis se presentó un nuevo método de síntesis de nanocristales de perovskitas de tipo ABX_3. El método permite la preparación de películas delgadas compuestas por nanocristales de perovskita encapsulados en matrices porosas formadas por nanopartículas de óxido metálico: pvk@MOx.

Se ha presentado una caracterización estructural completa de los materiales compuestos (matrices porosas de SiO_2 y nanocristales de perovskita) que destaca claramente la formación de las perovskitas dentro de los poros de las matrices. Además de un estudio del proceso de crecimiento de los nanocristales dentro de las matrices porosas, se presentó también un análisis de las propiedades ópticas y, en particular, del control sobre las propiedades de emisión (PL y PLQY) relacionado con los efectos del confinamiento cuántico. Hemos podido cambiar el entorno óptico de la matriz para modificar las propiedades de emisión de los nanocristales de perovskita. Esta modificación también resalta la versatilidad del método sintético tanto en lo que respecta a la matriz como a la composición química de las perovskitas. Esto nos permitió preparar una serie de películas flexibles y autosoportadas constituidas por la matriz porosa y los nanocristales de perovskita embebidos en una matriz polimérica. Los materiales así obtenidos han demostrado no solo funcionalidad mecánica, sino también la protección de las perovskitas de humedad extrema. También se ha demostrado cómo estos sistemas flexibles se pueden utilizar como laminas para la conversión de color en la nueva generación de LED. Se presentó por primera vez un estudio sobre la dependencia espectral del

índice de refracción y el coeficiente de extinción de los nanocristales de perovskita junto con su variación con respecto al tamaño. Se ha presentado un estudio de la fotoluminiscencia de nanocristales de perovskita a bajas temperaturas y altas presiones. Esta caracterización nos permitió distinguir la contribución de la expansión térmica y el acoplamiento electrón-fonón en la dependencia del *bandgap* con la temperatura, demostrando además cómo la variación con respecto al tamaño de los nanocristales. También se caracterizó la respuesta óptica no lineal del tercer orden de los nanocristales de $FAPbBr_3$, demostrando la posibilidad de utilizar esos nanocristales para la generación de tercer armónicos.

Finalmente se ha presentado la fabricación y caracterización de céldas solares y LED basados en nanocristales de perovskita encapsulados en matrices porosas de SiO_2. Además de la percolación de las cargas a través de la población de nanocristales dentro de las matrices aislantes, estas céldas revelaron una mejora en la estabilidad con el tiempo, en comparación con la célda *bulk*.

8. Bibliografía

1 WELLS, HORACE LEMUEL. ÜBER DIE CÄSIUM-UND KALIUM-BLEIHALOGENIDE. ZEITSCHRIFT FÜR ANORGANISCHE CHEMIE, 1893, 3.1: 195-210.

2 BHALLA, A. S.; GUO, RUYAN; ROY, RUSTUM. THE PEROVSKITE STRUCTURE—A REVIEW OF ITS ROLE IN CERAMIC SCIENCE AND TECHNOLOGY. MATERIALS RESEARCH INNOVATIONS, 2000, 4.1: 3-26.

3 MITZI, DAVID B. SYNTHESIS, STRUCTURE, AND PROPERTIES OF ORGANIC-INORGANIC PEROVSKITES AND RELATED MATERIALS. PROGRESS IN INORGANIC CHEMISTRY, 1999, 1-121.

4 SNAITH, HENRY J. PEROVSKITES: THE EMERGENCE OF A NEW ERA FOR LOW-COST, HIGH-EFFICIENCY SOLAR CELLS. THE JOURNAL OF PHYSICAL CHEMISTRY LETTERS, 2013, 4.21: 3623-3630.

5 KUNDU, SOUMYA; KELLY, TIMOTHY L. IN SITU STUDIES OF THE DEGRADATION MECHANISMS OF PEROVSKITE SOLAR CELLS. ECOMAT.

6 CHERRY, M.; ISLAM, M. SAIFUL; CATLOW, C. R. A. OXYGEN ION MIGRATION IN PEROVSKITE-TYPE OXIDES. JOURNAL OF SOLID STATE CHEMISTRY, 1995, 118.1: 125-132.

7 ZHU, PENGCHEN; ZHU, JIA. LOW-DIMENSIONAL METAL HALIDE PEROVSKITES AND RELATED OPTOELECTRONIC APPLICATIONS. INFOMAT, 2020, 2.2: 341-378.

8 JEAN, JOEL. GETTING HIGH WITH QUANTUM DOT SOLAR CELLS. NATURE ENERGY, 2020, 5.1: 10-11

9 YANG, ZHILI, ET AL. SPONTANEOUS EMISSION ENHANCEMENT OF COLLOIDAL PEROVSKITE NANOCRYSTALS BY A PHOTONIC CRYSTAL CAVITY. APPLIED PHYSICS LETTERS, 2017, 111.22: 221104.

10 SALIBA, MICHAEL, ET AL. PEROVSKITE SOLAR CELLS: FROM THE ATOMIC LEVEL TO FILM QUALITY AND DEVICE PERFORMANCE. ANGEWANDTE CHEMIE INTERNATIONAL EDITION, 2018, 57.10: 2554-2569.

11 SLOTCAVAGE, DANIEL J.; KARUNADASA, HEMAMALA I.; MCGEHEE, MICHAEL D. LIGHT-INDUCED PHASE SEGREGATION IN HALIDE-PEROVSKITE ABSORBERS. ACS ENERGY LETTERS, 2016, 1.6: 1199-1205.

12 BERA, DEBASIS, ET AL. QUANTUM DOTS AND THEIR MULTIMODAL APPLICATIONS: A REVIEW. MATERIALS, 2010, 3.4: 2260-2345.

13 EKIMOV, ALEXEY I.; EFROS, AL L.; ONUSHCHENKO, ALEXEI A. QUANTUM SIZE EFFECT IN SEMICONDUCTOR MICROCRYSTALS. SOLID STATE COMMUNICATIONS, 1985, 56.11: 921-924.

14 HUANG, HE, ET AL. LEAD HALIDE PEROVSKITE NANOCRYSTALS IN THE RESEARCH SPOTLIGHT: STABILITY AND DEFECT TOLERANCE. ACS ENERGY LETTERS, 2017, 2.9: 2071-2083.

15 SHAMSI, JAVAD, ET AL. METAL HALIDE PEROVSKITE NANOCRYSTALS: SYNTHESIS, POST-SYNTHESIS MODIFICATIONS, AND THEIR OPTICAL PROPERTIES. CHEMICAL REVIEWS, 2019, 119.5: 3296-3348.

16 GODIN, ROBERT, ET AL. TUNING CHARGE CARRIER DYNAMICS AND SURFACE PASSIVATION IN ORGANOLEAD HALIDE PEROVSKITES WITH CAPPING LIGANDS AND METAL OXIDE INTERFACES. ADVANCED OPTICAL MATERIALS, 2018, 6.5: 1701203.

17 TEN BRINCK, STEPHANIE; ZACCARIA, FRANCESCO; INFANTE, IVAN. DEFECTS IN LEAD HALIDE PEROVSKITE NANOCRYSTALS: ANALOGIES AND (MANY) DIFFERENCES WITH THE BULK. ACS ENERGY LETTERS, 2019, 4.11: 2739-2747.

18 SCHEIDT, REBECCA A.; ATWELL, COREY; KAMAT, PRASHANT V. TRACKING TRANSFORMATIVE TRANSITIONS: FROM CSPBBR3 NANOCRYSTALS TO BULK PEROVSKITE FILMS. ACS MATERIALS LETTERS, 2019, 1.1: 8-13.

19 RUBINO, ANDREA, ET AL. MESOPOROUS MATRICES AS HOSTS FOR METAL HALIDE PEROVSKITE NANOCRYSTALS. ADVANCED OPTICAL MATERIALS, 2020, 8.9: 1901868.

20 MALGRAS, VICTOR, ET AL. OBSERVATION OF QUANTUM CONFINEMENT IN MONODISPERSE METHYLAMMONIUM LEAD HALIDE PEROVSKITE NANOCRYSTALS EMBEDDED IN MESOPOROUS SILICA. JOURNAL OF THE AMERICAN CHEMICAL SOCIETY, 2016, 138.42: 13874-13881.

21 DIRIN, DMITRY N., ET AL. HARNESSING DEFECT-TOLERANCE AT THE NANOSCALE: HIGHLY LUMINESCENT LEAD HALIDE PEROVSKITE NANOCRYSTALS IN MESOPOROUS SILICA MATRIXES. NANO LETTERS, 2016, 16.9: 5866-5874.

22 WANG, HUNG-CHIA, ET AL. MESOPOROUS SILICA PARTICLES INTEGRATED WITH ALL-INORGANIC CSPBBR3 PEROVSKITE QUANTUM-DOT NANOCOMPOSITES (MP-PQDS) WITH HIGH STABILITY AND WIDE COLOR GAMUT USED FOR BACKLIGHT DISPLAY. ANGEWANDTE CHEMIE INTERNATIONAL EDITION, 2016, 55.28: 7924-7929.

23 DEMCHYSHYN, STEPAN, ET AL. CONFINING METAL-HALIDE PEROVSKITES IN NANOPOROUS THIN FILMS. SCIENCE ADVANCES, 2017, 3.8: E1700738.

24 LEE, HYO JOONG, ET AL. A FACILE PREPARATIVE ROUTE OF NANOSCALE PEROVSKITES OVER MESOPOROUS METAL OXIDE FILMS AND THEIR APPLICATIONS TO PHOTOSENSITIZERS AND LIGHT EMITTERS. ADVANCED FUNCTIONAL MATERIALS, 2018, 28.39: 1803801.

25 HIDALGO, NURIA, ET AL. CHARACTERIZATION OF MESOPOROUS THIN FILMS BY SPECULAR REFLECTANCE POROSIMETRY. LANGMUIR, 2012, 28.39: 13777-13782.

26 THANH, NGUYEN TK; MACLEAN, N.; MAHIDDINE, S. MECHANISMS OF NUCLEATION AND GROWTH OF NANOPARTICLES IN SOLUTION. CHEMICAL REVIEWS, 2014, 114.15: 7610-7630.

27 LIFSHITZ, ILYA M.; SLYOZOV, VITALY V. THE KINETICS OF PRECIPITATION FROM SUPERSATURATED SOLID SOLUTIONS. JOURNAL OF PHYSICS AND CHEMISTRY OF SOLIDS, 1961, 19.1-2: 35-50.

28 BRUS LE. ELECTRON–ELECTRON AND ELECTRON-HOLE INTERACTIONS IN SMALL SEMICONDUCTOR CRYSTALLITES: THE SIZE DEPENDENCE OF THE LOWEST EXCITED ELECTRONIC STATE. THE JOURNAL OF CHEMICAL PHYSICS. 1984 MAY 1;80(9):4403-9.

29 LIN, CHUN CHE; LIU, RU-SHI. ADVANCES IN PHOSPHORS FOR LIGHT-EMITTING DIODES. THE JOURNAL OF PHYSICAL CHEMISTRY LETTERS, 2011, 2.11: 1268-1277.

30 LEVY, OHAD; CHERKAEV, ELENA. EFFECTIVE MEDIUM APPROXIMATIONS FOR ANISOTROPIC COMPOSITES WITH ARBITRARY COMPONENT ORIENTATION. JOURNAL OF APPLIED PHYSICS, 2013, 114.16: 164102.

31 TAUC, J.; GRIGOROVICI, RADU; VANCU, ANINA. OPTICAL PROPERTIES AND ELECTRONIC STRUCTURE OF AMORPHOUS GERMANIUM. PHYSICA STATUS SOLIDI (B), 1966, 15.2: 627-637.

32 FOROUHI, A. R.; BLOOMER, I. Optical dispersion relations for amorphous semiconductors and amorphous dielectrics. Physical review B, 1986, 34.10: 7018.
33 HERZ, Laura M. How lattice dynamics moderate the electronic properties of metal-halide perovskites. The Journal of Physical Chemistry Letters, 2018, 9.23: 6853-6863.
34 SAIDI, Wissam A.; KACHMAR, Ali. Effects of electron–phonon coupling on electronic properties of methylammonium lead iodide perovskites. The journal of physical chemistry letters, 2018, 9.24: 7090-7097.
35 LAUTENSCHLAGER, P.; ALLEN, P. B.; CARDONA, M. Temperature dependence of band gaps in Si and Ge. Physical Review B, 1985, 31.4: 2163.
36 DAR, M. Ibrahim, et al. Origin of unusual bandgap shift and dual emission in organic-inorganic lead halide perovskites. Science advances, 2016, 2.10: e1601156.
37 FRANCISCO-LÓPEZ, Adrián, et al. Equal footing of thermal expansion and electron–phonon interaction in the temperature dependence of lead halide perovskite band gaps. The journal of physical chemistry letters, 2019, 10.11: 2971-2977.
38 FRANCISCO-LOPEZ, Adrián, et al. Pressure-induced locking of methylammonium cations versus amorphization in hybrid lead iodide perovskites. The Journal of Physical Chemistry C, 2018, 122.38: 22073-22082.
39 WASYLISHEN, Roderick E.; KNOP, Osvald; MACDONALD, J. Bruce. Cation rotation in methylammonium lead halides. Solid state communications, 1985, 56.7: 581-582.
40 MAIER, M.; KAISER, W.; GIORDMAINE, J. A. Intense light bursts in the stimulated Raman effect. Physical review letters, 1966, 17.26: 1275
41 BRAUNSTEIN, Rubin. Nonlinear optical effects. Physical Review, 1962, 125.2: 475.
42 GOVINDA, Sharada, et al. Can SHG Measurements Determine the Polarity of Hybrid Lead Halide Perovskites?. ACS Energy Letters, 2018, 3.8: 1887-1891.
43 JOHNSON, Justin C., et al. Third-order nonlinear optical properties of methylammonium lead halide perovskite films. Journal of Materials Chemistry C, 2016, 4.22: 4847-4852.
44 ABDELWAHAB, Ibrahim, et al. Highly enhanced third-harmonic generation in 2D perovskites at excitonic resonances. ACS nano, 2018, 12.1: 644-650.
45 BERESTENNIKOV, Alexander S., et al. Active meta-optics and nanophotonics with halide perovskites. Applied Physics Reviews, 2019, 6.3: 031307.
46 NASU, Hiroyuki, et al. Influence of matrix on third order optical nonlinearity for semiconductor nanocrystals embedded in glass thin films prepared by Rf-sputtering. Journal of non-crystalline solids, 2005, 351.10-11: 893-899.
47 KOJIMA, Akihiro, et al. Organometal halide perovskites as visible-light sensitizers for photovoltaic cells. Journal of the American Chemical Society, 2009, 131.17: 6050-6051.
48 LEE, Michael M., et al. Efficient hybrid solar cells based on meso-superstructured organometal halide perovskites. Science, 2012, 338.6107: 643-647.
49 BI, Dongqin, et al. Using a two-step deposition technique to prepare perovskite (CH3NH3PbI3) for thin film solar cells based on ZrO2 and TiO2 mesostructures. Rsc Advances, 2013, 3.41: 18762-18766.
50 YOO, So-Min, et al. An Equivalent Circuit for Perovskite Solar Cell Bridging Sensitized to Thin Film Architectures. Joule, 2019, 3.10: 2535-2549.
51 MILLER, Owen D.; YABLONOVITCH, Eli; KURTZ, Sarah R. Strong internal and external luminescence as solar cells approach the Shockley–Queisser limit. IEEE Journal of Photovoltaics, 2012, 2.3: 303-311.
52 TAN, Zhi-Kuang, et al. Bright light-emitting diodes based on organometal halide perovskite. Nature nanotechnology, 2014, 9.9: 687-692.

53 HWANG, SUN HYE, ET AL. SIZE-CONTROLLED SIO2 NANOPARTICLES AS SCAFFOLD LAYERS IN THIN-FILM PEROVSKITE SOLAR CELLS. JOURNAL OF MATERIALS CHEMISTRY A, 2014, 2.39: 16429-16433.

54 KWON, HYEOK-CHAN, ET AL. INVESTIGATING RECOMBINATION AND CHARGE CARRIER DYNAMICS IN A ONE-DIMENSIONAL NANOPILLARED PEROVSKITE ABSORBER. ACS NANO, 2018, 12.5: 4233-4245.